Cell physiology based pharmacodynamic modeling of antimicrobial drug combinations

Dissertation

zur Erlangung des akademischen Grades

doctor rerum naturalium (Dr. rer. nat.)

an der Mathematisch–Naturwissenschaftlichen Fakultät der

Christoph Philipp Hethey

Juli 2017

Published online at the
Institutional Repository of the University of Potsdam:
URN urn:nbn:de:kobv:517-opus4-401056
http://nbn-resolving.de/urn:nbn:de:kobv:517-opus4-401056

Hiermit versichere ich, dass die vorliegende Arbeit mit dem Titel “Cell physiology based pharmacodynamic modeling of antimicrobial drug combinations” selbständig von mir ausschließlich mit den angegebenen Mitteln angefertigt wurde und bisher an keiner weiteren Hochschule eingereicht worden ist.

Abstract

Mathematical models of bacterial growth have been successfully applied to study the relationship between antibiotic drug exposure and the antibacterial effect. Since these models typically lack a representation of cellular processes and cell physiology, the mechanistic integration of drug action is not possible on the cellular level. The cellular mechanisms of drug action, however, are particularly relevant for the prediction, analysis and understanding of interactions between antibiotics. Interactions are also studied experimentally, however, a lacking consent on the experimental protocol hinders direct comparison of results. As a consequence, contradictory classifications as additive, synergistic or antagonistic are reported in literature.

In the present thesis we developed a novel mathematical model for bacterial growth that integrates cell-level processes into the population growth level. The scope of the model is to predict bacterial growth under antimicrobial perturbation by multiple antibiotics *in vitro*.

To this end, we combined cell-level data from literature with population growth data for *Bacillus subtilis*, *Escherichia coli* and *Staphylococcus aureus*. The cell-level data described growth-determining characteristics of a reference cell, including the ribosomal concentration and efficiency. The population growth data comprised extensive time-kill curves for clinically relevant antibiotics (tetracycline, chloramphenicol, vancomycin, meropenem, linezolid, including dual combinations).

The new cell-level approach allowed for the first time to simultaneously describe single and combined effects of the aforementioned antibiotics for different experimental protocols, in particular different growth phases (lag and exponential phase). Consideration of ribosomal dynamics and persisting sub-populations explained the decreased potency of linezolid on cultures in the lag phase compared to exponential phase cultures. The model captured growth rate dependent killing and auto-inhibition of meropenem and—also for vancomycin exposure—regrowth of the bacterial cultures due to adaptive resistance development. Stochastic interaction surface analysis demonstrated the pronounced antagonism between meropenem and linezolid to be robust against variation in the growth phase and pharmacodynamic endpoint definition, but sensitive to a change in the experimental duration.

Furthermore, the developed approach included a detailed representation of the bacterial cell-cycle. We used this representation to describe septation dynamics during the transition of a bacterial culture from the exponential to stationary growth phase. Resulting from a new mechanistic understanding of transition processes, we explained the lag time between the increase in cell number and bacterial biomass during the transition from the lag to exponential growth phase. Furthermore, our model reproduces the increased intracellular RNA mass fraction during long term exposure of bacteria to chloramphenicol.

In summary, we contribute a new approach to disentangle the impact of drug effects, assay readout and experimental protocol on antibiotic interactions. In the absence of a consensus on the corresponding experimental protocols, this disentanglement is key to translate information between heterogeneous experiments and also ultimately to the clinical setting.

Zusammenfassung

Der Zusammenhang zwischen antibiotischer Exposition und antibakterieller Wirkung wird derzeitlich erfolgreich mithilfe von mathematischen Bakterienwachstumsmodellen studiert. Üblicherweise ignorieren diese Modelle jedoch die bakterielle Physiologie und Prozesse auf Zellebene. Es folgt, dass das mechanistische Einbinden von Wirkstoffeffekten auf Zellebene nicht möglich ist. Jedoch ist der zelluläre Wirkmechanismus besonders relevant für die Vorhersage, die Analyse und das Verständnis von Antibiotikainteraktionen. Leider gibt es keinen Konsens bezüglich des experimentellen Protokolls, um diese Interaktionen zu untersuchen. Das ist einer der Gründe, warum wir in der Literatur widersprüchliche Klassifizierungen von Antibiotikainteraktionen als additiv, synergistisch oder antagonistisch finden. In der vorliegenden Arbeit entwickelten wir ein neuartiges mathematisches Bakterienwachstumsmodel, welches Prozesse auf Zellebene in das Populationswachstum einbindet. Der Anwendungszweck dieses Models ist die Vorhersage bakteriellen Wachstums unter antimikrobieller Mehrfachexposition *in vitro*.

Um das zu erreichen, kombinierten wir die Zellebene beschreibende Daten aus der Literatur mit Wachstumsdaten für *Bacillus subtilis*, *Escherichia coli* und *Staphylococcus aureus*. Die die Zellebene beschreibenden Daten bezogen sich auf Wachstums-bestimmende Charakteristika einer Referenzzelle, unter anderem auf die ribosomale Konzentration und Effizienz. Die Wachstumsdaten beinhalteten umfangreiche Zeit-Absterbe-Kurven für klinisch relevante Antibiotika (Tetracyclin, Chloramphenicol, Vancomycin, Meropenem, Linezolid) und Zweifachkombinationen aus diesen.

Der neue Zellebenen-Ansatz erlaubt es erstmalig, einzelne und kombinierte Effekte der erwähnten Antibiotika für unterschiedliche experimentelle Protokolle gleichzeitig zu beschreiben. Insbesondere beziehen sich diese Unterschiede auf die Wachstumsphasen (Lag oder exponentiellen Phase). Die Berücksichtigung der ribosomalen Konzentration und persistenter Subpopulationen erklärte die verminderte Potenz von Linezolid gegen Kulturen in der Lag Phase im Vergleich zu Kulturen, die sich in der exponentiellen Phase befanden. Das Model erfasst Wachstumsraten-abhängiges Zelltöten und die Selbstinhibierung von Meropenem und—ebenso für Vancomycin—ein Wiederanwachsen der bakteriellen Kulturen aufgrund von adaptiver Resistenzentwicklung.

Stochastische Analysen der Interaktionsoberflächen zeigen, dass der ausgeprägte Antagonismus zwischen Meropenem und Linezolid zwar robust gegenüber Variation der Wachstumsphase und der Definition des pharmakodynamischen Endpunktes reagiert, jedoch empfindlich von der Zeitspanne des Experiments beeinflusst wird.

Desweiteren enthält der entwickelte Ansatz eine detaillierte Repräsentation des bakteriellen Zellzyklus. Wir nutzten diese Repräsentation, um Septierungsdynamiken während des Übergangs einer bakteriellen Kultur aus der exponentiellen Phase in die stationäre Phase zu beschreiben. Basierend auf einem neugewonnenen mechanistischen Verständnis für diese Übergänge, konnten wir außerdem die zeitliche Verzögerung erklären, die zwischen dem Anstieg der Zellanzahl und der Biomasse während des Übergangs von Lag zu exponentieller Phase auftritt. Außerdem reproduziert unser Modell den erhöhten intrazellulären RNA Massenanteil, der auftritt, wenn Bakterien Chloramphenikol ausgesetzt werden.

Zusammenfassend steuern wir einen neuen Ansatz bei, der es erlaubt, die Einflüsse von Wirkstoffeffekten, Endpunktdefinitionen und des experimentellen Protokolls zu entflechten. Da kein Konsens hinsichtlich eines entsprechenden experimentellen Protokolls existiert, ist eine solche Entflechtung der Schlüssel, um Informationen zwischen unterschiedlichen Experimenten—und letztendlich auch in die Klinik—zu transferieren.

In memory of Niklas Werner,
with whom I would have loved to discuss this work in more detail.

Acknowledgments

I would like to show my greatest appreciation to my supervisor Wilhelm Huisinga. His never ending passion for science is commendable and inspirational. Without his persisting patience and advice, this work would not have been possible. Furthermore, my extraordinary thanks go to my co-supervisor Charlotte Kloft for her valuable input on countless occasions. Due to this combined supervision, I always felt in good company to conduct research. Furthermore, I thank ...

- ... Sebastian Wicha for sharing the time-kill curve data. I noticed on many occasions that the data sets were thoughtfully designed by a modeler for a modeler.
- ... Niklas Hartung, Stephan Menz and Andreas Braunß for enlightening mathematical discussions from which I learned a lot.
- ... Jan Freijer for being my mentor.
- ... Alexander Solms, Sathej Gopalakrishnan, Matthias Theves, Iris Minichmayr and David Molke for supporting me in writing this thesis.
- ... Alexander Friedrich with whom I shared an office and who always had an open ear for my lamentations, thoughts and ideas.
- ... present and former colleagues in Berlin and Potsdam for the inspiring working atmosphere.

I acknowledge the Graduate Research Training Program PharMetrX for funding.

Finally, I express my deepest gratitude to Katinka Schneider for comforting me in stressful times. Thank you for all the sacrifices you made on my behalf.

Contents

1 Introduction **1**

2 Background of bacterial growth and its inhibition **5**
2.1 Bacterial population growth 6
2.1.1 Bacterial population size 6
2.1.2 Growth phases 7
2.2 Single cell replication 9
2.3 Balanced growth and the cell-state 11
2.4 Antibiotic drugs 12
2.4.1 Systematic classification of antibiotics 14
2.4.2 Pharmacological profiles for drugs used in this study 17
2.5 Bacteria 20
2.5.1 Clinical pathogens and Gram staining 20
2.5.2 *Escherichia coli* 21
2.5.3 *Staphylococcus aureus* 21
2.5.4 *Bacillus subtilis* 21
2.6 Antimicrobial *in vitro* activity 22
2.6.1 Time-kill curve assay 23
2.6.2 Antibiotic resistance 23
2.6.3 Persistence 24
2.7 Drug-drug interactions 25

3 Prototype cell-level model of bacterial population growth **27**
3.1 Growth in the absence of antibiotics 28
3.2 Cellular characteristics 30
3.3 Antibiotic perturbations 32
3.4 Metabolic adaptation processes 33
3.5 Summarized prototype cell-level model of bacterial population growth . . . 36
3.6 Applications of the prototype model 37
3.6.1 Single drug time-kill curves 37
3.6.2 Septation dynamics during shift-down 37
3.6.3 Impact of antibiotic exposure on RNA mass fraction 42
3.6.4 Lag between increase in cell number and biomass 42
3.7 Interim evaluation of the prototype model 44

4 Cell-level model for antibiotic combinations **47**
4.1 Overcoming the limitations of the prototype model 48
4.2 Linking the cell-state to bacterial population growth and *vice versa* 48
4.3 Integration of drug effects 51
4.3.1 Tetracycline 51
4.3.2 Vancomycin 52

4.3.3 Meropenem . . . 53
4.3.4 Linezolid . . . 55
4.4 Cell-level model of bacterial population growth for antibiotic combinations . 56
4.5 Pharmacodynamic summary endpoints for time-kill curve data . . . 57

5 Statistical approaches **59**
5.1 Cell-state estimation . . . 60
5.2 Bayesian inference . . . 60
5.3 Stochastic interaction surface analysis . . . 61

6 Model based analysis of antibiotic combinations and beyond **63**
6.1 Analysis of time-kill curves . . . 64
6.1.1 Reduced linezolid potency on lag phase bacteria . . . 64
6.1.2 Adaptive resistance . . . 66
6.1.3 Antibiotic interactions . . . 67
6.1.4 Eagle effect . . . 67
6.2 Impact of the experimental protocol on antibiotic interactions . . . 69
6.2.1 Pairwise comparison of drug combinations . . . 70
6.2.2 Systematic exploration of different experimental protocols . . . 71
6.2.3 Time and concentration dependency of interactions . . . 72

7 Discussion **75**

8 Conclusion **79**

A Appendix **93**
A.1 Persister fraction during exponential growth . . . 94
A.2 Comprehensive effect equations . . . 95
A.3 *E. coli* exposed to tetracycline . . . 97
A.4 Comprehensive time-kill curves *S. aureus* . . . 99

List of Figures

1.1 Overview of modeling approaches linking drug and population level 3

2.1 Bacterial population growth phases 8
2.2 Compartmentalization of the bacterial cell-cycle 11
2.3 Cellular characteristics as functions of the growth rate 13
2.4 Minimum inhibitory and bactericidal concentrations 22
2.5 Time-kill curve assay 23

3.1 Effects of antibiotics on bacterial growth dynamics 29
3.2 Bacterial population growth and persister fraction 30
3.3 Progress of cells through the maturation cycle 35
3.4 Time-kill curves (*E. coli*, TET, exp. phase, prototype model) 38
3.5 Goodness of fit plot prototype model 38
3.6 Septation dynamics 41
3.7 RNA mass fraction depends on growth rate and drug concentration 43
3.8 Lag time between increase in cell number and population mass 44

4.1 Sensitivity of lag phase duration to initial ribosomal concentration 50
4.2 Sensitivity of resistance development to corresponding EC50 value 52
4.3 Sensitivity of meropenem killing to growth medium 53
4.4 Sensitivity of the Eagle effect to meropenem exposure 55

6.1 Time-kill curves (*S. aureus*, selection) 65
6.2 Time-kill curves (*S. aureus*, LZD, exp. phase, validation) 66
6.3 Reported qualitative antibiotic interactions 70
6.4 Response and interaction surfaces 71
6.5 Time dependency of interactions 73

A.1 Time-kill curves (*E. coli*, TET, exp. phase) 98
A.2 Time-kill curves (*S. aureus*, MER, LZD, exp. phase) 99
A.3 Time-kill curves (*S. aureus*, MER, LZD, lag phase) 100
A.4 Time-kill curves (*S. aureus*, VAN, MER, exp. phase) 101
A.5 Time-kill curves (*S. aureus*, VAN, MER, lag phase) 102

List of Tables

2.1 Overview of bacterial counting techniques 7

3.1 Cellular characteristics as functions of the growth rate constant 31
3.2 Cell-cycle characteristics as functions of the doubling time 31
3.3 Strain- and drug-specific parameter estimates for the prototype model . . . 39
3.4 Experimental details on *E. coli* exposed to tetracycline 39
3.5 Experiment-specific parameter estimates for the prototype model. 40

6.1 Parameter estimates (*S. aureus*, growth and linezolid related) 68
6.2 Parameter estimates (*S. aureus*, vancomycin and meropenem related) . . . 69
6.3 Impact of the experimental protocol on antibiotic interactions 72

A.1 Parameter estimates (*E. coli*, growth and tetracycline related) 97

Chapter 1

Introduction

The looming antibiotic resistance crisis threatens the current success of anti-infective treatments [1, 2]. The extent of this success becomes visible when comparing the mortality associated with infectious diseases before and after the discovery of the first antibiotics [3]: while according to the Centers of Disease Control and Prevention, infectious diseases represented more than 50% of all causes of death for the US in the pre-antibiotic era in 1900 [4], this contribution to mortality decreased to less than 5% in 1998 [4]. These numbers highlight the deadly potential of infectious diseases and the vital dependency of society on efficacious (drug) therapies, particularly antibiotics.

While the demand for new antibiotics has increased due to epidemic resistance development [5, 6], the supply, i.e., the development of new antibiotics, has not been ensured. Consequentially, we are currently facing a period characterized by dwindling numbers of new entries of antibiotics into the market [5, 7, 8]. At the same time, effective therapy options based on the remaining drugs become more and more limited.

In cases where the risk of therapy failure would be fatal, clinical guidelines recommend to administer combinations of antibiotics. For example guidelines for treating pneumonia [9, 10] recommend dual combinations of meropenem with either linezolid or vancomycin as initial empiric therapy of hospital-acquired (non-ventilator-associated) pneumonia in high risk patients. In this indication, the extension of the antibacterial spectrum of the therapy motivates the combination of antibiotics, because the causative pathogen has usually not yet been identified during this critical first phase of treatment. Other motivations to combine antibiotics include faster clearance of infections [11], exploitation of synergies [12] or control of resistance development [11, 13].

A critical bottleneck in advancing antibiotic combination therapy is the lack of a quantitative understanding of the joint effect of drug combinations, even if the individual effects and mechanisms of action are generally well described [11]. Brute force *in vitro* testing of potential drug combinations is one option to improve this understanding, though it is cumbersome, time-consuming and does not necessarily provide insight into the reasons underlying observed interaction patterns [14]. A promising alternative are *in silico* studies based on combined pharmacokinetic (PK) and pharmacodynamic (PD) models that are driven by well designed *in vitro* data [15, 16].

Since the mechanism of action of antibiotics has been shown to be predictive of interaction patterns of antibiotic combinations [17], a physiological and mechanism based modeling approach is expected to be most powerful. Therefore, this thesis focuses on the development of a PD model to predict time-kill curves (TKC). In short, TKC are repeated measurements of the bacterial population size over time, with the addition of known concentrations of one or more antibiotic drugs. As TKC data resolve both, the time and the drug concentration dependency of bacterial growth, derived models can be seamlessly integrated into the PKPD context [15, 18]. Antibiotic PKPD models have been applied with increasing success in clinical practice [19–22].

It is a major and unmet challenge to represent the diversity of antibiotic drug targets and corresponding mechanisms of action in a single PKPD model. Conventionally, coarse grained models, which lack representation of cell-level processes and targets, are used to predict TKC data [15, 16, 23]. To overcome this limitation, the objective in this thesis was to develop a novel cell-level bacterial population growth model that allows for a mechanistic integration of drug actions of multiple antibiotics.

We achieved this by firstly exploring the "Background of bacterial growth and its inhibition" (p. 5), including experimental and theoretical considerations of "Bacterial population growth" (p. 6). As the bacterial cell-cycle links the "Single cell replication" (p. 9) to bacterial population growth, this process served as a starting point for developing a corresponding transit compartment model to describe the replication process. Together with the established [24, 25] concept of "Balanced growth and the cell-state" (p. 11),

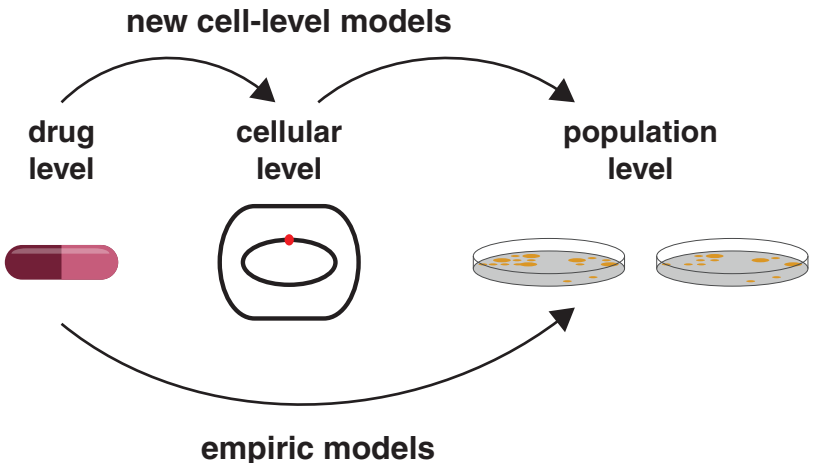

Approach	Associated data	Drug action included on	Comment
empiric models	time-kill curves	population level	simple structure, data driven
"Prototype cell-level model of bacterial population growth" (p. 27)	time-kill curves, cellular characteristics (RNA polymerase, ribosomes), cell-cycle characteristics	population and/or cellular level	complex structure, mechanism based
"Cell-level model for antibiotic combinations" (p. 47)	time-kill curves, cellular characteristics (ribosomes)	population and/or cellular level	simple structure, data driven, mechanism based

Figure 1.1: Overview of modeling approaches linking drug and population level. New developed cell-level models allow prediction of bacterial population growth while accounting for drug action on cellular level. Drug level includes pharmacokinetics of antibiotic drugs (indicated by capsule). Cellular level comprises, e.g., dynamics of intracellular concentrations of RNA polymerase or ribosomes (indicated by stylized cell). Population level refers to bacterial population growth and accounts for sub-populations like persisters (indicated by Petri dish).

we further developed this mathematical construct to the "Prototype cell-level model of bacterial population growth" (p. 27). Although extraordinary versatile in application—including the prediction of "Single drug time-kill curves" (p. 37), "Septation dynamics during shift-down" (p. 37) and the "Impact of antibiotic exposure on RNA mass fraction" (p. 42)—the prototype model was limited in its broader applicability for several reasons, see "Interim evaluation of the prototype model" (p. 44).

In order to overcome the limitations, we returned to our initial objective in "Cell-level model for antibiotic combinations" (p. 47) and thoroughly reduced our approach. The main lesson learned from the prototype model was that the ribosomes play a central role in reporting and predicting bacterial population growth in the PKPD context. Indeed, consideration of ribosomal dynamics allowed to correctly capture the reduced sensitivity of lag phase bacteria to linezolid compared to exponentially growing cultures. This, and other results, including the correct description of complex population growth dynamics and pharmacodynamic drug-drug interactions, are described in the chapter "Model based analysis of antibiotic combinations and beyond" (p. 63). For the first time, a cell-level PKPD model for antibiotic combinations systematically accounts for aspects of the experimental protocol including the growth phase. This allowed to perform an analysis of the "Impact of the experimental protocol on antibiotic interactions" (p. 69). We found the pronounced antagonism between meropenem and linezolid to be robust against variations in the growth phase and pharmacodynamic endpoint definition, but sensitive to a change in experimental duration.

The translational value of any *in vitro* data is limited by the lack of knowledge of how the experimental protocol influences the assay readout. As this thesis contributes a new approach to disentangle the impact of drug effects, assay readout and experimental protocol on antibiotic interactions, it offers new insights for experimenters and theorist alike. Since no consensus exists on the experimental protocol to assess antibiotic interactions, such insight is crucial to advance the field of anti-infective research.

Chapter 2

Background of bacterial growth and its inhibition

2.1 Bacterial population growth

A bacterial population refers to all individual bacteria in a defined experimental environment. Since the description of population growth necessitates the definition of population size, we outline typical quantification methods and related assumptions to determine this quantity in an *in vitro* setting. Classically, bacterial population growth is divided into several growth phases. We use the sequential framework of these growth phases to describe the biological background, introduce parameter notation and present empirical growth modeling approaches.

2.1.1 Bacterial population size

The development of the bacterial population size over time is a direct measure of how successfully bacteria colonize an environment. While repeated counting of the total population provides that dynamics, exhaustive counting is prohibitive for repeated measurements and not practical for large bacterial populations because of the resulting high work load. Instead, if the cells are predominantly in planctonic (free floating) state, it is commonly assumed that bacteria are well mixed in their environment (spatial homogeneity). It follows that the total bacterial population size can be approximated based on the analysis of reasonable large fraction of the environment, which is, i.e., the growth medium. Table 2.1 lists an overview of typical methods to quantify the bacterial population size.

Inference of the bacterial population size by indirect quantification methods (turbidity, bioluminescence and plating) requires the additional assumption that the number of bacteria is proportional to the assay readout. In the following we recapitulate an *exemplary* procedure to quantify the number of colony forming units (CFU) via plating, because it is a central unit throughout this thesis: from a constantly shaken reaction compartment confining the growth environment of a bacterial culture in some large volume (90 mL) the experimenter shall

(i) Extract a small volume (100 µL)

(ii) Dilute the extracted volume by a defined factor DF (usually between 1:10 and $1{:}10^7$)

(iii) Apply a fraction of the dilution onto an agar plate

(iv) Incubate the agar plate for a defined time (24 h)

(v) Count the macroscopically visible colonies (CFU)

(vi) Use the dilution factor to back-calculate the bacterial concentration in the reaction compartment in CFU/mL

The dilution factor DF is chosen based on the experimenters prior expectations such that a posteriori counted numbers of CFU are optimal with respect to the plate size. This dilatation factor also determines the lower limit of quantification (LLOQ) of the assay. Since the aim is to obtain plates which are neither empty nor overgrown, this often requires running several experiments in parallel using different values for DF. The main strength of the plating method is that it is an established method which is able to detect viable cells with minimal experimental equipment [26, p. 25]. Not counting dead cells and particles is of importance when performing experiments including antibiotic drugs, where a high number of dead bacteria is expected.

Table 2.1: Overview of bacterial counting techniques.

Method	Description	Time until result	Viability screen	Strengths	Weaknesses
Microscopic counts	Visual count of magnified bacteria	Minutes	Yes	Low LLOQ	Subjective
Flow cytometer	Analysis of cell stream	Real-time		High throughput	Expensive equipment
	a) Non-labeled cells (e.g., impedance in Coulter counter or CASY systems)		Yes	Nondestructive assay	Limited additional single-cell parameters (cell volume, viability)
	b) Labeled cells (e.g., fluorescence in FACS)		Yes	Multiparametric single-cell measurements, sub-population analysis	Complex method (combination of dye, fixation and laser excitation)
Turbidity	Determination of optical density (e.g., UV-VIS)	Real-time	No	High throughput, nondestructive assay	Indirect count via absorbtion, High LLOQ
Bioluminescence	ATP quantification via luciferase assay	Real-time	Yes	High throughput	Indirect cell count via biomarker
Plating	Count of macroscopic colonies after incubation	After incubation, e.g., 24 h	Yes	Simple experimental setup	Indirect cell count as colony forming unit

2.1.2 Growth phases

Any meaningful model of bacterial growth inhibition requires a proper baseline model describing bacterial population growth in the absence of drugs. Thus, we first focus on the growth phases observed in drug-free growth media. Early in the last century, in 1918, Buchanan described the typical growth curve of a batch culture, i.e., the development of the bacterial population size over time in a confined environment [27]. We reproduced the original trajectory from [27] to illustrate the sequence of bacterial population growth phases in Figure 2.1.

Lag phase

Per definition in [27], the lag phase is a time interval of *positive growth acceleration* after initial inoculation. In order to model the mechanisms governing this phase, it is of importance to understand the biological function and evolutionary benefit conveyed by this growth behavior.

From an evolutionists perspective, the conversion rate of nutrients into biomass is an important determinant of fitness, because a fast conversion rate allows to outgrow competitors in constant growth supporting environments [28]. The bacterial physiology determines this conversion rate via the abundance of growth limiting cellular components (ribosomes, DNA, cell wall, etc.). For all growth limiting cellular components, any increase in the abundance of one component implies savings at the cost others, because of a shared and limited cellular synthesis capacity [29]. Thus, the cellular synthesis capacity determines the abundance of growth limiting cellular components. On the transcriptional and translational level, the synthesis capacity is determined by the abundance of RNA polymerase (RNAP) [24] and ribosomes [24, 28, 30], respectively. Furthermore, the syn-

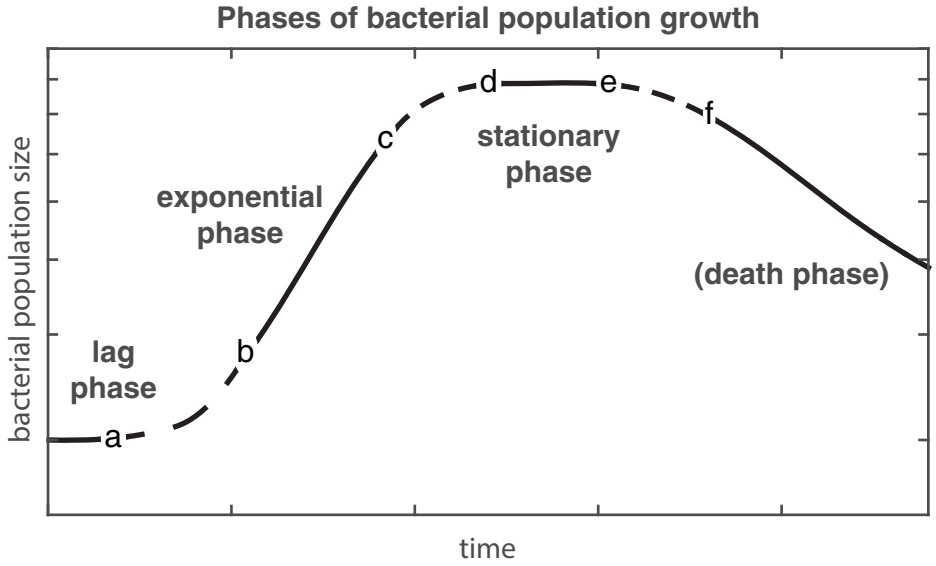

Figure 2.1: Bacterial population growth phases. Typical bacterial population growth curve in a batch culture (semilogarithmic scale). After inoculation, the bacteria start in a growth arrested state (lag phase). After a transition phase (dashed lines) with increasing growth rate ($a \to b$), the culture enters exponential growth ($b \to c$). Because of the limited abundance of nutrients and space in the confined growth environment, a transient phase with a slow down of growth ($c \to d$) leads to the stationary phase ($d \to e$). Eventually, for long experimental durations, the culture transits ($e \to f$) into a death phase. Reproduced from [27]

thesis capacity depends on the supply of energy and amino acids (aa), which is provided by the corresponding metabolic enzymes [30] and the growth environment. Changes in gene expression indicate an adaptation of the synthesis capacity during transition from lag into exponential phase [31]: the most up-regulations are observed in the functional categories related to the RNAP, the ribosomes, the fatty acid biosynthesis and the aa-tRNA synthesis. Ideal adaptation, i.e., an optimal balance between the components, is maintained, when the capacity of all individual components is fully utilized and therefore no resources for its production are wasted.

But how do bacteria approach and maintain a state of ideal adaptation, the so-called *cell maintenance*? Under the hypothesis that synthesis processes are irreversible investments, unconditioned cell maintenance imposes a risky strategy in changing environments. And indeed, bacteria typically dilute rather than actively recycle proteins [32] and ribosomes [33, 34]. As such the lag phase offers a protective mechanism against oversensitive adaption, conveying a moment of inertia to the cell maintenance.

Exponential growth

In the exponential phase a bacterial population size doubles at a constant frequency. Let $N = N(t)$ denote the total bacterial population size at some time t, then

$$\frac{\mathrm{d}}{\mathrm{d}t} N = k_{\mathrm{net}} \cdot N \tag{2.1}$$

describes the exponential growth using parameter k_{net}, which is the net exponential growth rate constant or so-called *Malthusian parameter* in 1/h. In a stochastic setting, the time to replication of a bacterial population is exponentially distributed with

$$T \sim \mathrm{Exp}(k_{\mathrm{net}}). \tag{2.2}$$

An often used re-parameterization is in terms of doubling time (or population half-life for $k_{\mathrm{net}} < 0$) defined via $\tau = \mathrm{SF} \cdot \log(2)/k_{\mathrm{net}}$, with τ in min and $\mathrm{SF} = 60\,\mathrm{min/h}$.

On the population level, τ quantifies the time interval in which the population size doubles $N(t+\tau) = 2 \cdot N(t)$. Furthermore, τ quantifies the time interval in which half of all individual cells replicate once. Thus, τ corresponds to the median of T. As a bacterial population consists of individually growing cells, the doubling time allows interpretations beyond the population level: for individual cells, τ characterized the expected doubling time. Note that individual cells may replicate more than or not at all in this time interval.

Stationary phase

Bacterial growth is typically limited by a so-called *carrying capacity*, representing the finite space and nutrient availability in a confined growth environment. Individual cells communicate the saturation of the population density via quorum sensing [35, 36], e.g., by secreting the signaling molecule Autoinducer-2 [36]. A quorum triggers changes in gene expression [35] which inhibit growth and ultimately prevent the bacterial concentration to exceed the carrying capacity.

On the population level, the logistic growth equation is the most simplistic model to describe the transition into stationary phase. The corresponding ordinary differential equation (ODE) is given by

$$\frac{\mathrm{d}}{\mathrm{d}t}N = k_{\mathrm{net}} \cdot (1 - N/N_{\max}) \cdot N, \tag{2.3}$$

where $N_{\max}$ denotes the bacterial carrying capacity. The ODE of the logistic growth equation has the analytical solution

$$N(t) = \frac{N_{\max}}{1 + \exp(-k_{\mathrm{net}} \cdot t) \cdot (\frac{N_{\max}}{N_0} - 1)}. \tag{2.4}$$

Beyond the logistic growth equation, there exists a variety of other, more complex growth models (e.g., Gompertz, Richards, Stannard, Schnute) as described in the comparative review [37].

2.2 Single cell replication

Bacterial population growth may be interpreted as the result of the replication of individual cells. Since the objective was to develop a cell-level model of bacterial population growth, we firstly investigated how single cell replication is linked to bacterial population growth. Therefore the bacterial cell-cycle was of interest. Once developed, this model served as a starting point to predict time-depended adaption processes during antibiotic exposure in "Metabolic adaptation processes" (p. 33).

The bacterial cell-cycle was divided into three phases, the B, C and D period (see Figure 2.2). During the B period, cells increased in mass. Start of a new round of chromosome replication marked the entry into the C period. The initiation of the septation process (indicated by invaginations of the cell envelope) marked the transition from the C to D period, which was completed with the division into two newborn cells.

The durations of the B, C and D periods depended on the growth rate constant [24]. For *E. coli* and *B. subtilis*, we compiled corresponding data from [24, 38, 39] and fitted continuous functions as suggested in [24], see Figure 2.3. For the corresponding equations and estimated parameters, see Table 3.2.

Cells skip the B period completely during fast growth [40]. To further speed up the chromosome replication, multiple origins of replication are initiated (multifork-replication), leading to overlapping division cycles ($\tau < \mathrm{B} + \mathrm{C} + \mathrm{D}$). For *E. coli*, the D period has been described as relatively constant over different growth rate constants [24].

We interpreted the bacterial cell-cycle as a maturation process leading to the division of a cell. To justify a final maturation stage we used the common [41] assumption that the number of growth limiting components is finite. For the definition of growth limiting components see the description of the "Lag phase" (p. 7).

This assumption allowed to define a transit compartment model for population growth similar to the Leslie matrix approach [42] in terms of describing population growth in an age structured framework: we described the bacterial cell-cycle by m maturation stages $s = 1, \ldots, m$, with cells gradually progressing from stage $s = 1$ (just after birth) to $s = m$ (just before division). The gradual progress was determined by transition rate constant k_{trans}. The transition rate constant k_{trans} was linked to the sum of the durations of the B, C and D period

$$k_{\text{trans}} = \frac{m}{\text{B} + \text{C} + \text{D}}. \tag{2.5}$$

Excursion to derive the number of transit compartments

The number of maturation stages m impacts the structure of the transit compartment model and determines the transition rate constant via eq. (2.5). In our case, this parameter was unknown. We exploited its link to the variability of the doubling time τ, represented by the coefficient of variation CV. Let the doubling time be the sum of m independent and identically distributed (i.i.d.) exponential random variables

$$\tau = \sum_{s=1}^{m} \tau_s,$$

where $\tau_s \sim \text{Exp}(k_{\text{trans}})$ is the time spent in a single maturation stage, then τ is Erlang distributed. The expected value of this Erlang distribution is given by

$$\mu = \mathbb{E}(\tau) = \mathbb{E}\left(\sum_{s=1}^{m} \tau_s\right) = m \cdot \mathbb{E}(\tau_s) = m/k_{\text{trans}},$$

which is equal to eq. (2.5). The variance of the doubling time is given by

$$\text{Var}(\tau) = \text{Var}\left(\sum_{s=1}^{m} \tau_s\right) = \sum_{s=1}^{m} \text{Var}(\tau_s) = \sum_{s=1}^{m} \frac{1}{k_{\text{trans}}^2} = \frac{m}{k_{\text{trans}}^2}.$$

With these first two moments and the definition $\text{CV}^2 = \text{Var}/\mu^2$ it follows that number of transit compartments is given by

$$m = \frac{1}{\text{CV}^2}.$$

To apply the Leslie matrix approach in the bacterial population growth context, we denoted the absolute number of cells in stage s by A_s. The rate of change for $A = (A_1, \ldots, A_m)$ over time is then described by the following system of ODEs

$$\frac{\text{d}}{\text{d}t} A_1(t) = 2k_{\text{trans}} \cdot A_m(t) - k_{\text{trans}} \cdot A_1(t) \tag{2.6}$$

$$\frac{\text{d}}{\text{d}t} A_s(t) = k_{\text{trans}} \cdot A_{s-1}(t) - k_{\text{trans}} \cdot A_s(t) \tag{2.7}$$

for $s = 2, \ldots, m$. The factor 2 in the first equation reflects the division of a single mother cell in stage $s = m$ into two daughter cells in stage $s = 1$. Since we were only interested

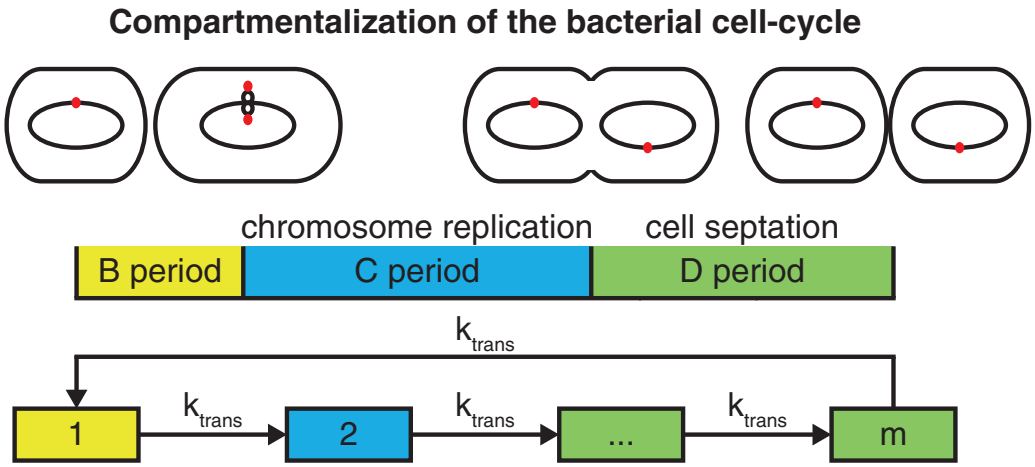

Figure 2.2: Compartmentalization of the bacterial cell-cycle. The prokaryotic cell-cycle is divided into the B, C and D period. The sketches in the upper panel depict a bacterial cell at different stages of the cell-cycle. The round boxes, inner ovals and red dots represent cell envelopes, chromosomes and origins of replication, respectively. During the B period, the cell increases in mass. Beginning of a new round of chromosome replication marks the entry into the C period. Start of the septation process indicates the transition from the C to D period, which is completed with the division into two cells. We used a transit compartment model to divide the cell-cycle in m compartments, each corresponding to a distinct cell-cycle phase and maturation stage. The cycle starts just after division with stage $s = 1$ and terminates just before division with stage $s = m$. Progress of a cell through the cell-cycle was characterized by rate constant k_{trans}. After division, two cells re-enter the cycle in the first compartment.

in the relative abundance $F_s = A_s / \sum_{s=1}^{m} A_s$, we determined the rate of change of the distribution of maturation stages $F = (F_1, \ldots, F_m)$ based on the chain rule, yielding

$$\frac{\mathrm{d}}{\mathrm{d}t} F_1(t) = 2k_{\text{trans}} \cdot F_m(t) - k_{\text{trans}}\big(1 + F_m(t)\big) \cdot F_1(t) \tag{2.8}$$

$$\frac{\mathrm{d}}{\mathrm{d}t} F_s(t) = k_{\text{trans}} \cdot F_{s-1}(t) - k_{\text{trans}}\big(1 + F_m(t)\big) \cdot F_s(t) \tag{2.9}$$

for $s = 2, \ldots, m$. During exponential growth, the distribution of maturation stages is stationary—a state called *balanced growth*. The steady state solution is given by

$$F_s^{\text{bg}} = \frac{2q}{(1+q)^s} \qquad \text{and} \qquad q = \sqrt[m]{2} - 1. \tag{2.10}$$

The stationary distribution of maturation stages in eq. (2.10) is equivalent to what has been postulated [25, p. 10] as the ideal age distribution during exponential growth $F_\alpha^{\text{bg}} = \log(2) \cdot 2^{(1-\alpha)}$ with relative age

$$\alpha = (s-1)/(m-1). \tag{2.11}$$

Note that $F^{\text{bg}} = (F_1^{\text{bg}}, \ldots, F_m^{\text{bg}})$ is not only time-invariant, but also independent of the growth rate constant. Unsurprisingly an exponentially growing bacterial culture comprises twice as many newborn cells ($s = 1$) compared to cells which are just before division ($s = m$).

2.3 Balanced growth and the cell-state

We have shown how the replication cycle links the maturation of individual cells to changes in the bacterial population size. To increase the level of detail of the modeling approach

up to a point where a mechanistic integration of antibiotic drug effects is feasible, we analyzed next, how cellular characteristics are related to bacterial population growth.

In this context it is useful to define *extensive* characteristics as characteristics describing the sum of all cells in a population [25, p. 9] (e.g., protein mass of the culture $P_{\mathrm{c,tot}}$ or population size N). During the exponential growth phase as defined in eq. (2.1), all extensive characteristics increase exponentially. *Intensive* characteristics represent cellular properties and refer to quantities per cell (e.g., protein mass per cell P_{c}). As such, intensive characteristics are time invariant during exponential, i.e., balanced growth [24, 43, 44].

We have pointed out that the distribution of maturation stages, i.e., the age distribution of the bacterial culture, is stationary during exponential growth, see eq. (2.10). We assumed for our model that each maturation stage was associated with a defined set of N_s cellular characteristics, which we henceforth call the cell-state

$$S = (S_1, S_2, \ldots, S_{N_s}). \tag{2.12}$$

From the experimentalists perspective, the cell-state describing an approximately half mature reference cell is of special interest because of the implied experimental simplifications: under the assumption that a cellular characteristic S_i increases exponentially with relative age α and doubles from cell birth to division (exponential growth law), it is this reference cell, whose value of S_i coincides with the corresponding extensive characteristic divided by the population size (see excursion on p. 14). For cellular characteristics describing parts of the cytoplasm including proteins, RNA, polyamines and glycogen, the exponential growth law is appropriate [45]. For the chromosome, on the contrary, the exponential growth law is inappropriate because of the discontinuity in DNA synthesis during the replication cycle [45], see Figure 2.2.

In 1958, Schaechter, Maaløe and Kjeldgaard [46] have made the surprising discovery that a cell-state of a bacterial population is primarily defined by the exponential growth rate constant. In other words, different growth media supporting similar growth rates lead to similar cellular characteristics of the growing bacteria. For *E. coli*, an extensive compilation of cellular characteristics for a range of growth rates has been published by Bremer and Dennis [24]. For *S. aureus* similar, but more sparse data are available [47, 48]. The cellular characteristics describe an approximately half mature reference cell, see excursion on p. 14. A selection of cellular characteristics is shown in Figure 2.3.

2.4 Antibiotic drugs

In this thesis, the term antibiotic refers to chemical compounds which kill bacteria or limit their growth at therapeutically usable concentrations. Unwanted side effects usually limit the application of chemical compounds as antibiotics. To link the antibiotic drug concentration C to a corresponding effect E, we typically used a sigmoidal Emax model

$$E = \frac{\mathrm{Emax} \cdot C^{\gamma}}{\mathrm{EC50}^{\gamma} + C^{\gamma}}. \tag{2.13}$$

The parameter EC50 denoted the concentration, at which half of the maximum effect Emax was exerted. The Hill factor γ quantified the steepness of the concentration-effect relationship. As we used the Emax model on many occasions also for different antibiotics, the definition of a uniform notation for the corresponding parameters was appropriate: in the sequel, we say that the drug or some related effector species exhibited an effect $E = E_{\mathrm{Abc,Xyz}}$ on a targeted process or cellular characteristic Xyz, if the corresponding concentration Abc was linked to the effect via the Emax model (2.13), parameterized in terms of $\mathrm{Emax} = \mathrm{Emax}_{\mathrm{Abc,Xyz}}$, $\mathrm{EC50} = \mathrm{EC50}_{\mathrm{Abc,Xyz}}$ and $\gamma = \gamma_{\mathrm{Abc,Xyz}}$.

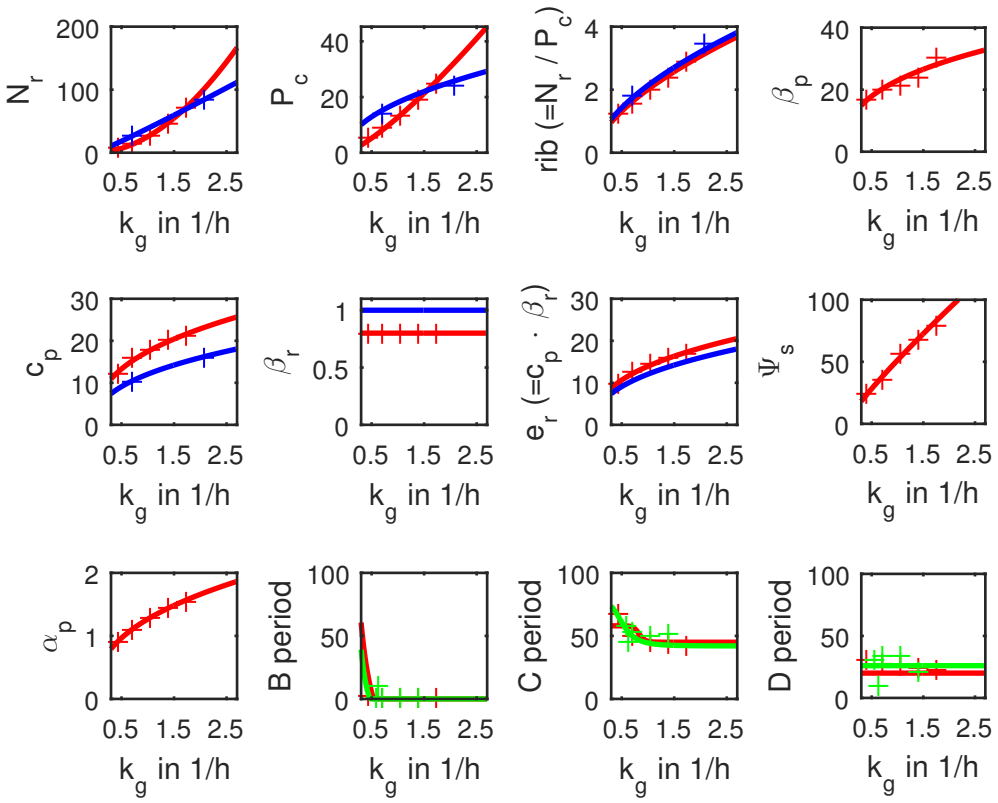

Figure 2.3: Cellular characteristics as functions of the growth rate. Growth rate is quantified via the exponential growth rate constant k_g. Experimental data for the organisms *E. coli* (red), *S. aureus* (blue) and *B. subtilis* (green) are shown as crosses. We fitted power functions to the data, represented by solid lines in corresponding color. From left to right, top panel: number of ribosomes (N_r), the protein mass per cell (P_c), ribosomal concentration (rib) and percentage of active RNA polymerase (β_p). Middle panel: peptide chain elongation rate per active ribosome (c_p), fraction of active ribosomes (β_r), ribosomal efficiency (e_r) and percentage of RNAP synthetizing rRNA and tRNA (Ψ_s). Bottom panel: percentage of total protein which is RNA polymerase α_p and duration of the individual cell-cycle periods. For description, parameterization and units, see Tables 3.1 and 3.2.

Excursion to derive the relative age of the reference cell

The cell-level data used in this thesis reportedly described the composition of an average cell in the population [24]. The authors state that the average cell is an approximately half mature cell. In the following, we contribute a theoretical justification for that claim. The cellular characteristics of the reference cell depend on the relative age α of the reference cell. For example, let $P_{c,\alpha} = \log(2) \cdot 2^{\alpha}$ describe the exponential increase of protein mass per cell up to division (in arbitrary units), assuming the exponential growth law. Next we determine for which α a cellular characteristic coincides with the corresponding extensive characteristic divided by the population size. In our example, the corresponding extensive characteristic is $P_{c,tot}$, which describes the total protein mass of a bacterial culture with

$$P_{c,tot} = N \int_0^1 P_{c,\alpha} \cdot F_{\alpha}^{bg} \, d\alpha.$$

As both, the corresponding extensive characteristic and the population size, are measurable without age fractionation of the bacterial population, such definition of the relative age of the reference cell implies considerable simplifications for the experimentalist [25, p. 11]. To determine the relative age of the reference cell, whose protein mass equals to the average cell mass $P_{c,tot}/N$, we used the inverse of this function

$$\hat{\alpha} = P_{c,\alpha}^{-1}(P_{c,tot}/N) = \frac{\log\left(2 \cdot \log\left(2\right)\right)}{\log\left(2\right)} \approx 0.47,$$

which describes an approximately half mature cell.

2.4.1 Systematic classification of antibiotics

Grouping antibiotics into classes is an essential tool for the clinician to start and switch treatments. Furthermore, grouping antibiotics enables researchers to analyze antibiotic interactions beyond the level of individual compounds. In the following, we present a classification system based on compound properties of numerous antibiotic substances. The properties referred (i) to the corresponding perturbed superordinate cellular process or structure, (ii) to the target and (iii) to the chemical class of the antibiotic, listed in decreasing hierarchical order in the classification system.

Example: The antibiotic linezolid (compound) belongs to the group of oxazolidinones (chemical class). The drug binds to the 50S subunit (target). On a larger scale, linezolid inhibits translation (perturbed superordinate cellular process or structure).

Superordinate cellular processes or structures

On the highest hierarchical level, we grouped antibiotics by the superordinate cellular process or structure perturbed by the individual compound. In particular we described the cell envelope, DNA replication, transcription and translation. Each of these processes or structures is vital for the bacterium—perturbations kill the cell or prevent replication. The description of the processes and structures was tailored to the 4 drugs which were used in this study and whose mechanism of action is described in “Pharmacological profiles for drugs used in this study” (p. 17).

Cell envelope. The cell envelope comprises the cell wall, inner membrane and for gram negative bacteria also an outer membrane (see "Clinical pathogens and Gram staining" (p. 20) for a definition of the Gram method). The cell envelope conveys structural integrity, which is necessary to maintain the hydrostatic pressure inside of the cell (turgor). Furthermore, the cell envelope controls the cellular influx and outflow of substances via porins and pumps, while the membranes represent diffusion barriers. The main constituent of the bacterial cell wall is peptidoglycan (also known as murein), which is a macromolecular polymer. Since **peptidoglycan synthesis** is essential and unique in bacteria, it is an excellent target for antibiotics. Peptidoglycan synthesis is initiated in the cytoplasma and completed in the exoplasmic space [49, 50]. The cytoplasmic part of the synthesis pathway is catalyzed by the enzymes MurA-F, MraY, MurG and flippase. The exoplasmic part is catalyzed by the enzymes flippase, glycosyltranferase and transpeptidase, where the last two are penicillin binding proteins (PBP). Enzymes of both parts, as well as the **cell membrane** are targeted by therapeutically relevant antibiotics.

DNA replication. In order to prevent the loss of genetic information when dividing in two, a bacterial cell replicates its DNA. Between replications, DNA is stored in a space-saving super-coiled state. The semi-conservative replication of DNA is catalyzed, amongst others, by the enzymes toposiomerase I, helicase, DNA polymerase and topoisomerase II (gyrase). The **toposiomerases** I and II de- and re-coil the DNA strands, respectively. The toposiomerase II is targeted by therapeutically relevant antibiotics. Beside the catalyzing enzymes for DNA replication, also the supply of substrates in form of nucleic acids represents targets for antibiotic perturbations. Many prokaryotes rely on the dihydropteroate pathway to obtain tetrahydrofolate (THF), which is essential for the synthesis of nucleic acids (e.g., adenine, guanine and thymidine). Since the dihydropteroate pathway is not present in eukaryotic cells, the inhibition of **THF synthesis** also represents an excellent target to inhibit bacterial growth.

Transcription. During transcription, RNA polymerase (RNAP) molecules move along de-coiled DNA strands and catalyze the synthesis of template mRNA strands. As such, the transcription depends on the preceding activity of **toposiomerases** and a steady supply of nucleic acids. Accordingly, inhibition of **THF synthesis** also impairs the transcription process. Furthermore, some antibiotics inhibit the activity of the prokaryotic **RNA polymerase** itself.

Translation. The translation process is classically divided into initiation, elongation and termination phase. During initiation, the ribosome is assembled as a complex from the following educts [51, p. 374]: the **30S ribosomal subunit** (comprising 16S rRNA), initiator fMet-tRNA, mRNA and the **50S ribosomal subunit** (comprising 5S and 23S rRNA). After this complex formation, the ribosome enters the elongation phase, where single amino acids are added sequentially to the growing protein strand. The ribosome in the elongation phase has three tRNA binding sites, termed P (peptidyl), A (aminoacyl) and E (exit) site. During the elongation process, charged tRNA enter the A site and leave the E site uncharged. The formation of a peptide bond between the transported amino acid and the C-terminal end of the growing peptide is catalyzed by the ribozyme peptidyl transferase. A termination codon induces the dissociation of the completed peptide, tRNA, mRNA and ribosome.

Other targets, specifically the **redox system**, did not fit into any of the above categories and were listed as miscellaneous superordinate cellular processes or structures. Effecting 11 of 178 grouped compounds, we consider this acceptable.

Targets and chemical classes

In the following trees we assigned chemical classes, including exemplary compounds, to targets. The 1st level indicates the target level of the classification system. The 2nd level comprises the targets. The 3rd and 4th level lists the corresponding chemical groups and compounds, respectively. The compounds used in this study are printed in bold.

- Targets
  - Peptidoglycan synthesis
    - Penicillins
      - Amoxicillin
      - Dicloxacillin
      - Methicillin
      - Nafcillin
      - Oxacillin
      - Ticarcillin
      - ...
    - Cephalosporins
      - Cefaclor
      - Cefadroxil
      - Cefuroxime
      - Cephalexin
      - ...
    - Monobactams
      - Aztreonam
      - Tigemonam
      - ...
    - Carbapenems
      - Doripenem
      - Ertapenem
      - Imipenem
      - **Meropenem**
      - ...
    - Glycopeptides
      - Moenomycin
      - Teicoplanin
      - Telavancin
      - **Vancomycin**
      - ...

- Targets
  - Cell membrane
    - Polypeptides
      - Polymyxin B
      - Colistin (=Polymyxin E)
      - Tyrothricin
      - Cecropin
      - Bacitracin
      - Gramicidin
      - Nisin
      - ...
    - Lipopepides
      - Daptomycin
      - ...
    - Aminoglycosides (atypical) . . . [52]
      - Chelocardin
      - Anhydrotetracycline
      - Anhydrochlortetracycline
      - ...
    - Other
      - Bacitracin
      - D-Cycloserin
      - Ethambutol
      - Ethionamid
      - Fosfomycin
      - Isoniazid
      - Loracarbef
      - Platensimycin
      - Teicoplanin
      - Triclosan
      - ...

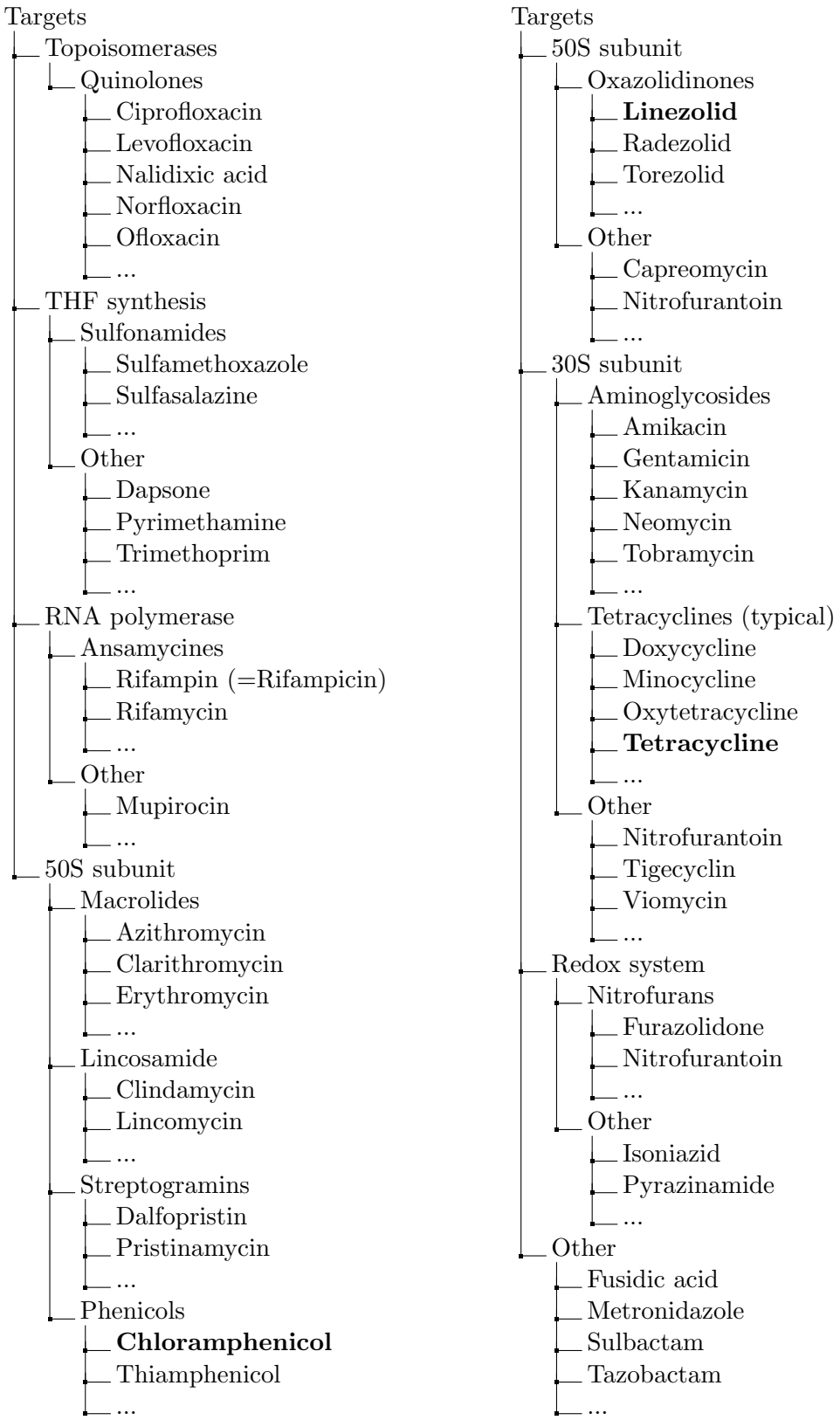

2.4.2 Pharmacological profiles for drugs used in this study

To highlight the importance of the individual antibiotics analyzed in this study, we describe in the following the pharmacological profile for the drugs. The pharmacological profile includes clinical indications, antimicrobial spectrum (see "Clinical pathogens and Gram staining" (p. 20) for definitions) and the mode of drug action of the compound.

The latter comprises a description of drug action on molecular level, as well as a characterization as either bacteriostatic or bactericidal. The characterization as bacteriostatic or bactericidal was based on the minimum inhibitory concentration (MIC) and minimum bactericidal concentration (MBC) of the compound, see Figure 2.4 for exemplary determination via serial dilution technique. Following [53], we consider a compound bacteriostatic if MBC/MIC < 5, and bactericidal otherwise. Note that the terms bacteriostatic and bactericidal may alternatively refer to the killing activity of the drug. In that case, bacteriostatic and bactericidal drug action differentiates between growth inhibition and death induction. The pharmacological profiles complement the corresponding paragraphs in "Integration of drug effects" (p. 51), where we discuss technical and modeling related aspects of the drugs.

Tetracycline

Tetracycline is a protein biosynthesis inhibitor and perturbs translation. The drug exhibits a low toxicity and a broad spectrum of activity (gram positive and gram negative bacteria including intracellular chlamydiae, mycoplasma and rickettsia) [20, p. 267]. It is used in treatment against community-acquired respiratory tract infections, infections of skin and skin structure and sexually transmitted diseases [20, p. 267]. Due to resistance, the drug is typically a secondary choice compared to other antibiotics and predominantly used against intracellular infections [20, p. 268]. The binding site of tetracycline is located on the 30S subunit of a 70S ribosome [54, 55] and interferes with the anticodon stem-loop of an tRNA which is charged with amino acids (aa), i.e., aa-tRNA at the A site [56]. Thus, the supply of amino acids is disrupted and translation is perturbed. Furthermore, under saturated cytoplasmic aa-tRNA concentrations, also the P site is blocked by tetracycline [57]. In both cases, bacterial growth is inhibited by reducing the fraction of active ribosomes [56]. The binding of tetracycline to the ribosomes is reversible and the drug effect is usually described as bacteriostatic [58].

Chloramphenicol

Chloramphenicol is a protein biosynthesis inhibitor that perturbs translation. The drug is considered a reserve antibiotic due to its severe side effects, including the potentially lethal bone marrow suppression. Therefore, its use is limited to severe infections, which are uncontrollable with other antibiotics [71]. Due to its excellent tissue penetration and broad antibacterial spectrum including gram positive and negative bacteria, it is used against several infectious diseases, e.g., meningitis and enteric fever [71]. Oral, topic and parenteral routes of administration are available. The binding site of chloramphenicol is located on the 50S subunit of a 70S ribosome. Specifically, the drug interacts with 23S rRNA nucleotides, which are part of the peptdidyl transferase cavity [56, 72]. The drug directly blocks the binding of aa-tRNA to the A site [72] and thus disrupts the consumption of amino acids. Typically, chloramphenicol is described as a bacteriostatic drug [56].

Vancomycin

Vancomycin is a cell wall active antibiotic that impairs the integrity of the cell envelope. Because of its activity against multi resistant Staphylococci, the glycopeptide vancomycin is an important drug to treat nosocomial infections. Vancomycin impairs the integrity of the cell envelope of gram positive bacteria. In particular, it interferes with the peptidoglycan synthesis by preventing the transglycosylation of the cell wall subunits [68]. Since the activity of the penicillin binding protein (PBP) transglycosylase is highest at the proximal side of the extracellular matrix [73], we consider this region as the target site and critical for drug action. On the molecular level, vancomycin binds to the D-Ala-D-Ala end of

Excursion about antibiotics and the stringent response

The stringent response is a protective mechanism limiting waste of cellular synthesis capacity in stressful conditions like nutrient deprivation or exposure to antibiotics. The stringent response is mediated via the alarmone (p)ppGpp. Along with limiting the cellular synthesis capacity and cell metabolism, (p)ppGpp stimulates resistance to drugs [59], persister [60, 61] and biofilm formation [62]. Thus, the stringent response impacts antibiotic drug action.

For proteinbiosynthesis inhibitors acting during the elongation phase of translation, it is the ribosomal binding time of the drug (τ_{drug}) which is predictive of the effect on (p)ppGpp [63, 64] in relation to the average time needed to complete a protein (τ_{protein}) and the average time needed to add a single amino acid (τ_{aa}), both referring to an elongation active ribosome. For *E. coli*, it is $\tau_{\text{protein}} \approx 16\,\text{s}$ and $\tau_{\text{aa}} \approx 0.05\,\text{s}$, assuming an average peptide chain elongation rate of 20 aa/s [65] and an average length of 317 aa per protein [66]. The following table is condensed from [63]:

Type I
$\tau_{\text{drug}} \leq \tau_{\text{aa}} \leq \tau_{\text{protein}}$

- Competitive inhibition
- Examples: no substance known

Type II
$\tau_{\text{aa}} \leq \tau_{\text{drug}} \leq \tau_{\text{protein}}$

- Activates stringent response
- Increases (p)ppGpp levels (activates RelA)
- Similar to heat-shock
- Similar to amino acid starvation
- Induces "translational pause"
- Premature termination of protein strands
- Examples: puromycin, streptomycin, kanamycin

Type III
$\tau_{\text{aa}} \leq \tau_{\text{prot}} \leq \tau_{\text{drug}}$

- Deactivates stringent response
- Decreases (p)ppGpp levels (deactivates SpoT)
- Similar to cold-shock
- Similar to *single* amino acid starvation
- Reduces fraction of active ribosomes
- Allosteric inhibition
- Examples: chloramphenicol, tetracycline, erythromycin, spiramycin, fusidic acid

In *E. coli* (p)ppGpp is regulated via a (p)ppGpp synthetase and a bifunctional synthetase / hydrolase, which are the enzymes RelA and SpoT, respectively [67, p. 343]. "RSH" proteins, i.e., RelA and SpoT homologes, are abundant in many organisms and were also recently characterized in *S. aureus* [61]. Vancomycin [68], linezolid [69] and beta-lactams including meropenem [70] have the same effect on the stringent response: activation.

the peptidoglycan precursor Lipid II [68], which is the substrate of the transglycosylation reaction. Vancomycin is typically described as a bactericidal drug [53].

Meropenem

Meropenem is a cell wall active antibiotic that impairs the integrity of the cell envelope. It belongs to the group of carbapenems and is considered a broad spectrum antibiotic because of its activity against gram positive and negative bacteria. Yet, it is not active against methicillin resistant *S. aureus* (MRSA) [74]. Furthermore, meropenem is classified as a reserve antibiotic. Therefore, its use is limited to severe, live threatening infection, e.g., sepsis. The drug inhibits the peptidase domain of multiple PBPs, preventing the transpeptidase to catalyze cross-linking of peptidoglycan [75]. The beta-lactam ring of meropenem is remarkably stable against hydrolyzation. Only a few of the hundreds of known beta-lactameses inactivate meropenem [76]. Meropenem is described, similar to other beta-lactam antibiotics, as a bactericidal drug [26, p. 11].

Linezolid

Linezolid is a protein biosynthesis inhibitor that perturbs translation. Linezolid belongs to the synthetic class of oxazolidinone antibiotics. The name oxazolidinone refers to the central heterocyclic ring present in all drugs of this class. Linezolid is reserved for severe nosocomial infections because of its outstanding feature to be active against multi resistant gram positive bacteria [77, 78]. The antibacterial spectrum includes MRSA, vancomycin intermediate *S. aureus* (VISA) and vancomycin resistant *S. aureus* (VRSA). Furthermore, linezolid exhibits total oral bioavailability [78] and excellent tissue penetration into almost all body organs [77], making the drug an indispensable tool for the clinician. Linezolid binds to the 23S rRNA of the 50S subunit of the ribosomes. More specifically, it binds to the A site, where the peptidyl transferase center is located [56]. As a unique mechanism of the oxazolidinones, linezolid acts during the initiation phase of translation. This phase is the rate limiting step of translation [78]. However, non-physiologically high drug concentrations are required to inhibit this step [56]. As such, the exact ribosomal state during the inhibition is yet inconclusive and under current research. Linezolid is considered as a bacteriostatic drug.

2.5 Bacteria

Bacteria is the taxonomic term referring to one of the three classical domains of life [79]: Bacteria, Archaea and Eukaryota. The bacterial domain comprises astoundingly adaptable microorganisms which survive even in harshest environments like the outer hull of the international space station (*Bacillus pumilus* [80]), in radioactive waste water of a nuclear plant (*Deinococcus radiodurans*) or in Arctic climates. Some bacteria cause diseases, i.e., they are pathogenic. In the sequel, we give an overview of clinically relevant pathogens and describe the bacteria considered in this thesis—including infections, therapy and mechanisms of resistance. Beside the bacterial type, clinical pathogens may also refer to viruses, fungi, prions and algae.

2.5.1 Clinical pathogens and Gram staining

In the clinical setting, key determinants of individual treatment success are pharmacokinetic properties of the antibiotic compound [21] and the spectrum of antimicrobial activity. As the diversity of bacteria is large, a full specification of the spectrum of antimicrobial activity is not feasible. Instead of specifying the susceptibility of individual organisms, coarse grained differentiations for groups of pathogens are used. One of the most common methods to group bacteria is the Gram method. This method differentiates almost all bacteria

based on their characteristic cell wall staining into gram positive and gram negative organisms [81]. The few exceptions include *Mycobacterium tuberculosis*, which results in gram neutral stain [82]. Clinically relevant gram positive pathogens are bacteria of the genera streptococcus, enterococcus and staphylococcus. Problematic in terms of limited treatment options [83] are infections with methicillin resistant *Staphylococcus aureus* (MRSA) and vancomycin resistant enterococci (VRE). The group of gram negative pathogens comprises *Haemophilus influenzae*, *Moraxella catarrhalis* and the family of Enterobacteriaceae including *Salmonella*, *Escherichia coli*, *Yersinia pestis*, *Klebsiella* and *Shigella*. Especially problematic [83] are bacteria which synthesize extended spectrum beta-lactamases (ESBL) or exhibit carbapenemase activity, in particular *Klebsiella* species and *Escherichia coli*. These bacteria require the use reserve antibiotics. Further problematic [83] are *Acinetobacter baumannii*, *Pseudomonas aeruginosa* and *Enterobacter* species due to extensive resistance development.

2.5.2 *Escherichia coli*

The gram negative bacterium *Escherichia coli* (*E. coli*) is rod shaped and potentially pathogenic. Its pathogenicity strongly depends on the site of colonization: interaction between the human host and *E. coli* are symbiotic when the colonization is limited to the gut. Outside the intestinal tract, *E. coli* causes a variety of diseases including infections of the urinary tract and meningitis. The ability of some strains to produce extended spectrum beta-lactamases (ESBL) implies serious clinical problems [83] as it renders antibiotics of the chemical classes penicillins, cephalosporines and monobactams as ineffective. As a model organism, the cellular physiology of *E. coli* is well known and quantitatively described [24]. Thus, the bacterium is an ideal candidate to develop the "Prototype cell-level model of bacterial population growth" (p. 27).

2.5.3 *Staphylococcus aureus*

The gram positive bacterium *Staphylococcus aureus* (*S. aureus*) is sphere shaped and potentially pathogenic. Serious corresponding infections include endocarditis, pneumonia, sepsis and toxic shock syndrome, which may all be nosocomial or community acquired. It is estimated that 20% of the worlds population are carriers of *S. aureus* [84]. Clinical difficulties in treating *S. aureus* infections arise due to resistance development against almost all antibiotics showing activity against the bacterium. In particular infections with methicillin resistant *S. aureus* (MRSA), vancomycin (intermediate) resistant *S. aureus* (VISA, VRSA) threaten patients worldwide and require the use of the reserve antibiotics like linezolid. Therefore our choice to analyze combinations of meropenem with either linezolid or vancomycin is of highest clinical interest: clincial guidelines [9, 10] recommend both dual combinations as first line therapy in the same indication (initial empiric therapy for hospital-acquired pneumonia (non-ventilator-associated) in high risk patients). The choice to use the methicillin susceptible *S. aureus* (MSSA) strain ATCC 29213 as a test organism is based on the high incidence for MSSA to be the pathogen causing hospital-acquired pneumonia [10]. The results based on TKC experiments with *S. aureus* are presented in "Model based analysis of antibiotic combinations and beyond" (p. 63).

2.5.4 *Bacillus subtilis*

The gram positive bacterium *Bacillus subtilis* (*B. subtilis*) is rod shaped and usually not pathogenic. Under stressful conditions, such as the transition from exponential into stationary phase, *B. subtilis* undergoes characteristic sporulation processes leading to the formation of extraordinary resistant endospores. Because of its high importance for the

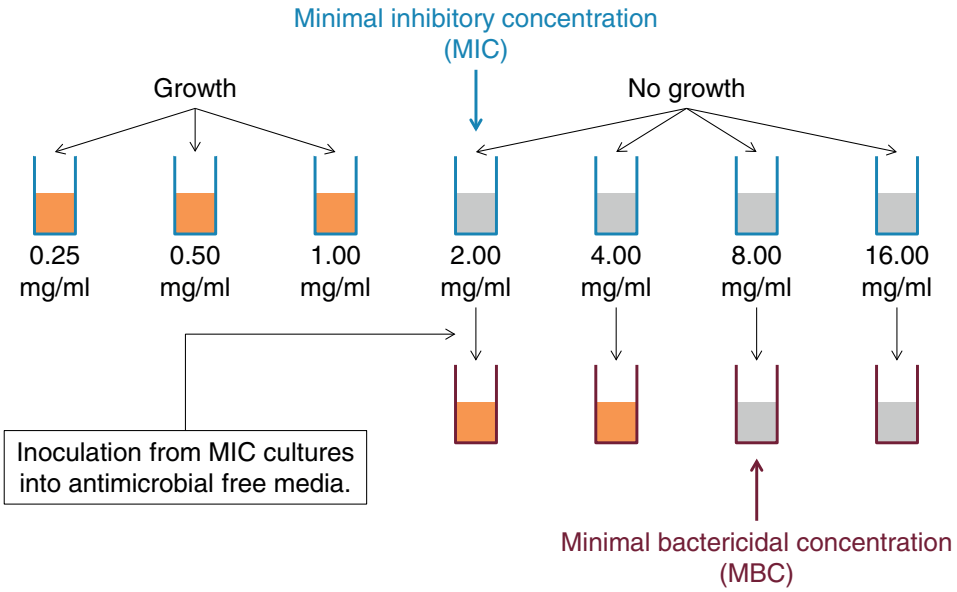

Figure 2.4: Minimum inhibitory and bactericidal concentrations. Determination of the minimal inhibitory and bactericidal concentration via serial dilution technique (twofold increments). After a first incubation step (20 h) the turbidity in the reaction vessels indicates growth (orange) or no growth (gray). The lowest concentration showing no growth is the minimal inhibitory concentration (MIC). To determine the minimal bactericidal concentration (MBC), those cultures who exhibit no growth are transfered into antibiotic free medium. The MBC is the lowest concentration, at which no growth is observed after a second incubation step.

industry, e.g., as fungicide or for biotechnological enzyme production, the organism is among the best analyzed bacteria, including a full sequencing of its genome [85]. In this study, we use morphological data from electron microscopy in [38, 39] to parameterize the cell-cycle of *B. subtilis*, see Table 3.2 and Figure 2.3. Application of the developed age structured cell-cycle model allowed to describe the transition from exponential into stationary phase with respect to the fraction of septated cells, see "Septation dynamics during shift-down" (p. 37).

2.6 Antimicrobial *in vitro* activity

The ability to culture bacteria *in vitro* allows to assess the effects of antibacterial drugs in the absence of animal or human hosts—with benefits (less sources of variability, more controlled environment, less expensive and more humane) and drawbacks (less translational power, no pharmacokinetic interactions) compared to corresponding *in vivo* experiments. In the anti infective setting, the most established *in vitro* assays are static assays in terms of reference to a single time point, which usually represents the end of the experiment. Among the static assays, the determination of the minimal inhibitory concentration (MIC) is the most prominent one. Harmonized protocols for individual bacterial species are available [86]. We summarized the in [86] suggested serial dilution technique in Figure 2.4.

A mayor drawback of static assays in general, and of the MIC determination in particular, is the exclusive reference to the end of the experiment. The MIC is not informative with respect to dynamic aspects like regrowth or ongoing prevention of bacterial growth, which both are critical information for the evaluation of antibacterial effects. In contrast, the TKC assay resolves the bacterial population size over time and thus gives a more detailed insight into bacterial population growth dynamics.

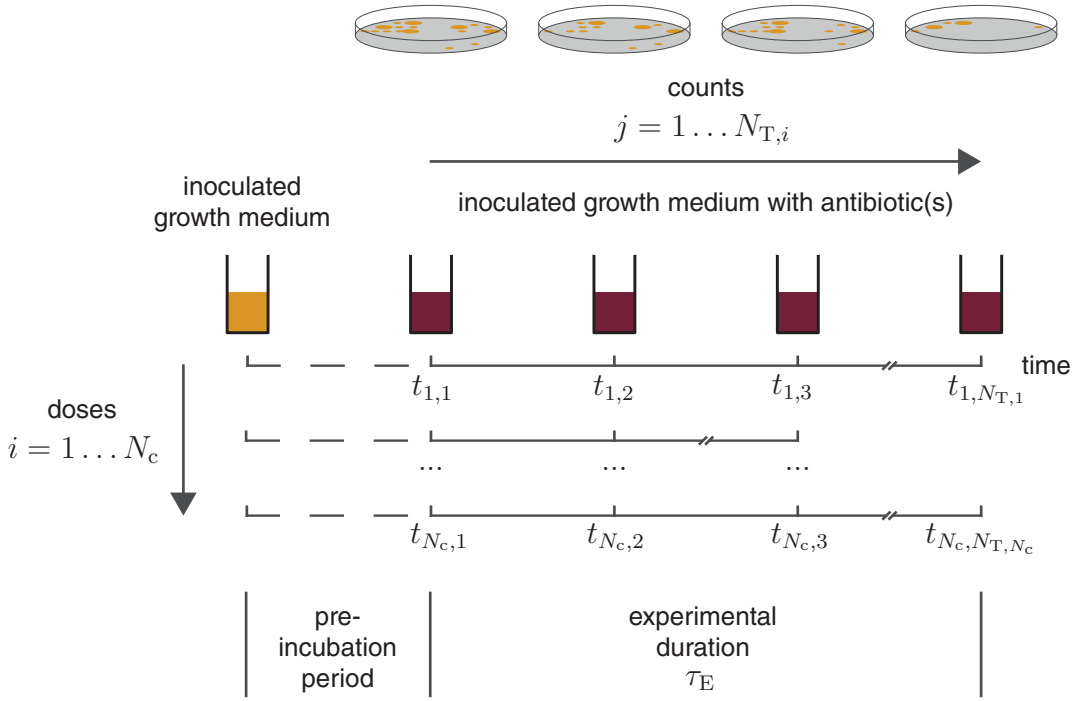

Figure 2.5: Time-kill curve assay. Time-kill curve observations $y_{\mathrm{obs},ij}$ are repeated counts of the bacterial population size over time $t_{i,j}$ after the addition of known doses of one or more antibiotics into the reaction vessel (indicated by red fill). The observations include N_{C} trajectories, each comprising $N_{\mathrm{T},i}$ measurements, i.e., counts. The figure illustrates viable plating as a counting technique. The duration of the pre-incubation period determines the growth phase at the start of the experimental duration.

2.6.1 Time-kill curve assay

Time-kill curve (TKC) observations are repeated counts of the bacterial population size over time after the addition of known doses of one or more antibiotics into the reaction vessel (for applicable counting techniques, see Table 2.1). In the static TKC assay, a standardized inoculum is pre-incubated in a constantly stirred or shaken reaction vessel before the antibiotic is added. The duration of the pre-incubation period is the key determinant for the initial growth phase (lag, exponential or stationary phase). The observation time interval defines the experimental duration τ_{E}. In dynamic TKC assays, additional pumps and filters enable control over the concentration time course of the antibiotic(s) to mimic *in vivo* pharmacokinetic profiles. Data from dynamic setups were not part of this study. However, extensive experimental durations up to $\tau_{\mathrm{E}} = 48\,\mathrm{h}$ lead to a significant change in drug concentrations due to degradation. Usually, several doses of the antibiotic(s) are explored in addition to control experiments without drugs. See Figure 2.5 for a schematic of the TKC methodology.

2.6.2 Antibiotic resistance

In clinical practice [87], antibiotic resistance is quantified via the MIC of an isolate: the isolate, that is a bacterial population, is considered resistant or susceptible with reference to MIC breakpoints. These breakpoints are based on previously determined MIC values for the same strain (as reported, e.g., in the EUCAST database [88]). Since antibiotic resistance threatens the (still) ongoing success of antibacterial therapies [2, 83] and represents a mayor driver of bacterial regrowth in time-kill curve (TKC) data [16, 89, 90] we outline general mechanisms of antibacterial resistance. On the cellular level, mechanisms of resistance are diverse and fall into the following categories [1]:

Firstly, prevention of access to the target due to reduced permeability or increased efflux. For example, *tet*(A-E,I,Y) genes encode for efflux pumps which confer resistance to tetracycline in *E. coli* [58]. Secondly, modifications in the antibiotic target, e.g., by mutation. And thirdly, modifications of the antibiotic, like the inactivation of chloramphenicol via the chloramphenicol acetyltransferase [91, p. 353].

A bacterial population may have inherited resistance, i.e., the bacteria are intrinsically resistant due to existing (mutated) genes, or they acquire resistance, which includes purely phenotypic (non-inherited) modifications [92]. The time-scale for acquiring resistance ranges from days to hours of antibiotic exposure. Such remarkable fast adjustments are termed *adaptive resistance* and rely on epigenetic factors, population heterogeneity, high mutation rates, gene amplification, efflux pumps and biofilm formation [93, 94].

In pharmacodynamic models based on the Emax function in eq. (2.13), adaptive resistance may decrease either the Emax parameter [89] or the drug concentration C [89], which is equivalent to an increase in the EC50 parameter.

Based on [89, 90], we developed a generic methodology to describe the time-depended development of adaptive resistance. Let $\mathrm{ARX} = \mathrm{ARX}(t)$ quantify the adaptive resistance against some antibiotic, with $0 \leq \mathrm{ARX} \leq 1$, where $\mathrm{ARX} = 1$ denoted full resistance. The concentration of the antibiotic is denoted by $\mathrm{X} = \mathrm{X}(t)$. With notation introduced for eq. (2.13), the reduced drug effect(s) were implemented by substituting the Emax and C components of the Emax function(s) effected by adaptive resistance with

$$\mathrm{Emax} \cdot (1 - \mathrm{ARX}) \qquad \text{or} \qquad C \cdot (1 - \mathrm{ARX}), \tag{2.14}$$

implying that ARX was in unit fractional reduction. The development of adaptive resistance was described as a time and drug concentration depending process with rate of change

$$\frac{\mathrm{d}}{\mathrm{d}t}\mathrm{ARX} = E_{\mathrm{X,ARX}} \cdot (\mathrm{ARX}_{\max} - \mathrm{ARX}) - k_{\mathrm{deg,ARX}} \cdot \mathrm{ARX} \tag{2.15}$$

where $E_{\mathrm{X,ARX}}$ denoted the selective pressure for resistance development and $k_{\mathrm{deg,ARX}}$ accounted for a corresponding fitness cost. The parameter $\mathrm{ARX}_{\max}$ represented the maximum adaptive resistance value, implying $0 \leq \mathrm{ARX} \leq \mathrm{ARX}_{\max} \leq 1$ for initial values $0 \leq \mathrm{ARX}(0) \leq \mathrm{ARX}_{\max} \leq 1$. The particularities of *S. aureus* resistance to meropenem and vancomycin, where we applied this methodology, are discussed in detail in the corresponding paragraphs in "Integration of drug effects" (p. 51).

2.6.3 Persistence

In contrast to resistance, which is defined with respect to the MIC of a whole bacterial population, persistence is the ability of a specialized sub-population to survive transient exposure to antibiotic concentrations far above the MIC [87]. The hallmark characteristic of persistence is reversible dormancy in form of a phenotypic switch [95, 96]. Re-inoculation of a persisting sub-population results in a similar MIC as the original population [87]. The trait of reversible dormancy is shared among persisters of numerous bacterial species [96], although the biological mechanisms are different. The mechanisms include toxin-antitoxin systems [97] and stationary phase respiration [98] (*E. coli*), or ATP depletion [99] (*S. aureus*).

While switching from persisting to growing state is usually described by single rate constant [95, 97], the effective rate of persister formation is stimulated by many factors [100]: environmental insults [100] (starvation, oxidative or acidic stress, heat shock), social engagement [100] (quorum sensing during transition to stationary phase [60, 101]) and exposure to antibiotics [101] are reported amongst others. The stimulation of persister formation is predominantly mediated via the alarmone ppGpp [97].

From an evolutionary perspective, persistence represents an "insurance policy" against antibiotic encounters [102] at the cost of reducing the reproductive capacity of the whole bacterial population (depending on the size of the persister fraction).

2.7 Drug-drug interactions

Patient medication often includes the simultaneous use of multiple drugs [103] with the aim to diversify or boost the effects of drug therapy. Drug-drug interactions on pharmacokinetic and pharmacodynamic level are the consequence, e.g., via shared metabolic capacity, crosstalk of signaling pathways [104] or chemical incompatibility [105]. Such interactions may critically impact the overall success (or failure) of drug therapy.

Let *pharmacodynamic summary endpoint* (PSE) quantify the overall success or failure of a two drug therapy. To emphasize the dependence of the PSE on the drug exposures(s), $\mathrm{PSE} = \mathrm{PSE}(A, B)$ denotes the summary endpoint of a combination of two drugs with exposures A and B, e.g., dose or initial concentrations.

The classification of drug combinations as *synergistic* or *antagonistic* is defined with respect to some reference. This reference is the definition of *additivity*, i.e., the *expected* PSE of a drug combination based on the single drug exposures. To this end, typically the concept of Bliss independence [106] or Loewe additivity [107] are used. Both definitions result in an *expected* endpoint assuming pure additivity. Other references have been derived from those basic definitions, see comparative review [108].

Bliss independence assumes independent drug action and effect additivity. As such, it is more appropriate for combinations with different mechanisms of drug action. We defined the expected endpoint based on Bliss independence by

$$\mathrm{PSE}_{\mathrm{Bliss}}(A, B) = \mathrm{PSE}(A, 0) + \mathrm{PSE}(0, B) - \mathrm{PSE}(A, 0) \cdot \mathrm{PSE}(0, B). \tag{2.16}$$

Note that "sham" combinations [107], where the interaction of a drug with itself is analyzed, do not result in unity of $\mathrm{PSE}(A, B)$ and $\mathrm{PSE}_{\mathrm{Bliss}}(A, B)$. Yet, we see this result not as a drawback, because sham combinations clearly violate the assumption of independent drug action and do not represent a realistic experimental scenario.

Loewe additivity automatically assumes dose additivity, because the dose of one drug is substituted by an equipotent dose of the other drug resulting in

$$\mathrm{PSE}_{\mathrm{Löwe},A} = \mathrm{PSE}\big(A + \mathrm{PSE}^{-1}(0, B), 0\big) \tag{2.17}$$

$$\mathrm{PSE}_{\mathrm{Löwe},B} = \mathrm{PSE}\big(0, B + \mathrm{PSE}^{-1}(A, 0)\big), \tag{2.18}$$

where PSE^{-1} maps one drug exposure to an equipotent exposure of the other drug such that both exposures result in the same response, i.e., $\mathrm{PSE}(A, 0) = \mathrm{PSE}(0, B)$. We differentiated between the substitution of exposure A or B (via $\mathrm{PSE}_{\mathrm{Löwe},A}$ and $\mathrm{PSE}_{\mathrm{Löwe},B}$, respectively) because of potentially heterodynamic drug combinations. Drug combinations are considered heterodynamic if the corresponding exposure–response functions are of different shape [107], e.g., different values for γ or Emax in the Emax model defined in eq. (2.13). The Loewe concept results for homodynamic, i.e., non-heterodynamic combinations in a unique expected endpoint

$$\mathrm{PSE}_{\mathrm{Löwe},A} = \mathrm{PSE}_{\mathrm{Löwe},B}. \tag{2.19}$$

This is not the case for heterodynamic combinations, where either one, two or none are defined. Accordingly, the Loewe is concept more appropriate than Bliss independence when two drugs have similar mechanisms of action and homodynamic behavior is expected.

Finally, we defined synergy or antagonism as deviation Δ of the predicted PSE (based on the predicted effect for the drug combination) from the expected PSE (based on the predicted effect for single drugs and its expected combined effect based on Bliss independence or Loewe additivity). For Bliss independence it is

$$\Delta_{\text{Bliss}}(A, B) = \text{PSE}(A, B) - \text{PSE}_{\text{Bliss}}(A, B), \tag{2.20}$$

and analogously for Loewe additivity. Well defined summary endpoints ($0 \leq \text{PSE} \leq 1$) imply $-1 \leq \Delta_{\text{Bliss}} \leq 1$, where negative deviation $\Delta_{\text{Bliss}} < 0$ indicates *antagonism*. Positive deviation $\Delta_{\text{Bliss}} > 0$ indicates *synergy*. No deviation $\Delta_{\text{Bliss}} = 0$ defines *additivity*.

Chapter 3

Prototype cell-level model of bacterial population growth

While susceptibility assays for MIC determination rely in general on good harmonization and international standards [86], the experimental setups for time-kill curves (TKC) are quite diverse in terms of protocol. A model that allows to account for these differences should integrate the following groups of parameters:

(i) strain-specific parameters, which are transferable between different experimental setups and thus broaden the applicability of the approach

(ii) drug-specific parameters that might be general or specific to a strain

(iii) experiment-specific parameters, which are expected to vary between experimental protocols

As a consequence, experimental data of diverse origin could be combined. Finally, the mechanistic integration of drug action is a prerequisite for understanding and quantifying the effect of antibiotic drug combinations. In the following, we develop a prototype cell-level model satisfying the mentioned criteria.

To this end, we first considered bacterial growth in the absence of antibiotics, and describe the characteristics of a reference cell in the bacterial population. Drug action was included by modulation of one or more of these characteristics—according to the mechanism of action of the drug.

Adaptational changes have been described [44] for bacterial cultures that are exposed to drugs for prolonged periods. Potentially relevant for antibiotic drug action, we accounted for such adaptations in the model. Finally, we also considered bacterial growth in changing growth environments.

3.1 Growth in the absence of antibiotics

Since bacterial persistence is a typical growth behavior observed in time-kill curves, we assumed for our model that the bacterial population consisted of two sub-populations: normal cells at counts $n = n(t)$ that grew, divided and were subject to cell death, and size of the persister population $p = p(t)$ that were dormant (yet alive). This results in the total bacterial population size

$$N = N(t) = n + p. \tag{3.1}$$

Two sub-populations are the minimum to account for a persisting population during drug exposure. In the model depicted in Figure 3.1, normal cells grew and died with rate constants k_g and k_d, both in units 1/h. Furthermore, growth was limited by a carrying capacity N_max, which accounted for experiment specific nutrient limitations, and—important for the consideration of persister cells—space limitations. The logistic term was introduced in eq. (2.3). Normal cells switched to persister phenotype and *vice versa* with effective rate constants $k_\mathrm{np,eff}$ and $k_\mathrm{pn,eff}$. Since the persister fraction was only observable during antibiotic exposure, the effective rates included basal and persister formation triggered by antibiotics. This yielded the following system of ODEs for the rate of change of normal and persister cells:

$$\frac{\mathrm{d}}{\mathrm{d}t}n = \big(k_\mathrm{g} \cdot (1 - (n+p)/N_\mathrm{max}) - k_\mathrm{d}\big) \cdot n - k_\mathrm{np,eff} \cdot n + k_\mathrm{pn,eff} \cdot p \tag{3.2}$$

$$\frac{\mathrm{d}}{\mathrm{d}t}p = k_\mathrm{np,eff} \cdot n - k_\mathrm{pn,eff} \cdot p \tag{3.3}$$

Experimental setups typically specify the starting inoculum $N(0) = n(0) + p(0)$. Depending on the experimental protocol, in particular the preparation of the bacterial culture

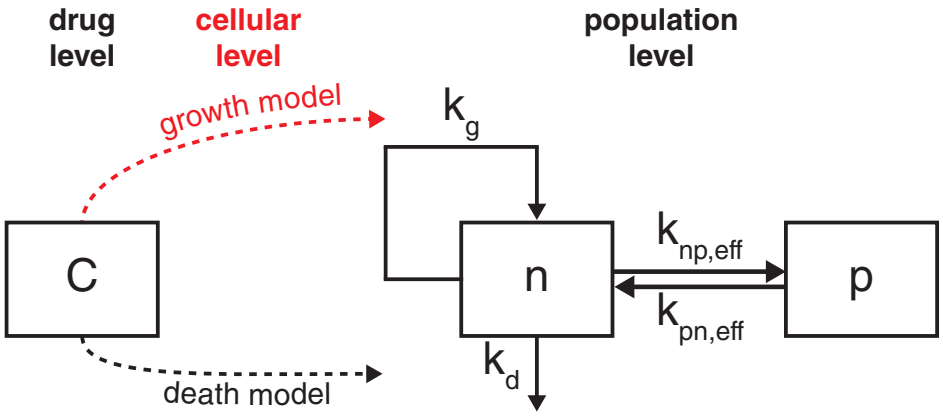

Figure 3.1: Effects of antibiotics on bacterial growth dynamics. On population level, the total concentration of cells N is sum of two sub-populations: normal, growing (n) and resting persister (p) cells. Switching from growing to resting state and back is described by rate constants $k_{\mathrm{np,eff}}$ and $k_{\mathrm{pn,eff}}$, respectively. Antimicrobial concentration C stimulated death rate constant k_{d} via death model and also inhibited growth according to growth model including cellular characteristics (red).

before the experiment, the relation between $n(0)$, $p(0)$ and $N(0)$ varied substantially. We parameterized the initial conditions as $n(0) = (1-f_{\mathrm{p}})\cdot N(0)$ and $p(0) = f_{\mathrm{p}}\cdot N(0)$. Thereby we defined the fraction of persister cells

$$f_{\mathrm{p}}(t) = \frac{p(t)}{n(t)+p(t)}. \tag{3.4}$$

A typical time course of $n(t)$, $p(t)$ and $f_{\mathrm{p}}(t)$ is shown in Figure 3.2. In the exponential phase, the persister fraction reached a quasi steady state

$$f_{\mathrm{p,exp}} \approx \frac{k_{\mathrm{np,eff}}}{k_{\mathrm{net}} + k_{\mathrm{np,eff}} + k_{\mathrm{pn,eff}}}, \tag{3.5}$$

in which normal cells largely out-competed persister cells (see "Persister fraction during exponential growth" (p. 94) for derivation). The persister fraction was parameterized in terms of the net growth rate constant

$$k_{\mathrm{net}} = k_{\mathrm{g}} - k_{\mathrm{d}}, \tag{3.6}$$

which described growth in the absence of capacity and nutrient limitations. Only this parameter is usually inferable from TKC data. To determine k_{g} and k_{d} from k_{net}, we assumed based on data in [109] that the probability of cell death per generation $p_{\mathrm{d}} = 0.01$ was constant across generations and cell maturations (no cell senescence). This yielded $k_{\mathrm{d}} = p_{\mathrm{d}} \cdot k_{\mathrm{g}}$ and finally

$$k_{\mathrm{g}} = k_{\mathrm{net}}/(1-p_{\mathrm{d}}) \qquad \text{and} \qquad k_{\mathrm{d}} = k_{\mathrm{net}} \cdot p_{\mathrm{d}}/(1-p_{\mathrm{d}}). \tag{3.7}$$

In the stationary phase the persister fraction was solely determined by the switching rate constants

$$f_{\mathrm{p,stat}} = \frac{k_{\mathrm{np,eff}}}{k_{\mathrm{np,eff}} + k_{\mathrm{pn,eff}}}. \tag{3.8}$$

Typically, we had $k_{\mathrm{np,eff}}, k_{\mathrm{pn,eff}} \ll k_{\mathrm{net}}$ [95], implying $f_{\mathrm{p,exp}} \ll f_{\mathrm{p,stat}}$ (see also Figure 3.2). Depending on the experimental protocol, the initial conditions were thus defined with the persister fraction reached in the exponential phase $f_{\mathrm{p}} = f_{\mathrm{p,exp}}$ or in the stationary phase $f_{\mathrm{p}} = f_{\mathrm{p,stat}}$.

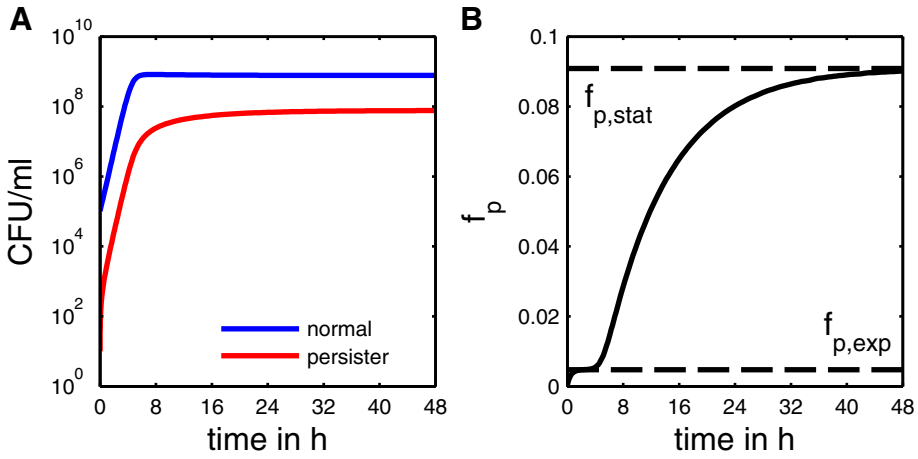

Figure 3.2: Bacterial population growth and persister fraction. *E. coli* B/r cells in drug-free media simulated with parameters estimated from the training data set as described in "Single drug time-kill curves" (p. 37). **(A)** Population dynamics during transition from exponential to stationary phase. **(B)** The persister fraction f_p exhibited two characteristic values (dashed lines): quasi steady state during the exponential phase $f_{\mathrm{p,exp}}$, followed by transition to steady state in stationary phase $f_{\mathrm{p,stat}}$, where the persister fraction became maximal.

3.2 Cellular characteristics

Antibiotic drug molecules act according to their mechanism of action on the cellular level. The effect of antibiotic drugs on the population level, observed and quantified as a change in bacterial population size, originates from drug induced perturbations on the cellular level. Thus, we explicitly included a cellular level into our model and a link to population growth and death. We exploited the interplay between growth rate and cellular characteristics, described in [24, 110]. To this end, we used the concept of the cell-state S, as introduced with eq. (2.12). The cell-state comprised cellular characteristics that allowed (i) to represent the mechanism of action of the drug by modulation of one or more of its elements; (ii) to capture key biological processes that determine growth; and (iii) to describe adaptational processes of the cells during prolonged drug exposition.

Based on definitions and notation in [24], we selected the cell-state $S = S_{i=1\ldots11}$ with

$$S = (\mathrm{nucl./prib.}, \mathrm{aa/pol.}, f_{\mathrm{t}}, \beta_{\mathrm{p}}, c_{\mathrm{s}}, \Psi_{\mathrm{s}}, \alpha_{\mathrm{p}}, c_{\mathrm{p}}, \beta_{\mathrm{r}}, P_{\mathrm{c}}, M_{\mathrm{cell}}) \,, \tag{3.9}$$

where, e.g., c_{p} denoted the peptide chain elongation rate per active ribosome, and β_{r} denoted the fraction of active ribosomes, see Tables 3.1 and 3.2. Given a detailed characterization of the cell-state at various growth rates, the individual cellular characteristics were determined solely from the growth rate constant [24, 46] via the mapping

$$k_{\mathrm{g}} \mapsto S_i(k_{\mathrm{g}}). \tag{3.10}$$

Bremer and Dennis had determined the relationship experimentally under various growth conditions corresponding to a range of growth rate constants [24]. Based on the experimental measurements for *E. coli* in [24], we estimated continuous representations, see Figure 2.3 and Tables 3.1 and 3.2. The estimation method is described in "Cell-state estimation" (p. 60).

Obviously, variations on the cellular level, i.e., changes in S_i, may impact growth. For antibiotic perturbations, we exploited the following two links between cellular characteristics and the growth rate constant. Firstly, each invertible cellular characteristic S_i (i.e., all S_i in Table 3.1 with $b_i \neq 0$) allowed to infer k_{g} as a function of S_i, i.e.,

$$S_i \mapsto k_{\mathrm{g}}(S_i). \tag{3.11}$$

Table 3.1: Cellular characteristics as functions of the growth rate constant. Cellular characteristics $S_i = a_i \cdot k_g^{b_i}$ for the reference *E. coli* and *S. aureus* cell as power functions of the exponential growth rate constant k_g in 1/h. Not available parameters are marked by N/A.

		E. coli		*S. aureus*		
S_i	**Description and units**	a	b	a	b	**References**
N_r	Number of 10^3 ribosomes per cell	25.50	1.89	37.96	1.07	[24, 47]
P_c	Protein mass per cell in 10^8 amino acid (aa) residues	12.70	1.28	16.75	0.48	[24, 47, 111]
c_p	Peptide chain elongation rate per active ribosome in aa/s	17.43	0.39	11.97	0.42	[24, 47]
β_r	Fraction of active ribosomes	0.80	0	1.00	0	[24]
Ψ_s	Fraction of active RNA polymerase synthesizing rRNA and tRNA in %	51.26	0.86	N/A	N/A	[24]
β_p	Fraction of active RNAP in %	22.95	0.36	N/A	N/A	[24]
α_p	Fraction of total protein that is RNAP in %	1.27	0.39	N/A	N/A	[24]
$P_{c,\mu g}$	Protein mass per 10^9 cells in µg	239.07	1.05	N/A	N/A	[24]
$R_{c,\mu g}$	RNA mass per 10^9 cells in µg	73.63	1.90	N/A	N/A	[24]
M_{cell}	Dry weight per 10^9 cells in µg	413.25	1.31	N/A	N/A	[24]
nucl./prib.	Ribonucleotide residues per rRNA precursor	6000	0	N/A	N/A	[24]
aa/pol.	Amino acid residues per RNAP core	3407	0	N/A	N/A	[24]
f_t	Fraction of stable RNA that is tRNA	0.14	0	N/A	N/A	[24]
c_s	Stable RNA chain elongation in nucleotides 1/s	85	0	N/A	N/A	[24]
nucl./rib.	Ribonucleotide residues per 70S ribosome	4566	0	N/A	N/A	[24]
f_s	Fraction of RNA that is stable RNA	0.98	0	N/A	N/A	[24]

Table 3.2: Cell-cycle characteristics as functions of the doubling time. Duration of the bacterial growth phases (B, C and D period) as functions of the doubling time τ, all in min. It is $D(\tau) = e$ and $C(\tau) = a + (b\tau^c)/(\tau^c + d^c)$, while $B(\tau) = \tau - C - D$ for $\tau > C + D$; and $B(\tau) = 0$ otherwise.

	Parameters					
Bacterium	a	b	c	d	e	**References**
E. coli	45	13	15	50	20	[24]
B. subtilis	42	35	4	80	26	[38, 39]

As expected, under balanced growth conditions, each cellular characteristic S_i resulted in the same growth rate constant $k_g(S_i)$. Secondly, it has been shown [24, 110] that the growth rate constant is also a function of a combination of key cellular characteristics:

$$S \mapsto k_g(S) = \mathrm{SF} \cdot \sqrt{\frac{\Psi_s(1-f_t)c_s\beta_p}{\text{nucl./prib.}} \frac{\alpha_p c_p \beta_r}{\text{aa/pol.}}}, \tag{3.12}$$

where the factor $\mathrm{SF} = 3600\,\mathrm{s/h}$ accounted for difference in units between c_s and c_p (in 1/s) and k_g (in 1/h). In summary, eqs. (3.10), (3.11) and (3.12) assumed that in the absence of drugs and during balanced growth, the growth rate constant predominantly determined the cell-state in a one-to-one relation. This interrelation was a key for our cell-level approach because it allowed to switch between the population and cellular level.

3.3 Antibiotic perturbations

During balanced growth, bacteria exhibit well defined cellular characteristics which ensure optimal growth, see "Growth phases" (p. 7) and "Balanced growth and the cell-state" (p. 11). Upon antibiotic exposure, this balance is perturbed. In the following, we define how these perturbations effect the cell-state.

Antibiotic effects are typically analyzed and quantified with respect to some control experiment without drugs. We used the control experiments to infer the associated control (net) growth rate constant $k_{\mathrm{net,c}}$. The control growth and death rate constants k_g and k_d were determined based on eq. (3.7). The corresponding cellular characteristics S_c defined a reference (control) cell-state according to eqs. (3.9) and (3.10). In our model, exposure to antibiotics was assumed to directly perturb one or more of the cellular characteristic of this reference cell-state according to the mechanism of action of the drug

$$S_c \underset{\text{antibiotic action}}{\longrightarrow} S_p, \tag{3.13}$$

where subscripts c and p abbreviate control and perturbed, respectively. As it is commonly done, we realized this via a variation of the parameters according to the introduced Emax model which linked the antibiotic concentration to the degree of perturbation (see example below). We termed these perturbed cellular characteristics "directly drug-controlled".

We considered the antibiotics tetracycline and chloramphenicol, both protein biosynthesis inhibitors that lower the fraction of active ribosomes β_r as described in detail in "Pharmacological profiles for drugs used in this study" (p. 17). To determine the resulting growth rate corresponding to the perturbed cell-state S_p, we assumed that the (invertible) cellular characteristic S_i with smallest corresponding growth rate constant $k_g(S_i)$ determined the perturbed growth rate constant, since it most severely limits growth. The assumption was based on the idea of Liebig's law of the minimum [112] and resulted in

$$k_{g,p} = \min_i k_g(S_i). \tag{3.14}$$

We modeled the induction of cell death from antibiotic exposure via the Emax model described in eq. (2.13). The relationship between antibiotic concentration, and growth / death effects is illustrated in Figure 3.1.

Example: Tetracycline at concentration C reduces the fraction of active ribosomes according to

$$\beta_{r,p} = \beta_{r,c} \cdot \left(1 - \frac{C^\gamma}{\mathrm{EC50}^\gamma + C^\gamma}\right), \tag{3.15}$$

where $\mathrm{EC50} = \mathrm{EC50_g}$ denoted the concentration corresponding to the half-maximal effect, and $\gamma = \gamma_\mathrm{g}$ denoted a Hill exponent. We assumed that tetracycline exposure may result in full, i.e., 100% inhibition of translation. This has been observed experimentally [113]. Additionally, we assumed that as an immediate consequence, the intracellular concentration of amino acids rises due to decreased translation. Because of the increased amino acid availability, the peptide chain elongation rate of the active ribosomes was assumingly effected via

$$c_\mathrm{p,p} = c_\mathrm{p,c} + (c_\mathrm{p,max} - c_\mathrm{p,c}) \cdot \frac{C^\gamma}{\mathrm{EC50}^\gamma + C^\gamma}, \tag{3.16}$$

with $c_\mathrm{p,max}$ denoting the maximal protein chain elongation rate in addition to the same notation as in eq. (3.15).

The product $e_\mathrm{r} = c_\mathrm{p} \cdot \beta_\mathrm{r}$ is known as the *ribosomal efficiency* [24]. Following exposure to tetracycline, the perturbed ribosomal efficiency $e_\mathrm{r,p}$ was strongly decreased. We assumed that no other cellular characteristic was directly drug-controlled by tetracycline. According to eq. (3.14), the reduced ribosomal efficiency $e_\mathrm{r,p}$ was the cellular characteristic that most severely impaired growth, i.e., $k_\mathrm{g,p} = k_\mathrm{g}(e_\mathrm{r,p})$. This example was analogously applied for chloramphenicol.

The drug effect on the death rate constant $k_\mathrm{d,p}$ was described as a sigmoid function

$$k_\mathrm{d,p} = k_\mathrm{d} + \mathrm{Emax} \cdot \frac{C^\gamma}{\mathrm{EC50}^\gamma + C^\gamma}, \tag{3.17}$$

where $\mathrm{Emax} = \mathrm{Emax_d}$ denoted the maximum induced death rate constant, C the drug concentration, $\mathrm{EC50} = \mathrm{EC50_d}$ the concentration of half-maximal effect, and $\gamma = \gamma_\mathrm{d}$ the Hill exponent.

3.4 Metabolic adaptation processes

During prolonged antibiotic exposure on the time-scale of hours, bacteria adjust their cell-state to adapt to the perturbations, eventually resulting in some adapted cell-state [44]. After defining the perturbed cell-state, we continue in the following to define this adapted cell-state

$$S_\mathrm{p} \underset{\text{adaptation}}{\longrightarrow} S_\mathrm{a}, \tag{3.18}$$

with associated growth rate constant $k_\mathrm{g,a}$. Subscripts p and a abbreviate perturbed and adapted, respectively. We assumed for simplicity that the gradual transition from the perturbed to the adapted growth rate constant followed a first-order adaptation process. We parameterized this process with rate constant λ. During the adaptation process, the growth rate constant $k_\mathrm{g} = k_\mathrm{g}(t)$ changed over time according to

$$\frac{\mathrm{d}}{\mathrm{d}t} k_\mathrm{g} = \lambda \cdot \left(k_\mathrm{g,a} - k_\mathrm{g}\right) \tag{3.19}$$

with $k_\mathrm{g}(0) = k_\mathrm{g,p}$ upon antibiotic exposure at time $t = 0$. To determine the adapted growth rate constant, we decomposed the cell-state S_a into three subsets: cellular characteristics S_direct that were directly effected by the drug; S_indirect that were indirectly effected by the drug, depending on the specific mechanism of action; and S_growth that were growth rate controlled and subject to the adaptation process.

Example: For tetracycline and chloramphenicol, the adapted cell-state was partitioned into the following groups: directly drug effected characteristics $S_\mathrm{direct} = (\beta_\mathrm{r}, c_\mathrm{p}, e_\mathrm{r})$ defined in S_p. As reported in [63, 114, 115], the peptide chain elongation rate c_p was

a sensor to induce changes in RNA ($R_{c,\mu g}$) and protein mass (P_c, $P_{c,\mu g}$) of the reference cell. Since c_p was directly perturbed by the antibiotic, we defined the indirectly drug effected characteristics as $S_{\text{indirect}} = (R_{c,\mu g}, P_c, P_{c,\mu g})$. Hence, for S_i as part of S_{indirect}, we assumed $S_i = S_i(c_{p,p})$. This functional dependence was realized by first determining the growth rate constant associated with $c_{p,p}$ in eq. (3.11), and then using this growth rate constant in eq. (3.10) to determine S_i. Growth rate controlled characteristics $S_{\text{growth}} = (\text{nucl./prib.}, \text{aa/pol.}, f_t, c_s, \Psi_s, \alpha_p, \beta_p, \text{B}, \text{C}, \text{D})$ with growth rate constant $k_{g,p}$. Together, this defined the adapted cell-state $S_a = (S_{\text{direct}}, S_{\text{indirect}}, S_{\text{growth}})$, and thus based on eq. (3.12) the adapted growth rate constant

$$k_{g,a} = k_g(S_a). \tag{3.20}$$

It remained to determine the adaptation rate constant λ in eq. (3.19). This was done based on a cell-cycle and maturation distribution model described in the section "Single cell replication" (p. 9). During balanced growth, cellular characteristics are largely time-invariant [24, 43, 44]. This was also the case for the distribution of maturation stages and cell ages [25, p. 10]. Upon a change of environment (a shift), e.g., a nutritional shift-up in the growth rate or shift-down due to antibiotic exposure, the pre-shift distribution was perturbed, resulting in a post-shift distribution. Over time, and if the environment remained constant, eventually a new time-invariant distribution was reached. We determined the adaptation rate constant λ from the dynamics of this adaptation process.

The cell-cycle characteristics shown in Figure 2.2 were functions of the target growth rate constant $k_{\text{post-shift}}$, i.e., $\text{B} = \text{B}(k_{\text{post-shift}})$, $\text{C} = \text{C}(k_{\text{post-shift}})$ and $\text{D} = \text{D}(k_{\text{post-shift}})$. The corresponding functions are defined and parametrized in Table 3.2. In the case of a drug-induced shift-down, we set $k_{\text{post-shift}} = k_{g,a}$, since the adapted growth rate constant described growth under prolonged antibiotic exposure.

For the strain *E. coli* B, Plank et al. [116] have estimated the coefficient of variation CV for the doubling time τ in several different growth media over three generations. They have inferred an approximately constant value of $\text{CV} = 0.226$ for a wide range of of doubling times ($35 \leq \tau \leq 95\,\text{min}$). For *B. subtilis*, we estimated based on data in [117] a similar value of $\text{CV} = 0.210$. According to the excursion on p. 10, this implied a comparable number of $m = 22$ and $m = 23$ stages for *E. coli* and *B. subtilis*, respectively.

Upon perturbation, the duration of the B and C periods changed (the D period was relatively constant). As a consequence, the overall progress of a single cell changed *within the cell-cycle*, i.e., its fractional completion of the cell-cycle. In contrast, progress of a single cell did not change *within its period*, i.e., the fractional completion of its B or C period.

Example: In Figure 3.3 the pre-shift and post-shift distributions are shown for the case of a shift-down from $k_g = 0.4/\text{h}$ to $k_{\text{post-shift}} = 0.2/\text{h}$. As exemplary cells, we choose those which have replicated half of their chromosome at the instant of the shift and were thus half-way in the C period ($s \approx 11$ of 22). In the post-shift distribution the same cells were located in a more mature stage ($s \approx 16$ of 22), due to the shifted duration of the cell-cycle periods.

The above outlined perturbation of the balanced growth distribution of maturation stages defined a perturbed post-shift distribution $F_{\text{post-shift}}$, which we used as the initial condition for eqs. (2.8)-(2.9), i.e., $F(t_0) = F_{\text{post-shift}}$. By setting $F_{\text{pre-shift}} = F_s^{\text{bg}}$ we assumed that the bacterial culture was initially in steady state age distribution. The post-shift distribution $F_{\text{post-shift}}$ was defined as follows:

$$F_{s,\text{post-shift}} = \omega_s \cdot F_{s,\text{pre-shift}}, \tag{3.21}$$

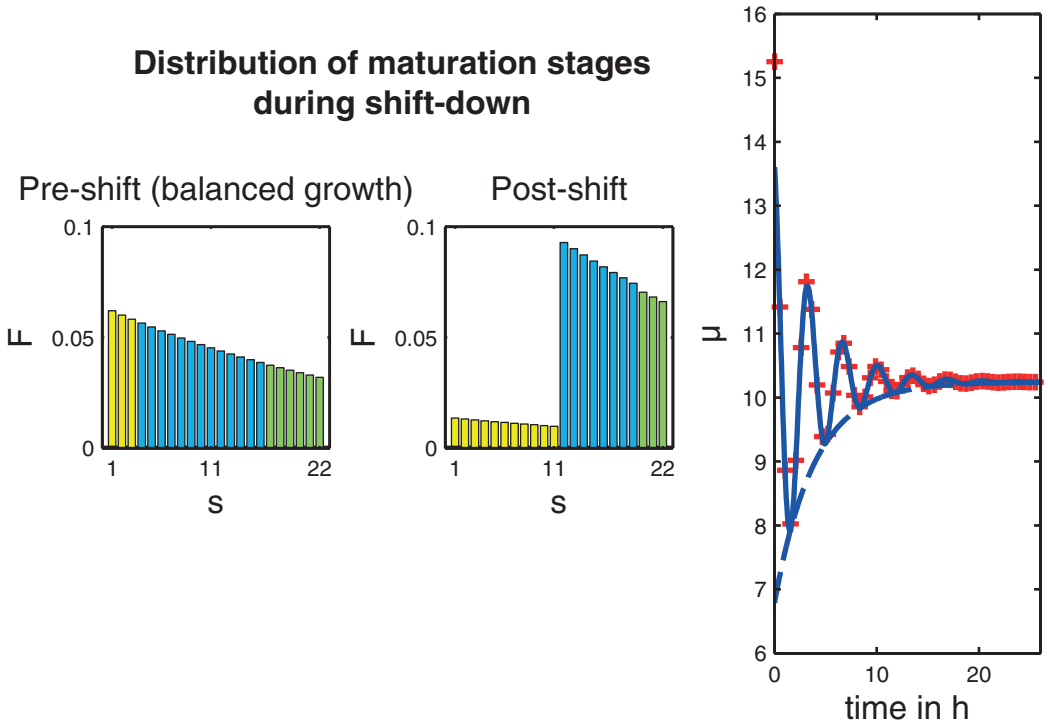

Figure 3.3: Progress of cells through the maturation cycle. Distribution of maturation stages during shift-down from pre-shift $k_{\mathrm{g}} = 0.4/\mathrm{h}$ to $k_{\text{post-shift}} = 0.2/\mathrm{h}$. Left histogram shows the normalized frequency F for each maturation stage s starting in balanced growth. Each stage is part of a cell-cycle period B (yellow), C (blue) or D (green). A shift-down lead to a temporal right-shift of this distribution, shown in the right histogram as the post-shift initial condition. Solving a system of ordinary differential equations, starting with the post-shift distribution, we determined the population mean of s—denoted by μ—over time (red crosses) which fitted a damped oscillation function (blue line). The transition rate constant λ was identified with the oscillatory damping rate constant (envelope function as dashed blue line).

where the re-weighting factor was defined as

$$\omega_s = \frac{\int_0^{B(k_\mathrm{g})} F_s^\mathrm{bg}\,\mathrm{d}s}{\int_0^{B(k_\text{post-shift})} F_s^\mathrm{bg}\,\mathrm{d}s}, \tag{3.22}$$

for all stages in the B period and analogously for $s \in C$ and $s \in D$.

Due to the discrete nature of the compartment model, a few special cases needed further specification: if no post-shift compartment was linked to the B or C period, which was the case for fast growth ($k_\text{post-shift} > 1/\mathrm{h}$) and very slow growth ($k_\text{post-shift} < 10^{-4}/\mathrm{h}$), respectively, then all pre-shift B or C period cells were transferred to the first post-shift compartment of the following period. The relative abundance of cells in the interval $[a, b]$ within one replication period $(B + C + D)$ were given by the following integral

$$\int_a^b F_s^\mathrm{bg}\,\mathrm{d}s = \frac{2q}{\log(q+1)\cdot(q+1)^{(a/(B+C+D)(m-1))+1}} \tag{3.23}$$

$$- \frac{2q}{\log(q+1)\cdot(q+1)^{(b/(B+C+D)(m-1))+1}}, \tag{3.24}$$

with $q = \sqrt[m]{2}-1$. Limits a and b were in unit min. The progress through the cell-cycle was denoted by stage s of total m stages. Hence, as before mentioned, each cell remained in its relative position *within its period*, but its overall progress changed *within the cell-cycle*, i.e., its stage relative to division.

We finally determined λ from the relaxation of the oscillating mean stage of cell-cycle progress $\mu(t) = \sum_{s=1}^{m} s \cdot F_s(t)$, as shown in Figure 3.3. The mean relative maturation stage followed a damped oscillation, described by

$$g(t) = \mu_\mathrm{ss} + a\cos(\nu \cdot t + \Phi)\exp\big((\lambda)\cdot t\big), \tag{3.25}$$

where μ_ss denoted the new stationary post-shift mean maturation stage, ν the frequency and Φ the phase shift. We estimated λ by fitting $g(t)$ to the predicted change of $\mu(t)$ over time.

As expected, the larger the variability of the doubling time τ in terms of CV, the shorter was the observed duration to reach balanced growth again. Oscillations arose from the unsteady re-entering of newborn cells into the cell-cycle until balanced growth was reached.

3.5 Summarized prototype cell-level model of bacterial population growth

In the following we summarize the detailed prototype model. The bacterial population was defined in terms of the concentrations of normal and persister cells, $n = n(t)$ and $p = p(t)$, respectively, and the growth rate constant $k_\mathrm{g} = k_\mathrm{g}(t)$. After some initial lag time, population growth was described by

$$\frac{\mathrm{d}}{\mathrm{d}t}n = \Big(k_\mathrm{g}\big(1-(n+p)/N_\mathrm{max}\big) - k_\mathrm{d}\Big)\cdot n$$

$$- k_\text{np,eff}\cdot n + k_\text{pn,eff}\cdot p \tag{3.26}$$

$$\frac{\mathrm{d}}{\mathrm{d}t}p = \; k_\text{np,eff}\cdot n - k_\text{pn,eff}\cdot p \tag{3.27}$$

$$\frac{\mathrm{d}}{\mathrm{d}t}k_\mathrm{g} = \lambda\cdot\big(k_\mathrm{g,a} - k_\mathrm{g}\big), \tag{3.28}$$

with initial values $n(0)$ and $p(0)$ resulting from eq. (3.4). We set the initial growth and death rate constants to the perturbed growth and death rate constants by $k_{\mathrm{g}}(0) = k_{\mathrm{g,p}}$ and $k_{\mathrm{d}} = k_{\mathrm{d,p}}$, according to eqs. (3.14) and (3.17). The parameters $N_{\max}$ and $k_{\mathrm{net,c}}$ were set to values as stated in the corresponding references or estimated separately. Finally, the values of λ and $k_{\mathrm{g,a}}$ were predicted using eqs. (3.12) and (3.25), respectively.

In the absence of a drug, death effects were negligible and the persister fraction could not be inferred from a growing culture. In this case, the part of our model describing the population dynamics, i.e., eqs. (3.26)-(3.28) simplified to good approximation to a logistic growth model, see eq. (2.3). The cell-cycle model described below eq. (3.19) remains compatible with this simplification as demonstrated in the prediction of septation dynamics.

3.6 Applications of the prototype model

In the following, we present results based on the prototype model. Beyond time-kill curve dynamics, we described septation dynamics and intracellular RNA mass fractions. Finally, we predicted the lag between increase in cell number and biomass.

3.6.1 Single drug time-kill curves

To study bacterial growth dynamics under antibacterial perturbations we assessed TKC experiments for different *E. coli* strains that have been exposed to static concentrations of tetracycline in several growth media.

We partitioned the data into training and test data sets. The resulting fit for the training data set is shown in Figure 3.4 A. Strain- and drug-specific parameters are summarized in Table 3.3, where *E. coli* B/r was used as a reference strain.

The parameter $\mathrm{EC50_d}$ exceeded its growth inhibiting pendant $\mathrm{EC50_g}$ by a factor of 50. This was in agreement with a high MBC/MIC ratio, which was expected for a bacteriostatic drug like tetracycline [53]. We did not observe a saturation of the killing rate even at high concentrations of tetracycline and thus fixed $\mathrm{Emax_d}$ to a high value to increase parameter identifiability. Missing saturation of the killing effect may be related to the quantification method in CFU/ml, which relied on the countable regrowth after drug removal and the resulting lower limit of quantification, see discussion on p. 77. The Hill coefficient γ_{g} was separately estimated based on data in [113] and fixed in subsequent analyses. Due to the sparse data situation for bactericidal drug concentrations, we furthermore fixed the switching rate constant $k_{\mathrm{pn,eff}}$ based on [95]. The parameter $k_{\mathrm{np,eff}}$ represented both, triggered persister formation (stationary phase and antibiotic exposure) and continuously generated non-growing cells, as a single rate constant.

We validated our predictions using data sets from experimental setups with different growth media and strains, as listed in Table 3.4. The different strains showed different sensitivities to tetracycline. Based on the validation data sets, we estimated an up to 16-fold variation in EC50 values, see experiment-specific parameters in Table 3.5. The model showed very good predictive power for all validation data sets, see Figure 3.5. For detailed information regarding strains, growth media, antibiotic concentrations, used counting techniques and duration of the experiments, see also Table 3.4.

3.6.2 Septation dynamics during shift-down

Funakoshi et al. [128] have simultaneously measured bacterial concentrations N and the fraction of septated cells f_{sep} for *B. subtilis* over time. Septated cells are cells which show signs of a binary fission, which ultimately leads to division [39]. While the bacterial

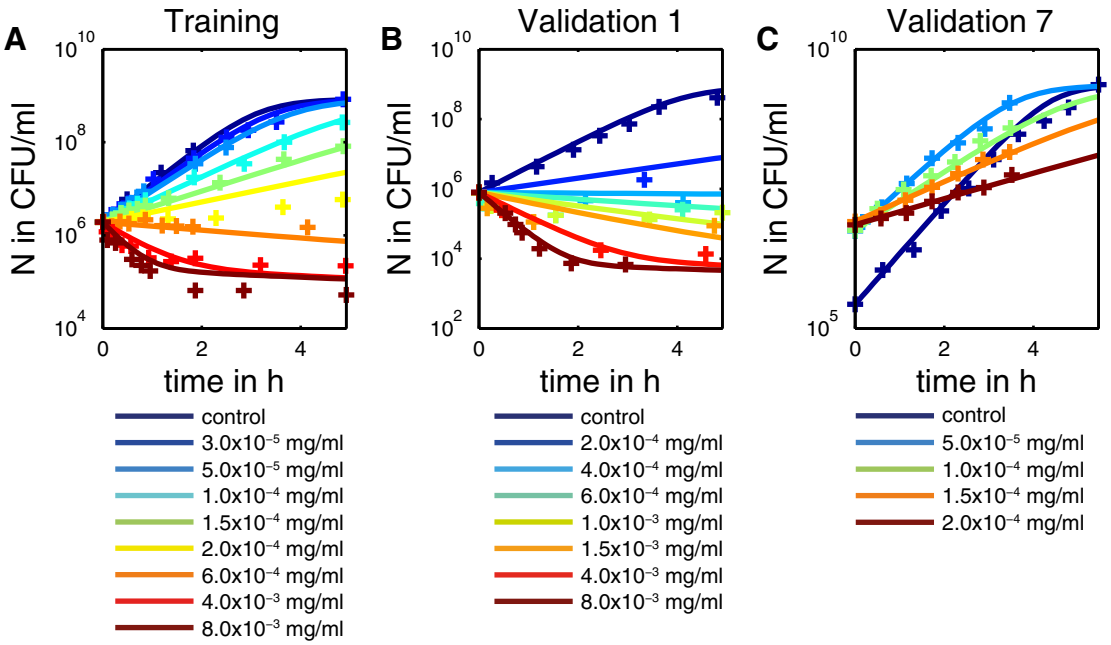

Figure 3.4: Time-kill curves (*E. coli*, TET, exp. phase, prototype model). *E. coli* B/r cells exposed to constant tetracycline concentrations. Bacterial concentrations N were measured over time (crosses) and simulated by the prototype model (solid lines). **(A)** The training data set was used to estimate the strain- and drug-specific parameters, which are summarized in Table 3.3. Experiment specific parameters were estimated individually for each data set (including validations) and are compiled in Table 3.5. For detailed information regarding the data sets, e.g., counting techniques or growth media, see Table 3.4. Exposure to bactericidal drug concentrations revealed a persisting sub-population which evaded eradication. Note that the persister related parameters were not estimated, but fixed based on literature data. **(B) & (C)** The predicted and observed time-kill curve data from validation sets 1 and 7 are shown representatively.

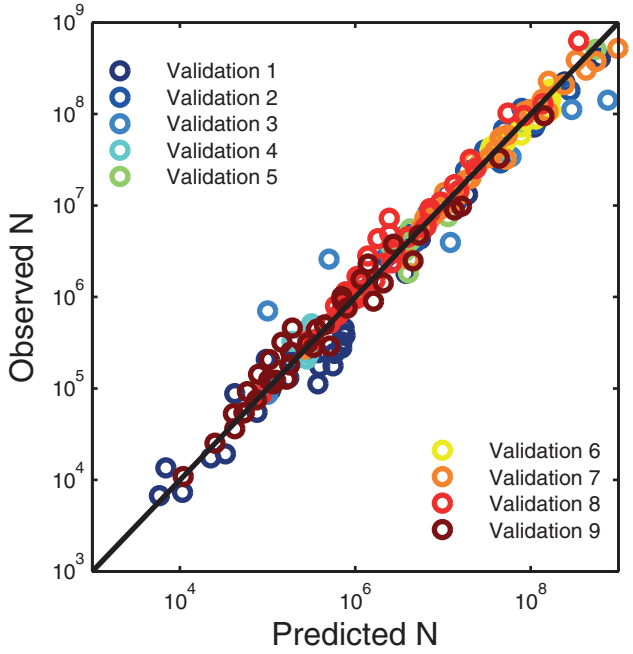

Figure 3.5: Goodness of fit plot prototype model. As validation, the detailed prototype model was evaluated with data from experiments with different *E. coli* strains and growth media, see Table 3.4. The goodness of fit plot shows the observed versus predicted bacterial concentrations N in CFU/ml. We observed excellent correlation between observations and model predictions.

Table 3.3: Strain- and drug-specific parameter estimates for the prototype model. Estimation was performed in the training dataset, where *E. coli* B/r was exposed to tetracycline.

Parameter	Unit	Comment	Value	References
$EC50_g$	mg/ml	EC50 tetracycline growth inhibition	0.0003	estimated
γ_g	-	slope factor tetracycline growth inhibition	1.42	[113]
$EC50_d$	mg/ml	EC50 tetracycline death induction	0.015	estimated
γ_d	-	slope factor tetracycline death induction	1	fixed
p_d	-	cell death per cell per generation	0.01	[109]
$k_{np,eff}$	1/h	effective switching rate constant ($n \to p$)	0.01	fixed
$k_{pn,eff}$	1/h	effective switching rate constant ($p \to n$)	0.1	[95]
$Emax_d$	1/h	Emax tetracycline death induction	10	fixed
$c_{p,max}$	aa/s	Maximum peptide chain elongation rate	28	[24, 118–120]

Table 3.4: Experimental details *E. coli* exposed to tetracycline. During the development of the prototype model, we used digitized data. The table comprises experimental methods and references to the corresponding data sources.

Dataset	Strain	Medium	Detection	Duration	Measurements	References
Training	*E. coli* B/r	Antibiotic medium 3	Viable plating	5 h	77	[121, Fig. 3]
Validation 1	*E. coli* B/r	Antibiotic medium 3	Viable plating	5 h	38	[121, Fig. 2]
Validation 2	*E. coli* B/r	Antibiotic medium 3	Viable plating	4 h	16	[122]
Validation 3	*E. coli* ATCC 25922	Mueller Hinton	Optical density	24 h	14	[123]
Validation 4	*E. coli* 51A0150	Mueller Hinton	Viable plating	24 h	8	[124]
Validation 5	*E. coli* ATCC 35218	Lysogeny broth	Viable plating	6 h	12	[125]
Validation 6	*E. coli* MG1655	Mueller Hinton	Optical density	5 h	27	[126]
Validation 7	*E. coli* B/r	Custom	Viable plating	6 h	40	[127, Fig. 4A]
Validation 8	*E. coli* B/r	Custom	Viable plating	6 h	36	[127, Fig. 4B]
Validation 9	*E. coli* B/r	Custom	Viable plating	6 h	37	[127, Fig. 4C]

Table 3.5: Experiment-specific parameter estimates for the prototype model. The listed parameter values were used to describe the listed datasets, where N_0 denoted the starting inoculum, $N_{\max}$ the carrying capacity, t_{lag} the lag time, $k_{\text{net,c}}$ the apparent control growth rate constant, f_{p} the method used to determine the initial persister fraction and SF_{EC50} was the scaling factor on EC50 values for strains other than *E. coli* B/r, which has been used in the training data set.

	Parameter values					
Dataset	N_0	$N_{\max}$	t_{lag}	$k_{\text{net,c}}$	f_{p}	SF_{EC50}
Training	1.92×10^6	8.5×10^8	0	2.0	stat.	1.0
Validation 1	7.84×10^5	8.5×10^8	0	1.7	exp.	1.0
Validation 2	1.15×10^6	10^9	0	2.6	exp.	1.0
Validation 3	10^5	3.3×10^{11}	4	2.2	exp.	16.0
Validation 4	3.16×10^5	4.7×10^9	0	1.7	exp.	10.5
Validation 5	4.23×10^6	10^{10}	0.5	2.0	exp.	3.0
Validation 6	3.53×10^7	2×10^8	2.7	1.2	exp.	5.0
Validation 7	several	2.3×10^9	0	2.1	exp.	1.0
Validation 8	several	2.3×10^9	0	2.1	exp.	1.0
Validation 9	several	2.3×10^9	0	2.0	exp.	1.0
Unit	CFU/ml	CFU/ml	h	1/h	-	-

population growth dynamics followed the typical course of a batch culture during the transition from exponential to stationary phase, the septation dynamics showed an abrupt increase in the fraction of septated cells at some time point, which we interpreted as the start of the transition process. Using only the prototype model, the time point of the start of the transition process and the population growth data, we were able to predict the septation dynamics.

By definition septated cells are in the D period, as illustrated in Figure 2.2. The solution of the logistic growth model in eq. (2.3) fitted the bacterial population dynamics. We estimated $N_0 = 1.6 \times 10^7\,\text{CFU/ml}$, $N_{\max} = 2.0 \times 10^8\,\text{CFU/ml}$ and $k_{\text{net}} = 1.10/\text{h}$. The resulting fit is shown in Figure 3.6 (A).

We determined the fraction of septated cells as $F_D = \sum_{s \in D} F_s$, where $s \in D$ denoted all indices s that corresponded to stages in the D period. Since the pre-shift distribution was determined during balanced growth, it was $k_{\text{g}} = k_{\text{net}}$ assuming that $k_{\text{d}} \ll k_{\text{g}}$. In the stationary phase, it was $k_{\text{net}} \approx 0$, implying $k_{\text{g}} \approx k_{\text{d}}$. Since the data did not allow to infer k_{d}, we assumed a physiologically-motivated range of (post-shift) growth rate constants $0.05 \leq k_{\text{post-shift}} \leq 0.1/\text{h}$. The resulting predictions are shown in Figure 3.6 (B) for five exemplary post-shift growth rates.

While the transition from exponential to stationary phase was gradual for the population dynamics, it was switch-like for the cell septation process. Our model correctly reproduced the septation dynamics without any estimation step involved. When the experiment was stopped, the fraction of septated cells was still decreasing without showing any signs of a new stationary level. Our model predicted an oscillatory approach to the new stationary level, including the steady state value itself. These oscillations resulted from replication waves, which were induced into the system by the change of growth rate—the bacterial culture became partially synchronous. To verify these predictions, one may exploit the prototype cell-level model to optimally design further experiments. From the predictions we moreover inferred that the time to reach steady state depended on the variability of the doubling time: the larger CV, the faster the steady state was reached.

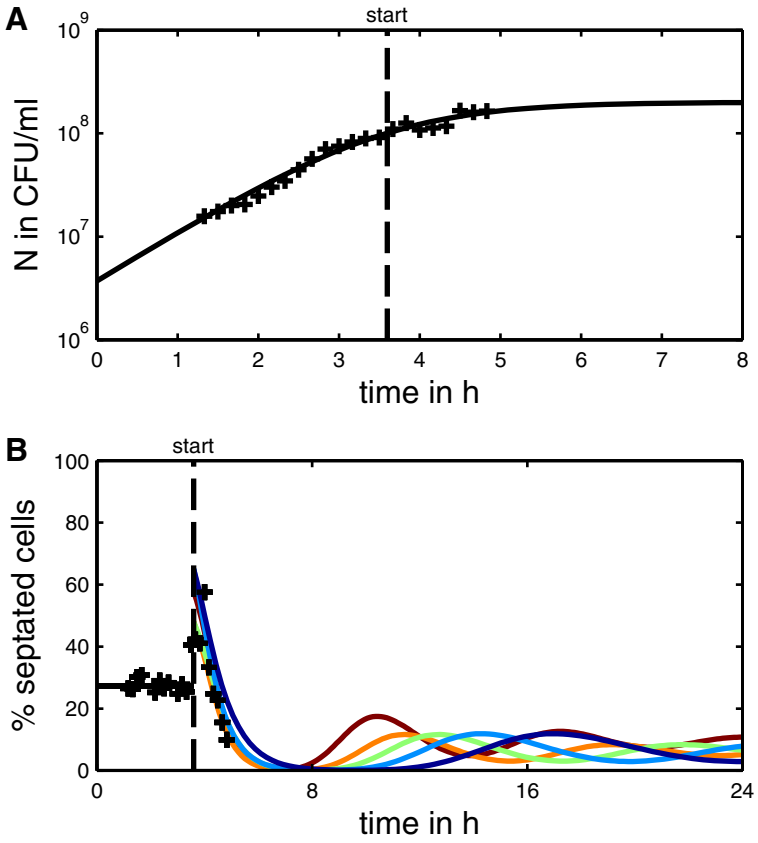

Figure 3.6: Septation dynamics. (A) Bacterial concentration N of *B. subtilis* (crosses) during transition from exponential to stationary phase. The fitted logistic growth model is shown as a black line. **(B)** Corresponding fraction of septated cells (crosses). Starting in balanced growth, the fraction of septated cells was predicted for a potential range of target growth rate constants, each as a single curve. Note that in the stationary phase, growth and death rate balanced each other. Each transition was characterized by an abrupt increase of the fraction of septated cells, which marked the start of a transition process. The extrapolation exhibited an oscillatory fade-out to a new steady state value, which was not apparent from the experimental data due to the short experimental duration.

3.6.3 Impact of antibiotic exposure on RNA mass fraction

In their innovative article on the regulation of cell-level characteristics, Scott et al. have found dramatically increased RNA mass fractions during exposure to protein biosynthesis inhibitors [44]. We challenged our model with this experimental data [44, Supplement]. In the corresponding experiments, the growth of *E. coli* B/r cells has been systematically controlled by the nutrient quality and exposure to chloramphenicol. The RNA and protein mass per cell have been quantified under balanced growth condition after prolonged drug exposure and was found to increase with drug concentration and nutrient quality. The prototype cell-level model was able to reproduce these dynamics.

In our model, the cellular RNA mass fraction $f_{\mathrm{RNA}} = R_{\mathrm{c},\mu\mathrm{g}}/P_{\mathrm{c},\mu\mathrm{g}}$ is the ratio of two cellular characteristics in the adapted cell-state. Chloramphenicol lead to a decreased fraction of active ribosomes and increased peptide chain elongation rates, as outlined in eqs. (3.15) and (3.16), respectively. The growth rate constant k_{net} decreased with increasing drug concentrations and approached static population sizes at high concentrations. This is in agreement with the bacteriostatic nature of the drug. Based on the data from [44], we estimated $\mathrm{EC50_g} = 0.0024\,\mathrm{mg/ml}$ and $\gamma_{\mathrm{g}} = 1.22$. Since reportedly only sub-lethal drug concentrations $C = 0, 0.0006, 0.0013, 0.0026$ and 0.0039 mg/ml were used [44], we assumed that death related effects on *E. coli* B/r were negligible for chloramphenicol concentrations $\mathrm{CHL} \leq 0.0039\,\mathrm{mg/ml}$. The experimental data and model predictions are shown in Figure 3.7. Across the six control experiments, f_{RNA} increased linearly with the apparent exponential growth rate $k_{\mathrm{net,c}}$ (black dashed line). In the model, this was the result of the relation between growth rate and cellular characteristics P_{c} and R_{c}. In the presence of drugs like chloramphenicol, the steepness of this linear relation changed and f_{RNA} was determined by both $k_{\mathrm{net,c}}$ and C (color coded thick lines).

The difference in f_{RNA} between the drug-perturbed and control state was maximal for nutritionally unfavorable media (small $k_{\mathrm{net,c}}$). In such media, cells are under stringent control. Therefore, the relaxation of the stringent control during the adaptation process has a marked impact on the cellular composition. This impact was a result of an increase in c_{p}. The smaller c_{p} in the control state, the more pronounced it can be adapted by the cell, up to the maximal peptide chain elongation rate $c_{\mathrm{p,max}}$ (limited by physical constraints). We estimated $c_{\mathrm{p,max}} = 28\,\mathrm{aa/s}$ per active ribosome, which is about 25% higher than the rate observed in experiments without drugs [24, 118–120] for *E. coli*. This indicated that the drug-induced translational block lead to higher translation rates of the remaining active ribosomes.

3.6.4 Lag between increase in cell number and biomass

Optical density measurements deliver fast and cheap information on the total biomass of the population—but lack information on the viable count (see Table 2.1). Colony counting fills this gap, but demands a high work load. The developed prototype cell-level model differentiated between cell number and population mass and thus linked both variables. For bacteria which have very long replication times, e.g., *Mycobacterium tuberculosis*, a lag time between an increase in cell number and in population bio-mass is potentially substantial and should be corrected for. Also the duration of the lag phase depends on the quantification method of the bacterial population size [129].

To demonstrate how a model based approach can translate between experiments with different quantification methods, we modeled a virtual experiment in which an *E. coli* B/r population was assumed to grow exponentially with $k_{\mathrm{g}} = 0.5/\mathrm{h}$. In this simulation, nutrients were added to the medium after 2 h supporting faster growth with $k_{\mathrm{g,p}} = 1.5/\mathrm{h}$. We predicted both, the change in population size N in number of cells and mass M in µg over time. To this end, we assumed the absence of a limiting carrying capacity,

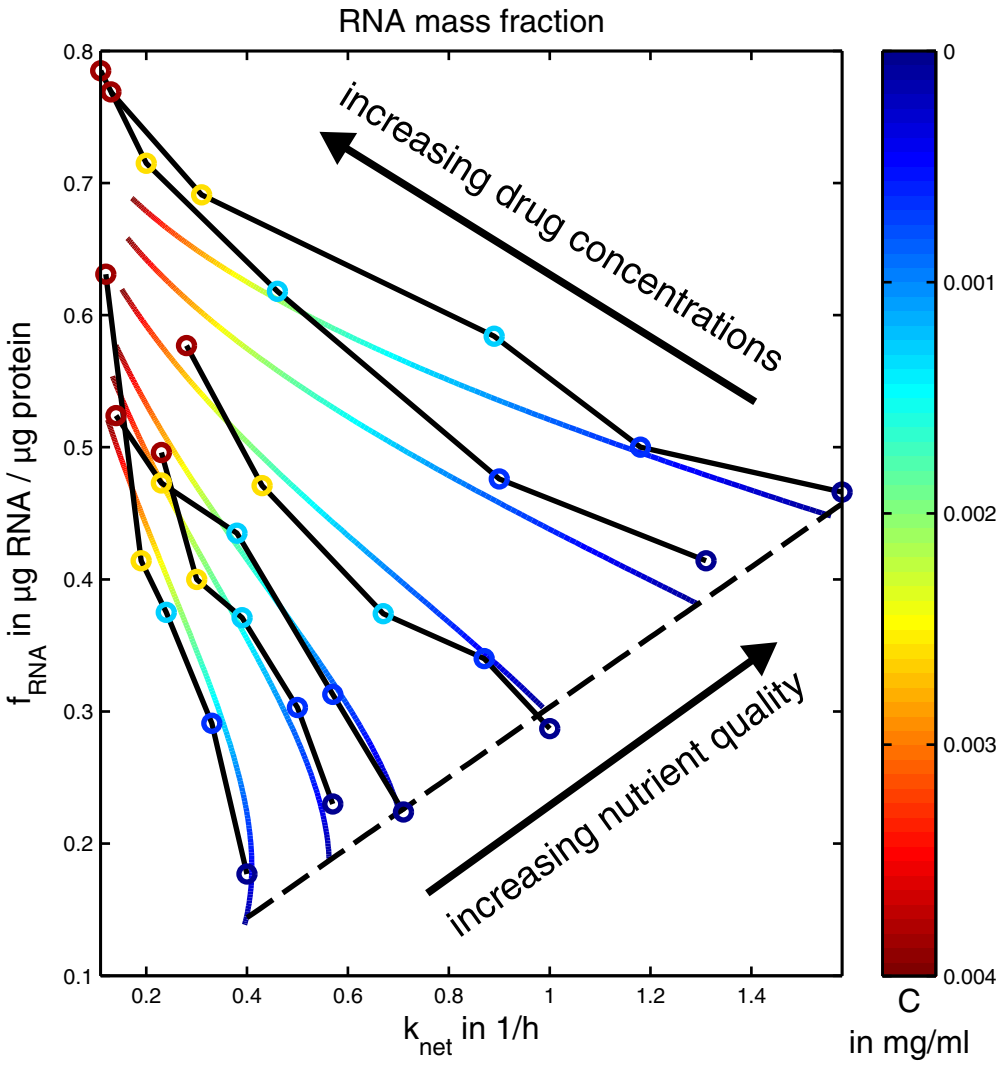

Figure 3.7: RNA mass fraction depends on growth rate and drug concentration. Bacterial cultures have been exposed to constant, sub-lethal concentrations of chloramphenicol (C) in different growth media (data from [44]). During balanced growth, the net exponential growth rate constant k_{net} and the cellular RNA mass fraction f_{RNA} have been determined. Experimental data as colored circles. Solid black lines indicate drug concentration series in the same growth medium. Thick color coded lines are predictions using the prototype model and are in good agreement with the data. The control experiments (deep blue circles) exhibited an apparently linear increase of f_{RNA} with k_{net} during exponential growth (black dashed line).

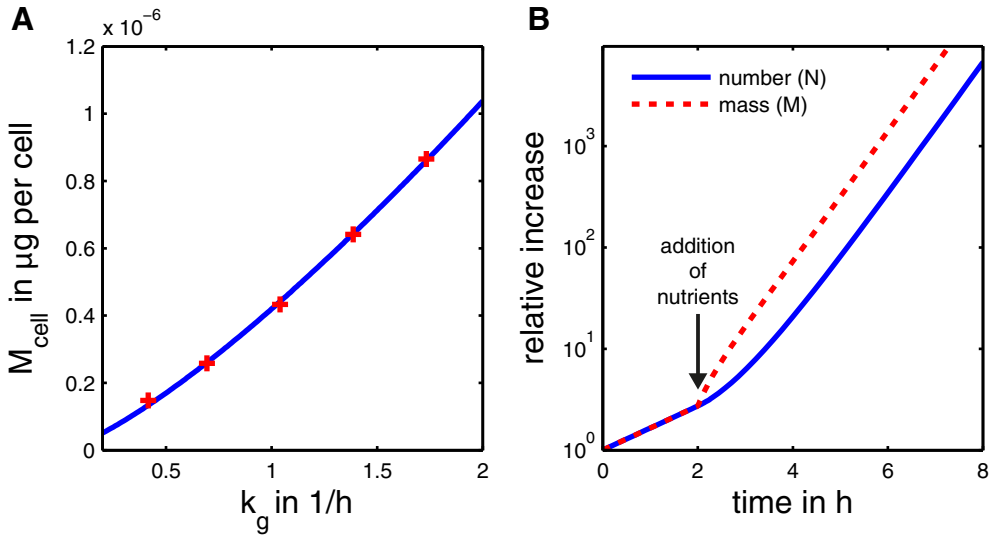

Figure 3.8: Lag time between increase in cell number and population mass. (A) Dry weight per cell M_{cell} as a function of the population growth rate k_{g}; experimental data (red crosses) and estimated power function (solid blue line). **(B)** Predicted relative increase in cell number N and population mass M over time for *E. coli* B/r in nutritional rich medium. After supplement of additional nutrients at $t = 2\,\text{h}$, the culture exhibited a lag between increase in cell number and population mass of $\approx 1\,\text{h}$.

i.e., $N \ll N_{\max}$. The population mass M was defined as the product of the dry weight of the reference cell M_{cell} (per 10^9 cells) and the bacterial concentration N, i.e., $M = N \cdot M_{\text{cell}}/10^9$. Note that since M_{cell} was in unit µg/10^9cells, it was mandatory to simulate N in unit cells rather than CFU. The change of k_{g} over time was given in eq. (3.19), with $k_{\text{g,p}}$ and $k_{\text{g,a}}$ denoting the growth rate constants before and after the modification of the growth medium. We predicted a transition rate constant of $\lambda = 0.8/\text{h}$.

Figure 3.8 B shows the relative increase in bacterial number N and population mass M for an initial inoculum size of $N(0) = 100$ cells. The increase in biomass exhibited no lag behavior, whereas the increase in cell number was delayed. We observed $\Delta t_{\text{lag}} \approx 1\,\text{h}$ between an increase in population mass $t_{\text{lag},M}$ and cell number $t_{\text{lag},N}$.

A plausible biological interpretation of this lag behavior has been presented in [30]: the increased supply of nutrients relaxed the stringent response, which first lead to increased expression of ribosomal and amino acid biosynthesis genes. For the definition of the stringent response, see the excursion on p. 19. Thus, the reference cell accumulated more ribosomes and increased in mass such that ribosomal concentrations increased, too. Secondary this lead to an accelerated cell division as cells passed cell-cycle periods faster compared to previous cycles. Eventually, the population reached balanced growth again.

3.7 Interim evaluation of the prototype model

The main advantage of the proposed model is the decomposition of parameters of different origins:

(i) strain-specific parameters

(ii) drug-specific parameters (for a given bacterial strain)

(iii) experiment-specific parameters

Consequentially, the model allowed to integrate data from different types of experiments and enabled a combined approach in a unified quantitative framework. Parameters of group (i) captured key cell-state characteristics of the reference strain and were estimated

based on literature data, see Tables 3.1 and 3.2. Additionally, this group of parameters included p_{d}, which denoted the probability of cell death per cell per generation (estimated based on data in [109]), $c_{\mathrm{p,max}}$ the maximum peptide chain elongation rate (manually inferred based on [24, 118–120]) and the switching rate constants $k_{\mathrm{np,eff}}$ (fixed based on TKC data including validation sets) and $k_{\mathrm{pn,eff}}$ (stated in [95]). Depending on the strain and parameter, individual elements of this group were representative for other bacterial strains as well: in our case, all strain-specific parameters were suitable to describe other strains in validation data sets, see Figure 3.5. Parameters of group (ii) described the perturbation of cellular characteristics by drug action and comprised the parameterization of the two Emax models ($\mathrm{EC50_g}$ (estimated on TKC data), $\mathrm{EC50_d}$ (estimated on TKC data), γ_{g} (estimated based on data from [113]), γ_{d} (fixed) and $\mathrm{Emax_d}$ (fixed)). Parameters of group (i) and (ii) are compiled in Table 3.3. Parameters of group (iii) accounted for the experimental features and comprised the maximum carrying capacity N_{max}, the lag-time t_{lag}, the control net growth rate constant $k_{\mathrm{net,c}}$, the initial inoculum N_0, and the scaling factor $\mathrm{SF_{EC50}}$, which accounted for the different drug sensitivities of the strains. The dichotomous parameter f_{p} represented the method of persister fraction initialization. Group (iii) parameters were manually inferred from the TKC data, see Table 3.5.

Overall, the parameterization included a minimal number of free parameters to be directly estimated from TKC data ($\mathrm{EC50_g}$ and $\mathrm{EC50_d}$). Accordingly, estimations were of low computational effort.

Although successful in many regards, a broader application of the prototype model was limited in a number of ways: firstly, and most important, the model required constant drug concentrations. Dynamic drug concentrations would necessitate repetitive evaluations of the perturbed and adapted cell-state at each time point, which is computationally highly inefficient. In the PKPD context this is a serious limitation. Secondly, the complexity of the model limited its applicability. While detailed data existed for *E. coli*, this is not the case for other bacteria. A reduced model—confined to parameters and a cell-state directly related to the TKC data—would allow application in less data rich situations. Thirdly, important aspects of TKC such as persistence were not or only rudimentary implemented. For example, we did not explicitly consider triggered persister formation as described in [95], because of the focus on the bacteriostatic drugs chloramphenicol and tetracycline. The persister-fraction is hardly quantifiable using viable plating or particle counting techniques in combination with bacteriostatic drugs. This is to be expected because the normal cells in a bacterial population are hardly eradicated at physiological concentrations and the detection methods quantify the total population size. An extension to more antibiotics (including bactericidal drugs like cell wall antibiotics) would allow the identification of more sophisticated mechanisms of persister formation.

The developed prototype model represents a “proof of concept” for the feasibility of a bacterial population growth model that integrates cell-level characteristics.

Chapter 4

Cell-level model for antibiotic combinations

4.1 Overcoming the limitations of the prototype model

In view of the shortcomings of the prototype model, we further developed the cell-level approach. As part of a cooperation with Prof. Charlotte Kloft and Sebastian Wicha (Department of Clinical Pharmacy and Biochemistry, Institute of Pharmacy, Freie Universität Berlin, Berlin, Germany), we obtained access to extensive *S. aureus* TKC data for vancomycin, meropenem and linezolid, including dual combinations. We focused on predicting bacterial population growth dynamics for these drug combinations and organism. We significantly reduced the cell-state complexity from 11 to 4 elements as described in "Linking the cell-state to bacterial population growth and *vice versa*" (p. 48), and implemented antibiotic drug action in "Integration of drug effects" (p. 51). This required an extension of the approach to cell wall antibiotics. Finally, in order to systematically analyze antibiotic interactions, we defined "Pharmacodynamic summary endpoints for time-kill curve data" (p. 57). The results based on this model are presented in "Model based analysis of antibiotic combinations and beyond" (p. 63).

4.2 Linking the cell-state to bacterial population growth and *vice versa*

To further develop the cell-level approach, we re-visit the work of Bremer and Dennis, on which we also based the prototype model. In their seminal work [24] Bremer and Dennis have established a quantitative relationship between the rate at which a bacterial population grows and its characteristics at the cellular level. They showed that the exponential growth rate constant can be predicted by the product of the ribosomal concentration and the ribosomal efficiency of a defined reference cell. As in [24], we defined the ribosomal concentration by

$$\mathrm{rib} = N_\mathrm{r}/P_\mathrm{c}, \tag{4.1}$$

where N_r denoted the number of ribosomes per cell in 10^3 ribosomes, and P_c the protein mass per cell in 10^8 amino acid (aa) residues. The ribosomal efficiency was defined by

$$e_\mathrm{r} = c_\mathrm{p} \cdot \beta_\mathrm{r}, \tag{4.2}$$

where c_p denoted the peptide chain elongation rate per active ribosome in aa/s, and β_r the fraction of active ribosomes. The ribosomal efficiency depended on the quality of the growth medium (quantified via the maximally supported growth rate constant in the control experiment $k_\mathrm{g,c}$), resulting in $e_\mathrm{r} = c_\mathrm{p}(k_\mathrm{g,c}) \cdot \beta_\mathrm{r}(k_\mathrm{g,c})$. Confirmed by a large body of experimental data, Bremer and Dennis [24] have established the following key relationship between the growth rate constant

$$k_\mathrm{g} = \mathrm{SF} \cdot \mathrm{rib} \cdot e_\mathrm{r}, \tag{4.3}$$

in 1/h and the cell-state, with SF = 0.036 in 10^5 s/h accounting for a conversion of units. Based on eqs. (4.1)-(4.3), we defined the cell-state

$$S = S_{i=1\ldots4} = (N_\mathrm{r}, P_\mathrm{c}, c_\mathrm{p}, \beta_\mathrm{r}) \tag{4.4}$$

that collected the key cellular characteristics to predict the growth rate constant of a bacterial population. Note that compared to the previously defined cell-state for the prototype model in (3.9), this considerably reduced the number of elements of the cell-state from 11 to 4. Schaechter et al. demonstrated in [46] for a variety of different growth media that cellular characteristics can be predicted by the bacterial population growth rate constant k_g, i.e, $N_\mathrm{r} = N_\mathrm{r}(k_\mathrm{g})$, $P_\mathrm{c} = P_\mathrm{c}(k_\mathrm{g})$ and $c_\mathrm{p} = c_\mathrm{p}(k_\mathrm{g})$. This relationship has been

applied in numerous modeling approaches [24, 44, 130] and was used here to determine the ribosomal concentration in control experiments during exponential, i.e., balanced growth based on

$$\mathrm{rib_c} = N_\mathrm{r}(k_\mathrm{g,c})/P_\mathrm{c}(k_\mathrm{g,c}). \tag{4.5}$$

We utilized data from [24, 47, 48] describing a reference cell of approximately mean maturation, see excursion on p. 14. Figure 2.3 depicts the corresponding growth rate dependency of the cell-state for *E. coli* B/r and *S. aureus* MF32. For the parameterization of the power functions, see Table 3.1. These power functions, combined with eq. (4.3), allowed to switch between the population growth rate constant and the cell-state, which is a key element of the cell-level bacterial population growth model.

A shortcoming of the prototype model was the lack of a time-continuous representation of the cell-state. To overcome this limitation, we defined a corresponding equation describing the rate of change of the cell-state over time. Active ribosomal RNA degradation was found to be negligible during exponential growth [34, 131]. Thus, we assumed that the rate of change of the ribosomal concentration was solely determined by ribosomal synthesis with rate constant $k_\mathrm{syn,rib}$ and dilution due to cell growth with rate constant k_dil. Assuming that ribosomal RNA degradation was negligible in all growth phases, it followed that

$$\frac{\mathrm{d}}{\mathrm{d}t}\mathrm{rib} = k_\mathrm{syn,rib} - k_\mathrm{dil} \cdot \mathrm{rib}, \tag{4.6}$$

with $k_\mathrm{dil} = k_\mathrm{g}$. By definition, the ribosomal concentration is time-invariant during balanced growth ($\mathrm{d\,rib}/\mathrm{d}\,t = 0$). Exploitation of the balance between ribosomal synthesis and dilution in eq. (4.6) resulted in

$$k_\mathrm{syn,rib} = k_\mathrm{g} \cdot \mathrm{rib_c}, \tag{4.7}$$

with $\mathrm{rib_c}$ defined in (4.5). This allowed to infer the ribosomal synthesis rate constant from the control experiment.

Time-kill curve experiments show remarkable differences in population growth dynamics depending on the experimental protocol. In particular, as it has been demonstrated in [16] that large differences resulted from the choice whether the culture started in lag or exponential phase. Increased ribosome synthesis has been described as a hallmark characteristic of the transition of a bacterial culture from lag into exponential growth phase [30, 31]. To account for ribosomal dynamics in a bacterial population growth model, we described the rate of change of the total bacterial concentration $N = N(t)$ by the following system of equations

$$\frac{\mathrm{d}}{\mathrm{d}t}N = k_\mathrm{g} \cdot N \tag{4.8}$$

$$k_\mathrm{g} = \mathrm{SF} \cdot \mathrm{rib} \cdot c_\mathrm{p} \cdot \beta_\mathrm{r} \tag{4.9}$$

$$\frac{\mathrm{d}}{\mathrm{d}t}\mathrm{rib} = k_\mathrm{syn,rib} - k_\mathrm{g} \cdot \mathrm{rib} = k_\mathrm{g} \cdot \big(\mathrm{rib_c} - \mathrm{rib}\big), \tag{4.10}$$

with $\mathrm{SF} = 0.036$ in $10^5\,\mathrm{s/h}$ accounting for a conversion of units. The above cell-level bacterial population growth model explicitly accounted for the dependence of $k_\mathrm{g} = k_\mathrm{g}(t)$ on the ribosomal concentration $\mathrm{rib} = \mathrm{rib}(t)$, which in turn was influenced by the initial ribosomal concentration $\mathrm{rib}(0) = \mathrm{rib_0}$ and the growth medium (via $\mathrm{rib_c}$). To explicitly differentiate between lag and exponential phase experiments, we choose

$$\mathrm{rib_0} = \begin{cases} \mathrm{rib_c} & \text{for experiments starting in exponential phase} \\ \mathrm{rib_{0,lag}} & \text{for experiments starting in lag phase.} \end{cases} \tag{4.11}$$

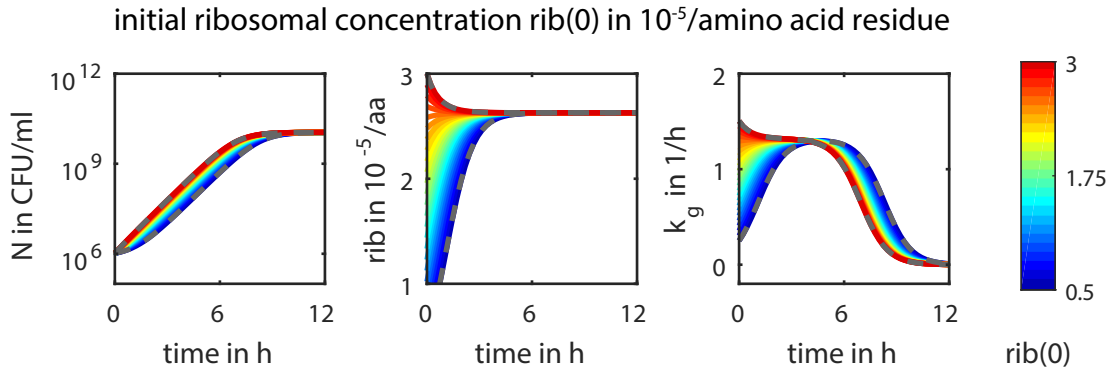

Figure 4.1: Sensitivity of lag phase duration to initial ribosomal concentration. Dynamics of total bacterial concentration N, intracellular ribosomal concentration rib and growth rate constant k_g depending on the initial ribosomal concentration rib(0). As can be seen from the bacterial population growth dynamics, the initial ribosomal concentration determined the duration of the lag phase. Over time rib approached rib_c, which is the predicted ribosomal concentration in balanced growth. The range of simulation results is marked by gray dashed lines. Simulations based on lag phase *S. aureus* cultures in drug-free growth media without persisters. Remaining parameters as in Tables 6.1 and 6.2.

Since $\text{rib}_{0,\text{lag}}$ was unknown, it was estimated from the TKC data. Thereby we assumed that the initial ribosomal concentration and the quality of the growth medium were the main determinants of the lag. The quality of the growth medium was represented in the model by the estimated control growth rate constant $k_{g,c}$ and determined rib_c via eqs. (4.5) and (4.10). The sensitivity of the model predictions with respect to the rib_0 estimate is visualized in Figure 4.1. The figure demonstrates that the time-kill curve dynamics can be used to inform the rib_0 estimate.

To account for antibiotic tolerant sub-populations, we considered two different cell-types: normal cells with concentration $n = n(t)$ and non-growing, yet viable persister cells with concentration $p = p(t)$. Hence,

$$N = n + p. \tag{4.12}$$

In contrast to normal cells, which grow and are effected by antibiotics, persister cells exhibit antibiotic tolerance and reversible dormancy as described in "Persistence" (p. 24).

While antibiotic induced death effects can be significant, we assumed non-antibiotic induced death effects to be negligible. In *E. coli*, e.g., non-antibiotic induced death effects have been described as relatively low [109] with death rate constant $k_d \approx 0.01 \cdot k_g$. To account for the transition into stationary phase, we used the logistic term introduced in eq. (2.3). In the absence of antibiotics, the following system of differential equations described the sub-population dynamics

$$\frac{\mathrm{d}}{\mathrm{d}t}n = (k_g - k_d) \cdot n - k_{np,\text{eff}} \cdot n + k_{pn,\text{eff}} \cdot p \tag{4.13}$$

$$\frac{\mathrm{d}}{\mathrm{d}t}p = k_{np,\text{eff}} \cdot n - k_{pn,\text{eff}} \cdot p \tag{4.14}$$

$$k_g = \text{SF} \cdot \text{rib} \cdot c_p \cdot \beta_r \cdot \big(1 - (n+p)/N_{\max}\big) \tag{4.15}$$

$$\frac{\mathrm{d}}{\mathrm{d}t}\text{rib} = k_g \cdot (\text{rib}_c - \text{rib}), \tag{4.16}$$

with $\text{SF} = 0.036$ in $10^5\,\text{s/h}$ accounting for a conversion of units. Bacterial growth was limited by a carrying capacity $N_{\max}$, representing nutrient and space limitations. We used the common [89] assumption that the effective rate of persister formation is proportional to the logistic term, i.e., $k_{np,\text{eff}} = k_{np} \cdot (n+p)/N_{\max}$. Based on the observation that

persisters are more abundant in slowly growing or growth arrested cultures [98], this assumption seemed legitimate. The parameter k_{np} quantified switching from the growing to the persisting state during stationary phase. Switching back from persisting to growing state was described by the effective switching rate constant $k_{\mathrm{pn,eff}} = k_{\mathrm{pn}}$. Antibiotics may impact both, the rate of persister formation and re-entering into the growing state [100]. The initial values of normal and persister cells were parameterized by the persister fraction f_{p} with $n(0) = (1 - f_{\mathrm{p}}) \cdot N(0)$ and $p(0) = f_{\mathrm{p}} \cdot N(0)$, respectively. Since normal cells largely out-compete persisters in the exponential phase, as shown in Fig. 3.2, we assumed that the persister fraction was negligible for experiments starting in the exponential growth phase

$$f_{\mathrm{p}} = \begin{cases} 0 & \text{for experiments starting in exponential phase} \\ f_{\mathrm{p,lag}} & \text{for experiments starting in lag phase.} \end{cases} \tag{4.17}$$

Since $f_{\mathrm{p,lag}}$ was in general unknown, it was estimated from the data.

4.3 Integration of drug effects

Antibiotics perturb bacterial growth by interfering with growth and/or death related processes. In the following, we describe how we implemented the drug action for the antibiotics tetracycline, vancomycin, meropenem and linezolid. The cell-state of the cell-level model for antibiotic combinations allows for a cell-level integration of drug action of protein biosynthesis inhibitors like tetracycline and linezolid. Drug effects of cell-wall active antibiotics vancomycin and meropenem were integrated empirically on the population level because the cell-state excluded characteristics describing the bacterial cell wall. On many occasions we linked an antibiotic drug concentration C to a corresponding effect E by the sigmoidal Emax model described in eq. (2.13) using the corresponding notation.

4.3.1 Tetracycline

The total extracellular concentration of the protein biosynthesis inhibitor tetracycline was denoted by TET. In the following, we define tetracycline related growth and death effects. Furthermore, the model allowed to estimate the drug effects on the persister dynamics.

Supported by our TKC data, we assumed that tetracycline induces a death effect $E = E_{\mathrm{TET,d}}$ resulting in

$$k_{\mathrm{d}} = E_{\mathrm{TET,d}}. \tag{4.18}$$

Tetracycline has been described to exert a growth inhibiting effect by reducing the fraction of active ribosomes [56]. In our model, the fraction of active ribosomes was termed β_{r}. We accounted for the reduced fraction of active ribosomes with effect $E = E_{\mathrm{TET,g}}$ on β_{r}, resulting in a reduction of the growth rate

$$k_{\mathrm{g}} = \mathrm{SF} \cdot \mathrm{rib} \cdot c_{\mathrm{p}} \cdot \beta_{\mathrm{r}}(1 - E_{\mathrm{TET,g}}), \tag{4.19}$$

with $\mathrm{SF} = 0.036$ in 10^5 s/h accounting for a conversion of units. Both effects require the binding of tetracycline to the ribosomes [56], such that $C = \mathrm{TET} \cdot \mathrm{rib}$ was the effector species. We normalized the effector species by $\mathrm{rib_c}$ resulting in

$$C = \mathrm{TET} \cdot \mathrm{rib}/\mathrm{rib_c}. \tag{4.20}$$

Thus, the estimated EC50 values had units mg/l and were with reference to balanced growth (where $C = \mathrm{TET}$). This normalization of the effector species is equivalent to scaling the potency parameters $\mathrm{EC50_{TET,g}}$ and $\mathrm{EC50_{TET,d}}$ by the dimensionless factor $\mathrm{rib_c}/\mathrm{rib}$. We accounted for drug induced modification of the persister formation via

$$k_{\mathrm{np,eff}} = k_{\mathrm{np}} \cdot (1 + E_{\mathrm{TET,p}}). \tag{4.21}$$

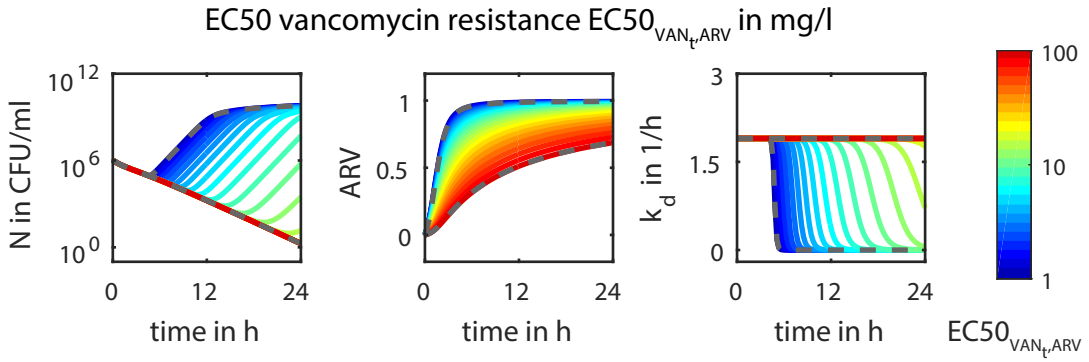

Figure 4.2: Sensitivity of resistance development to corresponding EC50 value. Dynamics of bacterial concentration N, adaptive resistance against vancomycin ARV and death rate constant k_d depending on the onset of adaptive resistance development (quantified by $\mathrm{EC50}_{\mathrm{VAN_t,ARV}}$). The range of simulation results is marked by gray dashed lines. Simulations based on lag phase *S. aureus* cultures exposed to vancomycin $\mathrm{VAN}(0) = 8\,\mathrm{mg/l}$. Remaining parameters as in Tables 6.1 and 6.2. ARV in unit fractional immunity.

Since switching back to normal state depends on the synthesis of key proteins (e.g., antitoxins in *E. coli* [97]), the corresponding switching rate constant

$$k_{\mathrm{pn,eff}} = k_{\mathrm{pn}} \cdot (1 - E_{\mathrm{LZD,g}}) \tag{4.22}$$

was also effected by the growth-inhibiting effect of the protein biosynthesis inhibitor tetracycline. The model accounted for a decay of the extra-cellular drug concentration by a first order process with rate constant $k_{\mathrm{deg,TET}}$.

4.3.2 Vancomycin

Vancomycin prevents the cross-linking of growing peptidoglycan strands and had thus to reach the proximal inner regions of the cell wall for causing lethal cell wall damage. We observed regrowth in TKC where vancomycin was used alone or in combination with meropenem. The developed model accounted for vancomycin related cell death and the development of adaptive resistance, see eqs. (2.14) and (2.15).

An increased cell wall thickness has been reported in [132] for vancomycin intermediate resistant *S. aureus* strains (such as the used ATCC 29123 [133]), which linearly correlated with the minimal inhibitory concentration for vancomycin [134]. A plausible mechanism for this morphological adaptation is an overproduction of false target structures which leads to a binding of vancomycin molecules in the non-critical distal regions of the cell wall [135].

In our model, the vancomycin concentration at the target site

$$\mathrm{VAN_t} = \mathrm{VAN} \cdot (1 - \mathrm{ARV}) \tag{4.23}$$

was expressed as a fraction of the total extracellular concentration $\mathrm{VAN} = \mathrm{VAN}(t)$. Increasing wall thickness conferred adaptive resistance against vancomycin $\mathrm{ARV} = \mathrm{ARV}(t)$ with $0 \leq \mathrm{ARV} \leq \mathrm{ARV_{max}}$. The impaired diffusion of the drug to the target site was the mechanism of resistance. The maximum adaptive resistance against vancomycin was denoted by $\mathrm{ARV_{max}}$, where the maximum $\mathrm{ARV_{max}} = 1$ confers total immunity against the antibiotic and the minimum $\mathrm{ARV_{max}} = 0$ represents normal sensitivity.

It turned out that the data did not allow to infer a maximum adaptive resistance against vancomycin (likelihood profiling as described in [136]). In agreement with the data, we set the corresponding parameters to $\mathrm{ARV_{max}} = 1$. The impact of this fixation is shown in Figure 4.2. The adaptive resistance ARV approaches one inevitably, i.e.,

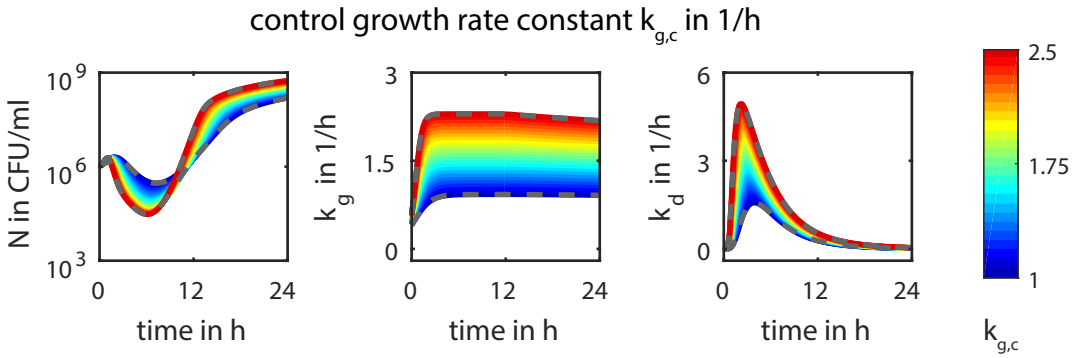

Figure 4.3: Sensitivity of meropenem killing to growth medium. Dynamics of bacterial concentration N, growth rate constant k_g and death rate constant k_d depending on the growth medium (quantified in the cell-level model for antibiotic combinations as control growth rate constant $k_\mathrm{g,c}$). Meropenem killing critically depends on growing cells as indicated by the change of nadir in $N(t)$ and maximum of $k_\mathrm{d}(t)$. The decreased killing after 6 h is related to the development of adaptive resistance against meropenem (ARM, not shown). The range of simulation results is marked by gray dashed lines. Simulations based on lag phase *S. aureus* cultures exposed to meropenem MER(0) = 0.0625 mg/l. Remaining parameters as in Tables 6.1 and 6.2.

drug concentration independent. Accordingly, simulations for vancomycin concentrations far beyond the tested concentration range will predict regrowth at some (very late) time point.

The mechanisms driving the increasing cell wall thickness during exposure to vancomycin include selection and metabolic adaption [134]. We represented the effect of vancomycin blocking the cellular disposition of itself with $E_{\mathrm{VAN_t,ARV}}$, which was linked to $\mathrm{VAN_t}$. In view of the faster adaptive resistance development in experiments starting in exponential phase, we empirically scaled the extent of the effect by k_g and $\mathrm{rib}/\mathrm{rib_c}$, see eq. (A.18). The dynamics of adaptive resistance development against vancomycin were described in eq. (4.33) and visualized in Figure 4.2. The vancomycin related death effect was accounted for via $k_\mathrm{d} = E_{\mathrm{VAN_t,d}}$, see eq. (A.17). The effect of vancomycin on the persister formation was quantified in $E_{\mathrm{VAN,p}}$, see eq. (A.19).

4.3.3 Meropenem

For meropenem, we observed following four effects experimentally: regrowth, auto inhibition, death induction and increased persister formation. We accounted for all of them in the model. Since the cellular disposition of the drug was reported [1] to be closely linked to the development of drug resistance, we explicitly modeled the meropenem concentration at the target site ($\mathrm{MER_t}$). The target site is localized at the outer surface of the cytoplasmic membrane and inside the cellular splitting system [137] where the targeted penicillin binding proteins are located [50, 138]. The peripheral cell wall separates this space from the growth medium. We denoted the total meropenem concentration in the growth medium with $\mathrm{MER} = \mathrm{MER}(t)$. We assumed a fast equilibrium

$$\mathrm{MER_t} = \mathrm{MER} \cdot (1 - \mathrm{ARM}), \tag{4.24}$$

where ARM summarized factors impairing the effectiveness of the antibiotic against normal cells in form of adaptive resistance against meropenem with $\mathrm{ARM} = \mathrm{ARM}(t)$ and $0 \leq \mathrm{ARM} \leq \mathrm{ARM_{max}}$.

For the dynamics of adaptive resistance development against meropenem, we applied the same methodology as for vancomycin with the same limitations with respect to the non-identifiability of the estimate for maximum adaptive resistance. As for vancomycin, the adaptive resistance against meropenem is related to the cellular disposition of the drug.

For meropenem, several cellular mechanisms lead to adaptive resistance development: (i) decreased influx, (ii) modification of target PBPs, (iii) induction of beta-lactamases (iv) increased efflux.

To answer the question which of the mechanisms is relevant for the experiments with *S. aureus* ATCC 29213, we discuss each of them in detail. We ruled out mechanism (i) since gram positive bacteria like *S. aureus* lack an outer membrane. The over-expression of selective porins is known for gram negative bacteria only. Mechanism (ii) typically confers high level beta-lactam resistance (MRSA) from the acquisition of the mecA gene [139, 140], which encodes for a modified target structure. ATCC 29213 is MSSA and has been reported to be mecA negative [86]. Meropenem is substrate only for a few of the hundreds of currently known beta-lactamases [76], where predominantly extended spectrum beta-lactamases, carbapenemase and metallo beta-lactamases show activity. Although *S. aureus* ATCC 29213 is beta-lactamase positive [133], it has weak activity of those beta-lactamases [86]. If (iii) would be true, one would expect the addition of ATCC 29213 cells to increase the extracellular degradation rate of meropenem—also because of the lytic activity of the drug [141], which would release the beta-lactamases from the periplasm to the growth medium. In growth medium comprising a growing bacterial culture, a degradation rate constant $k_{\mathrm{deg,MER}} = 0.0144/\mathrm{h}$ has been measured [142] in comparison to $k_{\mathrm{deg,MER}} = 0.0190/\mathrm{h}$, which has been determined in sterile growth medium [16]. Thus, the bacterium induced degradation was negligible (for tested inoculation sizes). This result has also been confirmed in [143], where no significant increase in degradation rate was observed for non-sterile compared to sterile growth medium. Regarding mechanism (iv): efflux pumps which are expressed in *S. aureus* include AbcA, which has medium affinity to hydrophilic drugs like meropenem [144] and no affinity to vancomycin [145]. The regulation of such efflux pumps has been described to depend on drug exposure [146]. All in all, we expect mechanism (iv) to be the dominant mechanism conferring adaptive resistance against meropenem for this strain. Yet, only additional experiments including a precise quantification of meropenem in the growth medium could ultimately differentiate between mechanism (iii) and (iv).

We observed in the TKC data that the onset of meropenem killing and development of resistance was delayed with respect to the time point when the drug was added. We assumed that the development of meropenem resistance is a delayed, time dependent process. Microscopic observation studies showed that beta-lactam killing is typically delayed between one or two doubling times [138]. Accordingly, we assumed that cells with a faster metabolism (in terms of growth rate constant) had shorter response times with respect to meropenem effects. Therefore, we introduced a growth depending effector species for meropenem, termed eMER = eMER(t), which accounted for the delay of all meropenem effects. The rate of change of this species is described in eq. (4.35).

For the induction of adaptive resistance via the corresponding effect $E_{\mathrm{MER,ARM}}$, see eq. (A.22). The differential equation eq. (4.34) defines the transition of the bacterial population from meropenem sensitivity to resistance.

With respect to a mechanistic representation of the meropenem related death effects, we investigated the key mechanism causing the staphylococcal cell death during exposure to the beta-lactam antibiotic meropenem. According to [138], the death effect was a growth dependent lytic process involving a fatal placement of so-called *murosomes* during the replication cycle. Thus, $E_{\mathrm{eMER,d}}$ was linked to the delayed effector species eMER and its extent was scaled by the growth rate constant k_{g}, see eq. (A.20).

The delay of the meropenem effector species, as well as, the meropenem related death effect depend on the growth rate constant. As a consequence, the growth medium directly influences the TKC dynamics for meropenem. This influence is visualized in Figure 4.3. If a medium supports fast growth, it also results in a pronounced killing effect of meropenem.

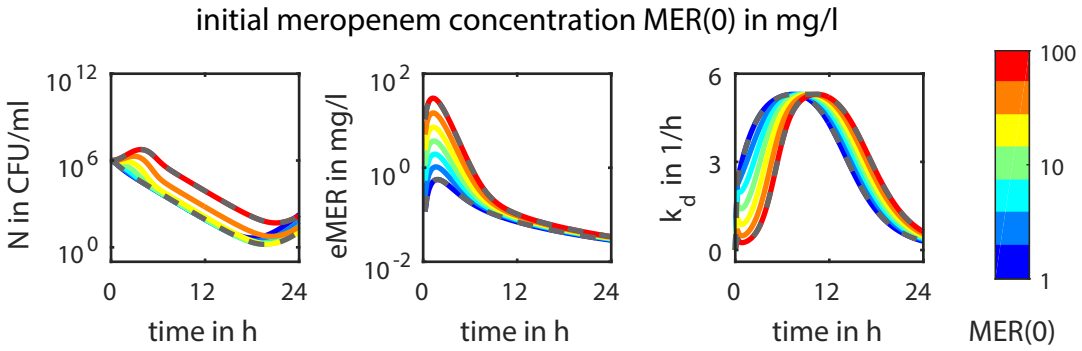

Figure 4.4: Sensitivity of the Eagle effect to meropenem exposure. Dynamics of bacterial concentration N, meropenem effector species eMER and death rate constant k_d depending on the initial meropenem concentration MER(0). The paradoxically reduced killing of beta-lactams at highest concentrations is known as the Eagle effect. The range of simulation results is marked by gray dashed lines. Simulations based on lag phase *S. aureus* cultures. Remaining parameters as in Tables 6.1 and 6.2.

For beta-lactams the so-called *Eagle effect* is reported [147]: high antibiotic concentrations can result in a reduced killing activity compared to medium-high concentrations. We also observed this effect in the TKC data where *S. aureus* was exposed to meropenem, see Figure 6.1 (G,I), (H,J). We accounted for the Eagle effect in the characterization of the death rate constant for meropenem $k_\mathrm{d} = E_{\mathrm{eMER,d}}(1 - E_{\mathrm{MER_t,E}})$ by introducing the self-inhibitory effect $E_{\mathrm{MER_t,E}}$ in eq. (A.21). For an explanation of the Eagle effect, see corresponding paragraph in "Model based analysis of antibiotic combinations and beyond" (p. 63). The effect of meropenem on the persister formation was quantified by $E_{\mathrm{MER,p}}$, as defined in eq. (A.23). Since we did not observe a saturation of the Eagle effect the Emax model was not fully identifiable. We resolved the identifiability problem by setting $\mathrm{Emax}_{\mathrm{eMER,E}} = 1$. Accordingly, extrapolation far beyond the tested concentrations (e.g., $\mathrm{MER}(0) > 100\,\mathrm{mg/l}$) are not supported by the current parameter values of the model. The impact of the Eagle effect on meropenem drug action was demonstrated in Figure 4.4 for a range of meropenem concentrations.

4.3.4 Linezolid

Linezolid and tetracycline show similarities with respect to their mechanism of drug action because both drugs inhibit protein biosynthesis by targeting the ribosomes, as described on p. 20. Accordingly the implementations of both drugs were similar in our cell-level approach. Therefore we keep the following description of the implementation of linezolid short. For a detailed description, see "Tetracycline" (p. 51). We accounted for linezolid induced growth inhibition, death induction and persister formation.

The growth inhibiting effect of linezolid was modeled as a lowered fraction of active ribosomes, as reported in [56]. An inhibition term was added to eq. (4.3). Thereby linezolid effected growth indirectly via

$$k_\mathrm{g} = \mathrm{SF} \cdot \mathrm{rib} \cdot c_\mathrm{p} \cdot \beta_\mathrm{r}(1 - E_{\mathrm{LZD,g}}), \tag{4.25}$$

where $\mathrm{SF} = 0.036$ in unit $10^5\,\mathrm{s/h}$ accounted for a conversion of units. Beyond growth inhibition, linezolid also exerted bactericidal drug action $k_\mathrm{d} = E_{\mathrm{LZD,d}}$, see eq. (A.25). Linezolid effects originate from a drug–ribosome complex [56] and we scaled the sensitivity parameters $\mathrm{EC50}_{\mathrm{LZD,g}}$ and $\mathrm{EC50}_{\mathrm{LZD,d}}$ accordingly. Furthermore, linezolid modified the persister formation via $E_{\mathrm{LZD,p}}$, see eq. (A.26). As a protein biosynthesis inhibitor, linezolid inhibited the switching back from persisting to growing state ($E_{\mathrm{LZD,g}}$, see eq. (A.24)) by modulation of the effective switching rate constant $k_{\mathrm{pn,eff}} = k_\mathrm{pn}(1 - E_{\mathrm{LZD,g}})$.

4.4 Cell-level model of bacterial population growth for antibiotic combinations

We summarize the introduced model components in a comprehensive system of ODEs including drug effects for tetracycline, vancomycin, meropnem and linezolid. Again, we use the nomenclature introduced below eq. (2.13) for the drug effects $E = E_{\mathrm{Abc,Xyz}}$, resulting in

$$\frac{\mathrm{d}}{\mathrm{d}t}n = (k_\mathrm{g} - k_\mathrm{d}) \cdot n - k_\mathrm{np,eff} \cdot n + k_\mathrm{pn,eff} \cdot p \tag{4.26}$$

$$\frac{\mathrm{d}}{\mathrm{d}t}p = k_\mathrm{np,eff} \cdot n - k_\mathrm{pn,eff} \cdot p \tag{4.27}$$

$$k_\mathrm{g} = \mathrm{SF} \cdot \mathrm{rib} \cdot c_\mathrm{p} \cdot \beta_\mathrm{r}(1 - E_\mathrm{TET,g})(1 - E_\mathrm{LZD,g}) \cdot \big(1 - (n+p)/N_\mathrm{max}\big) \tag{4.28}$$

$$k_\mathrm{d} = E_\mathrm{TET,d} + E_\mathrm{VAN_t,d} + E_\mathrm{eMER,d}(1 - E_\mathrm{eMER,E}) + E_\mathrm{LZD,d} \tag{4.29}$$

$$k_\mathrm{np,eff} = k_\mathrm{np} \cdot (1 + E_\mathrm{TET,p}) \cdot (1 + E_\mathrm{VAN,p}) \cdot (1 + E_\mathrm{MER,p}) \cdot (1 + E_\mathrm{LZD,p}) \cdot (n+p)/N_\mathrm{max} \tag{4.30}$$

$$k_\mathrm{pn,eff} = k_\mathrm{pn} \cdot (1 - E_\mathrm{TET,g}) \cdot (1 - E_\mathrm{LZD,g}) \tag{4.31}$$

$$\frac{\mathrm{d}}{\mathrm{d}t}\mathrm{rib} = k_\mathrm{g} \cdot (\mathrm{rib_c} - \mathrm{rib}) \tag{4.32}$$

$$\frac{\mathrm{d}}{\mathrm{d}t}\mathrm{ARV} = E_\mathrm{VAN_t,ARV} \cdot (\mathrm{ARV_{max}} - \mathrm{ARV}) \tag{4.33}$$

$$\frac{\mathrm{d}}{\mathrm{d}t}\mathrm{ARM} = E_\mathrm{eMER,ARM} \cdot (\mathrm{ARM_{max}} - \mathrm{ARM}) \tag{4.34}$$

$$\frac{\mathrm{d}}{\mathrm{d}t}\mathrm{eMER} = k_\mathrm{g} \cdot \big(\mathrm{MER} \cdot (1 - \mathrm{ARM}) - \mathrm{eMER}\big) \tag{4.35}$$

$$\frac{\mathrm{d}}{\mathrm{d}t}\mathrm{TET} = -k_\mathrm{deg,TET} \cdot \mathrm{TET} \tag{4.36}$$

$$\frac{\mathrm{d}}{\mathrm{d}t}\mathrm{VAN} = -k_\mathrm{deg,VAN} \cdot \mathrm{VAN} \tag{4.37}$$

$$\frac{\mathrm{d}}{\mathrm{d}t}\mathrm{MER} = -k_\mathrm{deg,MER} \cdot \mathrm{MER} \tag{4.38}$$

$$\frac{\mathrm{d}}{\mathrm{d}t}\mathrm{LZD} = -k_\mathrm{deg,LZD} \cdot \mathrm{LZD}, \tag{4.39}$$

with $N = n + p$ and $\mathrm{SF} = 0.036$ in $10^5\,\mathrm{s/h}$ accounting for a conversion of units. For an alternate representation of the drug effects, see "Comprehensive effect equations" (p. 95).

The initial value for normal cells was set to $n(0) = (1 - f_\mathrm{p}) \cdot N(0)$, with $N(0) = N_0$ and $p(0) = f_\mathrm{p} \cdot N(0)$ for the persister cells. We determined the persister fraction f_p according to eq. (4.17). For experiments that started in lag phase, the initial ribosomal concentration $\mathrm{rib}(0) = \mathrm{rib}_0$ was unknown and therefore estimated. For exponential phase cultures $\mathrm{rib}(0)$ can be determined from eq. (4.5) via $\mathrm{rib}(0) = \mathrm{rib_c}$. The initial drug concentrations TET(0), VAN(0), MER(0) and LZD(0) were chosen according to the experimental protocol. Since no increased adaptive resistance against meropenem and vancomycin has been described for *S. aureus* ATCC 29213, we defined $\mathrm{ARV}(0) = \mathrm{ARM}(0) = 0$. The effector species for meropenem was initialized at $\mathrm{eMER}(0) = 0$.

Since the effects of the antibiotics on the persister formation were similarly observed in all experiments including drugs, the data did not allow to infer the concentration dependency of these effects. To still account for them, we set corresponding EC50 parameters to a hundredth of the lowest experimentally tested drug concentration. This allowed to infer the extent of these effects in terms of estimates for the Emax parameters.

4.5 Pharmacodynamic summary endpoints for time-kill curve data

Time-kill curve data provide detailed information on the antibacterial *in vitro* dynamics. Sometimes, however, it is desirable to reduce TKC data to a single numerical quantity, the so-called pharmacodynamic summary endpoint (PSE) [15], e.g, to classify the interaction of antibiotic combinations. The numerous PSE definitions proposed in literature have been divided into two classes by Firsov et al. [148]: either having integral character, when referring to time and amplitude of the time-kill trajectory, or having snapshot character when referring to a single time point. To study the impact of the choice of the PSE on the evaluation of antibiotic interactions, we define in the sequel two exemplary cases: an integral endpoint ($\mathrm{PSE_{IE}}$) and a snapshot endpoint ($\mathrm{PSE_N}$).

The integral endpoint was chosen to depend on the area under the TKC, defined as

$$\mathrm{AUTKC} = \int_0^{\tau_\mathrm{E}} \log(N)\,\mathrm{d}t, \tag{4.40}$$

where τ_E denoted the experimental duration. To allow for a probabilistic interpretation, which was needed in eq. (2.16), the endpoint was normalized with respect to the control experiment, resulting in

$$\mathrm{PSE_{IE}} = 1 - \frac{\mathrm{AUTKC_{drug}}}{\mathrm{AUTKC_c}}. \tag{4.41}$$

The snapshot endpoint was chosen to depend on the population size at the end of the experiment, resulting in

$$\mathrm{PSE_N} = 1 - \frac{\log\big(N_\mathrm{drug}(\tau_\mathrm{E})\big)}{\log\big(N_\mathrm{c}(\tau_\mathrm{E})\big)}. \tag{4.42}$$

To emphasize the dependence of the PSE on the drug concentration(s) in the TKC experiments, $\mathrm{PSE}(A, B)$ denoted the summary endpoint of a combination of two drugs with initial concentrations A and B. The classification of antibiotic combinations as synergistic or antagonistic required a definition of additivity, i.e., the expected PSE of an antibiotic drug combination based on the single drug exposures. To this end, we used the concept of Bliss independence as defined in eq. (2.16).

To be well defined in terms of $0 \leq \mathrm{PSE} \leq 1$, we assumed $N \geq 1\,\mathrm{CFU/ml}$ (resulting in $\log(N) \geq 0$) and $\mathrm{AUTKC_{drug}} \leq \mathrm{AUTKC_c}$. Both are reasonable assumptions in our context due to the lower limit of quantification $\mathrm{LLOQ} = 10\,\mathrm{CFU/ml}$ in the TKC data and the expected antimicrobial effect of the antibiotics.

Chapter 5

Statistical approaches

The presented cell-level approach utilizes data describing the cell-level as well as bacterial population growth data in terms of time-kill curves (TKC). In the following we describe, how we estimated parameters on both kinds of data. Furthermore, we describe how we performed the stochastic interaction surface analysis resulting in a discrete classification of antibiotic interactions.

5.1 Cell-state estimation

The data informing the cell-state was measured in different growth media and resulting discrete values of the exponential growth rate constant $k_{\mathrm{g,c}}$. In order to allow a broad application of the approach, we estimated a continuous representation of the cell-state S over a range of exponential growth rate constants $k_{\mathrm{g,c}}$. For each element of the cell-state, we assumed this representation to follow the power function of the form

$$S_i = a_i \cdot (k_{\mathrm{g,c}})^{b_i}. \tag{5.1}$$

We chose this form because it represented an appropriate balance between model complexity and accuracy of the description of the data. Based on data in [24, 47, 48], we estimated parameters a_i and b_i for *E. coli* B/r and *S. aureus* MF32 with the least squares method. The parameters are summarized in Table 3.1. Experimental data and predictions are shown in Figure 2.3. Due to the sparse data situation for *S. aureus*, we constrained the optimization using the identity condition $k_{\mathrm{g}} = k_{\mathrm{g}}\big(S(k_{\mathrm{g}})\big)$, with $k_{\mathrm{g}}\big(S\big) = \mathrm{SF} \cdot \mathrm{rib}(k_{\mathrm{g}}) \cdot \beta_{\mathrm{r}} \cdot c_{\mathrm{p}}(k_{\mathrm{g}})$, as introduced in eq. (4.3).

5.2 Bayesian inference

In this section we define predictions, observations and the statistical model as used for the analysis of time-kill curve data in "Model based analysis of antibiotic combinations and beyond" (p. 63). These analyses included parameter estimation and uncertainty quantification via sampling based methods which we also describe in the following paragraphs.

Model predictions and observations. Let $\theta \in \mathbb{R}^{N_{\mathrm{T}}}$ denote the vector of parameters of length $N_{\mathrm{T}} > 0$. Using the structural model in eqs. (4.26) to (4.37) with the model predicted total number of bacteria $N(t_{ij};\theta) = N = n + p$, we obtained the model predictions as a function of time and parameters

$$y_{\mathrm{pred},ij} = N(t_{ij};\theta) \qquad \text{with} \qquad i = 1 \ldots N_{\mathrm{C}} \qquad \text{and} \qquad j = 1 \ldots N_{\mathrm{T},i}. \tag{5.2}$$

The index i denoted the ith time-kill trajectory and j denoted the jth time point. This indexing is illustrated in Figure 2.5. Note that θ also includes covariates like drug exposure and growth phase. We obtained these predictions by numerically solving the referenced ODEs of the structural model using the Matlab 2015a built in function `ode45` (or `ode15s` in cases when the model was stiff as indicated by warnings with the non-stiff solver). Observations were denoted by $y_{\mathrm{obs},ij}$.

Statistical model. As it is commonly done for TKC and recommended in [15], we log-transformed model predictions and observations. Furthermore we made the common assumption [149] that the observations $y_{\mathrm{obs},ij}$ are realizations of the random variable

$$\log(\boldsymbol{Y}_{ij}) = \log(y_{\mathrm{pred},ij}) + \epsilon_{ij}, \qquad \epsilon_{ij} \sim \mathcal{N}(0, \sigma^2) \tag{5.3}$$

with independent and identically distributed errors ϵ_{ij} parameterized by zero mean and variance $\sigma^2 > 0$. The log transformation implies an exponential error model on the original scale

$$\boldsymbol{Y}_{ij} = y_{\text{pred},ij} \cdot \exp(\epsilon_{ij}). \tag{5.4}$$

We disregarded all values below the lower limit of quantification (LLOQ = 10 CFU/ml). Since most censored data had replicates with other dilution factors and the number of effected data points was low (1% of all measurements), we expected that the overall impact of the censoring on the analysis was also low.

Maximum likelihood estimation. Based on above assumptions, the likelihood function $\mathcal{L} = \mathcal{L}\big(\theta \mid (y_{\text{obs},ij})\big)$ is defined as

$$-2\log(\mathcal{L}) \propto \frac{1}{\sigma^2} \sum_{i=1}^{N_\text{C}} \sum_{j=1}^{N_{\text{T},i}} \big(\log(y_{\text{obs},ij}) - \log(y_{\text{pred},ij})\big)^2. \tag{5.5}$$

It remained to determine variance σ^2 for the likelihood function. To this end, we exploited that given the additive normally distributed error defined in eq. (5.3), the ML estimate θ_ML is identical to the least squares estimate

$$\theta_\text{ML} = \underset{\theta}{\operatorname{argmin}} \sum_{i=1}^{N_\text{C}} \sum_{j=1}^{N_{\text{T},i}} \big(\log(y_{\text{obs},ij}) - \log(y_{\text{pred},ij})\big)^2, \tag{5.6}$$

where $y_{\text{pred},ij}$ was a function of θ according to eq. (5.2). We determined θ_ML via corresponding minimizations using Matlab 2015a bounded Nelder Mead simplex algorithm followed by the constraint nonlinear optimization algorithm `fmincon`. We estimated variance σ^2 based on the error distribution in eq. (5.3) and θ_ML.

Parameter sampling. We quantified the uncertainty in the model predictions as a combination of uncertainty in parameter estimates (based on the MCMC samples) and residual variability (based on the ML estimate). Samples of the posterior were obtained by Markov chain Monte Carlo (MCMC) methods. We chose the Delayed Rejection Adaptive Metropolis (DRAM) MCMC algorithm [150] because of its good performance in high dimensions [151]. If not stated otherwise, we used flat (non-informative) priors for all parameters. We tested for non-convergence of the DRAM-MCMC sampler by computing the Gelman Rubin [152] potential scale reduction factor $\hat{R}$ as defined in [153, p. 604] over $k = 3$ chains. The chains started from highly dispersed initials and contained 10^5 samples each (disregarding 2.5×10^4 samples burn-in period). The factor $\hat{R}$ diagnoses the non-convergence of the sampler by comparing the variance based on θ in the target distribution and the average variance of the k chains [153, p. 605]. All inferences satisfied $\hat{R} < 1.2$ as recommended in [152].

For a Monte Carlo simulation of a single TKC trajectory, we sampled once from the posterior. The residual error was added for each of the $N_{\text{T},i} = 100$ equidistant time points by sampling independent and identically from the error distribution in eq. (5.3). We computed the 5th to 95th percentiles of the prediction interval based on 10^3 simulations.

5.3 Stochastic interaction surface analysis

One of the main aspects of this thesis is the analysis of antibiotic combinations and resulting interactions. Previously, we defined the pharmacodynamic summary endpoint (PSE) and the deviation from additivity Δ_Bliss, see “Pharmacodynamic summary endpoints for

time-kill curve data" (p. 57). It remained to derive a discrete classification as additive, synergistic and antagonistic of an antibiotic interaction based on Δ_{Bliss}. To this end, we used our model and the sampled parameters. Based on the simulation of a TKC trajectory (using the same parameter set for the corresponding drug-free control curve), we derived the pharmacodynamic summary endpoint (PSE) and the deviation from additivity Δ_{Bliss}. After repeated Monte Carlo simulations ($n = 250$), an interaction was classified as *additive*, if we did not reject the null hypothesis that the realizations of Δ_{Bliss} were from a normal distribution with mean equal to zero and unknown variance. We used the one-sample t-test at the 5% significance level to test this hypothesis. If significant deviation was detected, we characterized the interaction based on the sign of the mean of the Δ_{Bliss} distribution: positive = *synergy* and negative = *antagonism*.

To allow insight into the antibiotic interactions over a range of concentrations for two antibiotics, we applied this methodology on a concentration grid. The bounds of the concentration grid based on the estimated potencies (EC50 values) of the drugs (15x15, logarithmically spaced $10^{-4} \leq \text{VAN}(0) \leq 100\,\text{mg/l}$, $10^{-6} \leq \text{MER}(0) \leq 100\,\text{mg/l}$ and $10^{-4} \leq \text{LZD}(0) \leq 100\,\text{mg/l}$).

Chapter 6

Model based analysis of antibiotic combinations and beyond

In this chapter we present the results obtained based on the "Cell-level model for antibiotic combinations" (p. 47). First we describe the dynamics of the extensive time-kill curve (TKC) data. The TKC data were challenging because of the diverse observed phenomena: we found a reduced linezolid potency on lag phase bacteria, adaptive resistance development, antibiotic interactions and the Eagle effect.

As we observed a considerable impact of the growth phase on the TKC dynamics, we expected also a potential impact on the interactions. We used the cell-level model for antibiotic combinations to quantify the impact of the experimental protocol (growth phase, experimental duration and the endpoint definition) on antibiotic interactions. We found that in some (but not all) cases the classification of antibiotic interactions was strongly influenced by the experimental protocol.

6.1 Analysis of time-kill curves

TKC dynamics capture bacterial population growth during exposure to one or more antibiotics. In addition to the TKC data, the developed model relied on the availability of cellular characteristics as a function of growth. For *E. coli*, the most extensive compilation is available [24] (four measurements per cell-level characteristic, see Figure 2.3). Therefore, we first used TKC data from [121, Fig. 3] for *E. coli* to study the ability of the proposed model to predict bacterial growth in the exponential phase while exposed to a wide range of tetracycline concentrations (bacteriostatic and bactericidal). We used the Bayesian approach described in section "Bayesian inference" (p. 60) for all subsequent parameter inference on TKC data.

In the TKC experiments, exponentially growing *E. coli* B/r cultures have been exposed to constant concentrations of tetracycline (77 CFU measurements for a range of increasing tetracycline concentrations up to 0.008 mg/l). The data showed no signs of regrowth, as expected for the short experimental duration $\tau_E = 4\,h$. As seen in Figure A.1, the model fit is in good agreement with the experimental data (see Table A.1 for parameter estimates). The estimated variance of the residual error was $\sigma^2 = 0.1853$. The results successfully demonstrate the ability of the model to predict bacterial population growth from the cellular level of a reference cell, when cellular characteristics are perturbed by a drug for a wide range of initial concentrations.

For the clinically relevant *S. aureus* strain ATCC 29213, an extensive TKC dataset was analyzed, which has been specifically designed to study drug-drug-interactions (2442 CFU measurement in 82 distinctive experimental setups), combined with more sparse cell-level data. In addition to experiments starting in exponential phase, the TKC data included experiments in which the antibiotics vancomycin, meropenem and linezolid have been added directly after inoculation during the lag phase. A detailed experimental protocol can be found in [16]. All data and predictions are plotted in Figures A.2, A.3, A.4 and A.5. Overall, the model fits are in very good agreement to the experimental data (see Table 6.1 and Table 6.2 for parameter estimates). The estimated variance of the residual error was $\sigma^2 = 2.3172$. In the following we analyze key aspects of the TKC data.

6.1.1 Reduced linezolid potency on lag phase bacteria

For drug-free control experiments with *S. aureus*, the differences between lag and exponential phase cultures were (hardly) distinguishable and confined to the initial phase, see Figure 6.1 (A,B). In contrast, the bacterial population dynamics differed substantially between exponential and lag phase when exposed to linezolid, as shown in Figure 6.1 (C,D). For example, linezolid acted bacteriostatic on lag phase bacteria, even at the highest tested initial concentration of 32 mg/l. For the same concentration, linezolid exerted bacterici-

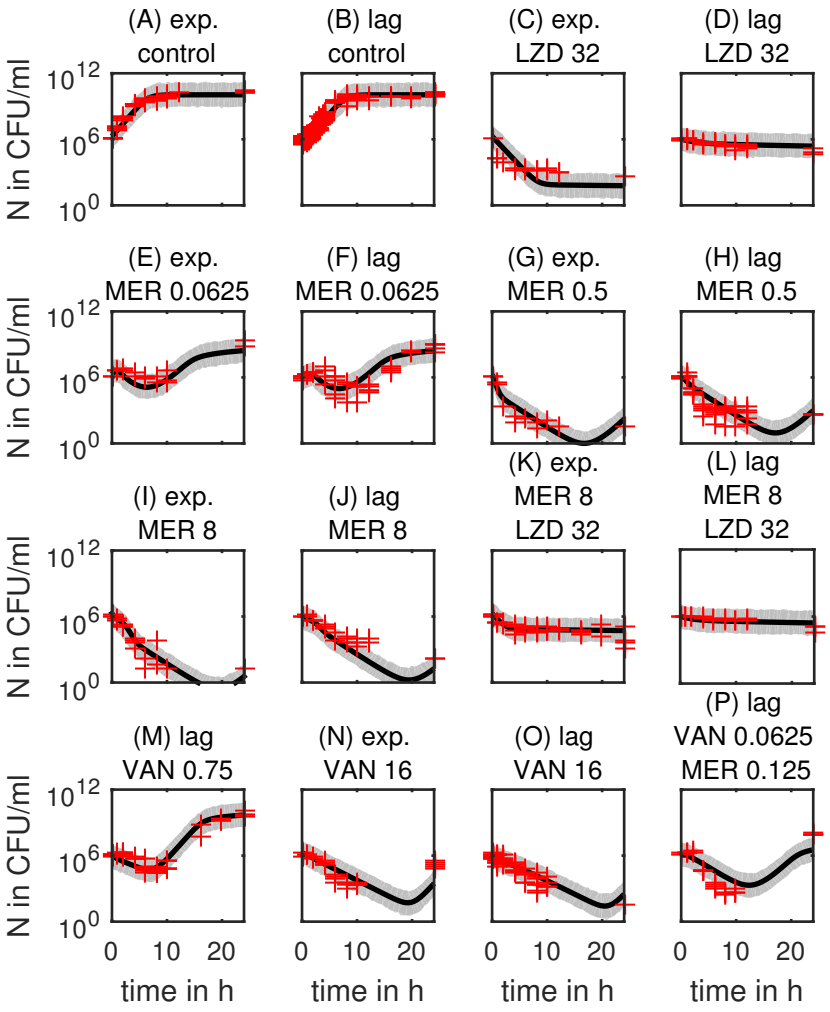

Figure 6.1: Time-kill curves (*S. aureus*, selection). *S. aureus* cultures in lag and exponential (exp.) phase exposed to antibiotic combinations. Selection shows: Negligible impact of growth phase in control experiments (A,B). Considerable impact of growth phase in experiments with linezolid (C,D). Delayed onset of meropenem drug action (E,F). Eagle effect, i.e., paradoxically decreased killing activity at higher meropenem concentrations (G,I). Less pronounced Eagle effect on lag phase cultures (H,J). Linezolid antagonizes meropenem drug action (I,K) and (J,L). Regrowth during vancomycin exposure (M,N,O) combined with meropenem (P). Data as red crosses. Solid black line is simulation based on the maximum a posteriori estimate. Gray area represents 0.05 to 0.95 quantile of prediction interval. Initial drug concentrations for vancomycin (VAN), meropenem (MER) and linezolid (LZD) in mg/l. For a comprehensive list of time-kill curves, see Figures A.2, A.3, A.4 and A.5.

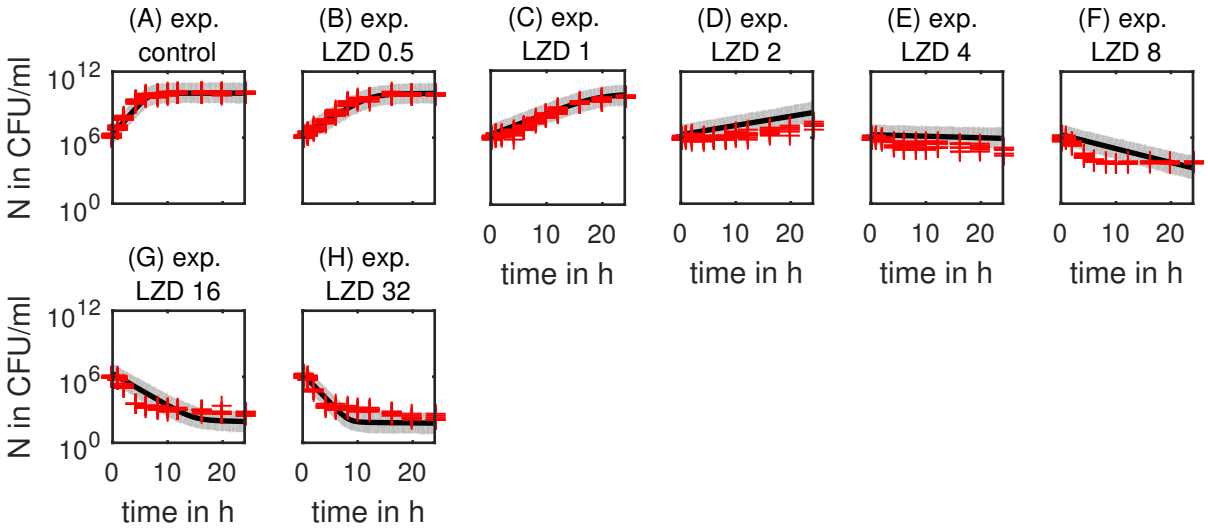

Figure 6.2: Time-kill curves (*S. aureus*, LZD, exp. phase, validation). Using the estimates from the main dataset, we described exponential phase cultures exposed to different initial concentrations of linezolid (LZD) in mg/l. Data as red crosses. Solid black line is simulation based on the maximum a posteriori estimate. Gray area represents 0.05 to 0.95 quantile of prediction interval.

dal effects when added to exponential phase cultures. This surprising difference can be explained based on our cell-level approach: in the model, the differences between lag and exponential phase experiments were represented by the persister fraction and the initial ribosomal concentration. The latter was estimated as $\mathrm{rib}_0 = \mathrm{rib}_\mathrm{c} = 2.63 \times 10^{-5}$/aa for exponential phase cultures and $\mathrm{rib}_0 = 0.93 \times 10^{-5}$/aa for lag phase cultures, impacting the linezolid potency as described for tetracycline in eq. (4.20). The persister fraction was initially much higher in lag phase cultures $f_\mathrm{p} = 0.42$, while it was negligible in the exponential phase.

The ability to simultaneously analyze TKC data in lag and exponential growth phases is a key benefit of our approach. The cell-level model allows to link the resulting differences in TKC dynamics to cellular characteristics, such as the ribosomal concentration and thereby mechanistically explains the reduced drug action of linezolid on lag phase cultures.

We validated the predictive power of the model for linezolid using a separate dataset (844 CFU measurements in 8 distinctive experimental setups) with the same strain and quantification method but different growth medium (see [23] for details). As shown in Figure 6.2, the model predictions are in good agreement with the data.

6.1.2 Adaptive resistance

Resistance development threatens the success of antibiotic treatments and is a driver for regrowth of a bacterial culture. We observed regrowth in experiments involving exposure to either vancomycin, meropenem or to a combination of the two antibiotics, see Figure 6.1 (E,F,M,N,P). Meropenem significantly degraded during the experimental time-course ($k_{\mathrm{deg,MER}} = 0.019$/h [16]), contributing to the observed regrowth. Degradation alone, however, was not sufficient to explain the observed regrowth (indicated by a model misfit, where more regrowth was observed than predicted, data not shown). Additionally, adaptive resistance development can contribute to regrowth. The model accounted for mechanisms of drug resistance against vancomycin and meropenem. Both mechanisms, assumingly efflux pumps and cell-wall thickening, lowered the effective drug concentrations at the target site and may be preexistent as less susceptible subpopulations. For a detailed description of the biological mechanisms and corresponding implementation, see "Integration of drug effects" (p. 51).

6.1.3 Antibiotic interactions

Both, the meropenem–linezolid and the vancomycin–meropenem combination, are recommended in guidelines for use in clinical practice [9, 10]. A combination of high initial concentrations of meropenem and linezolid resulted in a reduced killing activity compared to single drug meropenem exposure in exponential and lag phase experiments, see Figure 6.1 (I,J) compared to (K,L). Meropenem induced killing required ongoing progression of cells through the replication cycle and, implying continued protein biosynthesis [138]. Since linezolid impairs growth by inhibition of protein biosynthesis, it also lead to a reduced susceptibility of the bacteria to meropenem compared to single drug exposure to the beta-lactam. Lag phase bacteria benefit from the same protection mechanism against meropenem. In the model, the protection was represented by defining the death effect of meropenem to be proportional to the growth rate constant, see eq. (A.20).

We observed that based on the mechanism of drug action in the model and the corresponding predictions, linezolid did not impair vancomycin effects in the developed model. This combination, however, is not of clinical interest because of the overlapping antibacterial spectra. Furthermore, against MRSA, the vancomycin–linezolid combination showed antagonistic effects *in vitro* [154]. In contrast, the addition of meropenem enhanced the killing effect of vancomycin, as shown in Figure 6.1 (M,P), where the vancomycin concentration dramatically differed by more than an order of magnitude.

6.1.4 Eagle effect

One of the challenges during model development was that we observed a paradoxically decreased killing activity at increased drug concentrations for meropenem, a phenomenon known as the Eagle effect [147]. The Eagle effect was more pronounced in lag phase experiments compared to exponentially growing cultures, as seen in the initial slope in Figure 6.1 (G,I) and (H,J). Possible mechanisms how meropenem antagonized its own killing effect (auto-inhibition) include: (i) decreased protein-biosynthesis (via stringent response [155] and activation of the cell wall stress stimolon [156]); and (ii) decreased activity of autolysins [157–159]. The latter is also a consequence of the former, according to the surface stress theory [160]. This theory assumes that ongoing protein synthesis drives the autolytic activity. Since meropenem killing depends on the intrinsic activity of autolytic enzymes [138], both mechanisms contribute to the Eagle effect. In the model, an auto-inhibition term on the meropenem related death effect represented this phenomenon, see eqs. (A.21) and (4.29). Overall, the Eagle effect was reasonably well described.

Table 6.1: Parameter estimates (*S. aureus*, growth and linezolid related).

Parameter	Unit	Comment	Maximum a posteriori estimate with 0.05 and 0.95 quantiles of the marginals in brackets exponential phase	lag phase	Bounds / Reference
$\log(N_0)$	log(CFU/ml)	initial inoculum	14.44 (14.27–14.63)	13.85 (13.68–13.97)	$[0, \log(10^8)]$
rib_0	10^{-5}/aa	initial ribosomal concentration	rib_c	0.93 (0.72–1.25)	fixed and $[0, +\infty]$
f_p	-	initial persister fraction	0	0.42 (0.31–0.61)	fixed and $[0, 1]$
$k_{g,c}$	1/h	control growth rate constant	1.43 (1.31–1.53)		$[0, +\infty]$
$\log(N_{max})$	log(CFU/ml)	carrying capacity	23.13 (22.71–23.68)		$[\log(10^8), +\infty]$
k_{np}	1/h	switching rate constant (stationary phase, $n \to p$)	0.48 (0.17–1.06)		$[0, +\infty]$
k_{pn}	1/h	switching rate constant ($p \to n$)	0.74 (0.69–0.79)		$[0, +\infty]$
$k_{deg,LZD}$	1/h	degradation rate constant of linezolid	0.000101		[143]
$EC50_{LZD,g}$	mg/l	EC50 linezolid growth inhibition, scales with rib_c/rib	0.58 (0.49–0.71)		$[0, +\infty]$
$EC50_{LZD,d}$	mg/l	EC50 linezolid death induction, scales with rib_c/rib	96 (78–121)		$[0, +\infty]$
$Emax_{LZD,d}$	1/h	Emax linezolid death induction	5		fixed
$EC50_{LZD,p}$	mg/l	EC50 linezolid persister formation	0.0050		fixed
$Emax_{LZD,p}$	-	Emax linezolid persister formation	0.32 (-0.21–1.47)		$[-1, +\infty]$

Slope factors $\gamma_{LZD,g}$, $\gamma_{LZD,d}$, $\gamma_{LZD,p}$ and maximum effect $Emax_{LZD,g}$ were fixed to 1 to increase parameter identifiability

Table 6.2: Parameter estimates (*S. aureus*, vancomycin and meropenem related).

Parameter	Unit	Comment	Maximum a posteriori estimate with 0.05 and 0.95 quantiles of the marginals in brackets exponential phase	lag phase	Bounds / Reference
$k_{\mathrm{deg,VAN}}$	1/h	degradation rate constant of vancomycin	0.0039		[143]
$\mathrm{EC50}_{\mathrm{VAN_t,d}}$	mg/l	EC50 vancomycin death induction	0.496 (0.481–0.510)		$[0, +\infty]$
$\gamma_{\mathrm{VAN_t,d}}$	-	slope factor vancomycin death induction	17 (10–98)		$[0, +\infty]$
$\mathrm{Emax}_{\mathrm{VAN_t,d}}$	1/h	Emax vancomycin death induction	1.90 (1.78–2.01)		$[0, +\infty]$
$\mathrm{EC50}_{\mathrm{VAN_t,ARV}}$	mg/l	EC50 vancomycin adaptive resistance	12.23 (10.80–13.56)		$[0, +\infty]$
$\mathrm{Emax}_{\mathrm{VAN_t,ARV}}$	-	Emax vancomycin adaptive resistance, scales with $\mathrm{rib}/\mathrm{rib_c}$	1		fixed
$\mathrm{EC50}_{\mathrm{VAN,p}}$	mg/l	EC50 vancoymcin persister formation	0.000625		fixed
$\mathrm{Emax}_{\mathrm{VAN,p}}$	-	Emax vancoymcin persister formation	32 (21–62)		$[-1, +\infty]$
$k_{\mathrm{deg,MER}}$	1/h	degradation rate constant of meropenem	0.019		[143]
$\mathrm{EC50}_{\mathrm{eMER,d}}$	mg/l	EC50 meropenem death induction	0.0539 (0.0490–0.0621)		$[0, +\infty]$
$\gamma_{\mathrm{eMER,d}}$	-	slope factor meropenem death induction	4.59 (3.59–6.24)		$[0, +\infty]$
$\mathrm{Emax}_{\mathrm{eMER,d}}$	1/h	Emax meropenem death induction, scales with $k_{\mathrm{g}}(t)$	4.35 (3.41–6.36)		$[0, +\infty]$
$\mathrm{EC50}_{\mathrm{eMER,E}}$	mg/l	EC50 meropenem auto-inhibition	2.05 (1.05–5.61)		$[0, +\infty]$
$\mathrm{EC50}_{\mathrm{eMER,ARM}}$	mg/l	EC50 meropenem adaptive resistance	0.804 (0.740–0.870)		$[0, +\infty]$
$\mathrm{EC50}_{\mathrm{MER,p}}$	mg/l	EC50 meropenem persister formation	0.00015625		fixed
$\mathrm{Emax}_{\mathrm{MER,p}}$	-	Emax meropenem persister formation	905 (513–2059)		$[-1, +\infty]$

The maximum adaptive resistances $\mathrm{ARV}_{\mathrm{max}}$, $\mathrm{ARM}_{\mathrm{max}}$, slope factors $\gamma_{\mathrm{VAN_t,ARV}}$, $\gamma_{\mathrm{VAN,p}}$, $\gamma_{\mathrm{eMER,E}}$, $\gamma_{\mathrm{eMER,ARM}}$, $\gamma_{\mathrm{MER,p}}$ and maximum effects $\mathrm{Emax}_{\mathrm{VAN_t,ARV}}$, $\mathrm{Emax}_{\mathrm{eMER,E}}$, $\mathrm{Emax}_{\mathrm{eMER,ARM}}$ were fixed to 1 to increase parameter identifiability

6.2 Impact of the experimental protocol on antibiotic interactions

There is a plethora of different experimental setups to assess antibiotic interactions *in vitro*, including checkerboard, E-test and TKC assays [161]. Especially for the latter, a harmonized experimental protocol (including standardized metrics) is still to be established. Even for the same compounds and strain, contradicting categorizations of the interaction with respect to additivity, synergy or antagonism are reported [14]—a result which we additionally confirmed across publications, see Figure 6.3.

Our new developed *in silico* approach allows to understand these contradictory categorizations. We analyzed the impact of the experimental protocol in terms of different drug concentrations, growth phases, experimental durations and endpoint definitions. Start-

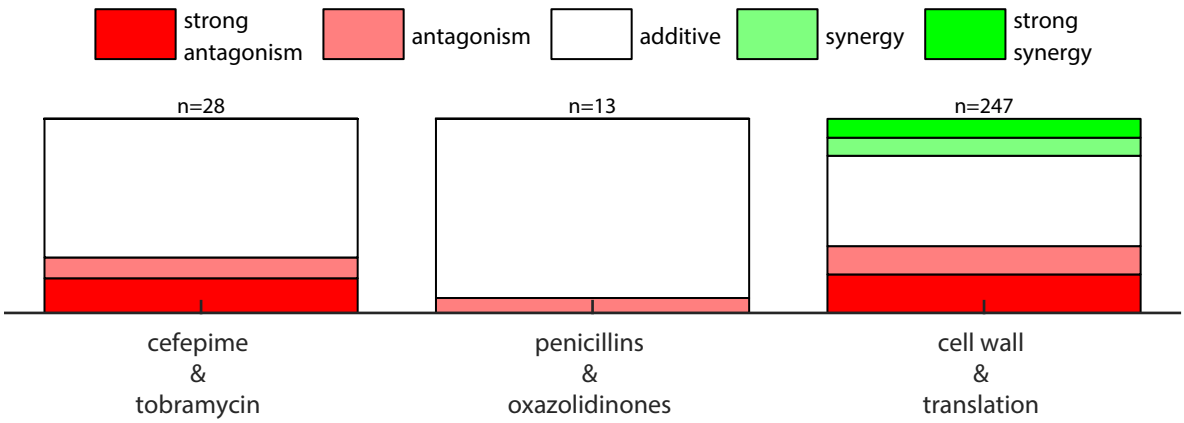

Figure 6.3: Reported qualitative antibiotic interactions. In total $n = 382$ reports were compiled from literature. Reports classified interactions as antagonistic, additive or synergistic across different *in vitro* assays, interaction indices and bacterial species. The interaction classifications showed similar variability when grouped as compounds (cefepime & tobramycin) and chemical class (penicillins & oxazolidinones). When we clustered the antibiotics by perturbed superordinate cellular processes or structures (cell wall & translation), the pattern was more heterogeneous. This example demonstrates that the cellular mechanism of drug action for a chemical class of antibiotics is predictive for the interaction pattern, as previously described in [17].

ing the analysis with first comparing the drug combinations meropenem–linezolid and vancomycin–meropenem with respect to response and interaction surfaces for a single experimental protocol, we then systematically explore diverse experimental protocols. Finally, we demonstrate how the experimental duration impacts the interaction between meropenem and linezolid.

6.2.1 Pairwise comparison of drug combinations

As antibiotic response is related to the corresponding drug exposure, we expected that antibiotic interactions are impacted by the initial concentrations of the drugs. Previously, we described how the antibiotic response in terms of resulting TKC dynamics can be reduced to a single numerical quantity called pharmacodynamic summary endpoint (PSE), see "Pharmacodynamic summary endpoints for time-kill curve data" (p. 57). In addition to the exposures, also the experimental protocol is of relevance for the PSE. The quantification of an antibiotic interaction was obtained by using the PSE in the definition of the deviation from additivity in eq. (2.20). The combination of response and interaction allowed to determine the response and interaction surfaces as described in "Drug-drug interactions" (p. 25).

To get insight into the concentration dependency, we simulated the response and interaction surfaces over a range of initial concentrations for combinations of vancomycin, meropenem and linezolid. The results for *S. aureus* are shown in Figure 6.4 for the integral endpoint $\mathrm{PSE} = \mathrm{PSE}_{\mathrm{IE}}$ as response (experimental protocol: lag phase, $\tau_{\mathrm{E}} = 24\,\mathrm{h}$).

For meropenem–linezolid, the corresponding interaction surface indicates antagonism for clinically relevant concentrations [16]. For vancomycin–meropenem and the same experimental protocol, the interaction surface indicated mostly additive interactions with a small region of synergy, showing superiority compared to meropenem combined with linezolid. The vancomycin–meropenem combination was also superior with respect to the maximum response compared to the meropenem–linezolid combination. For visualization of the response surfaces, see Figure 6.4.

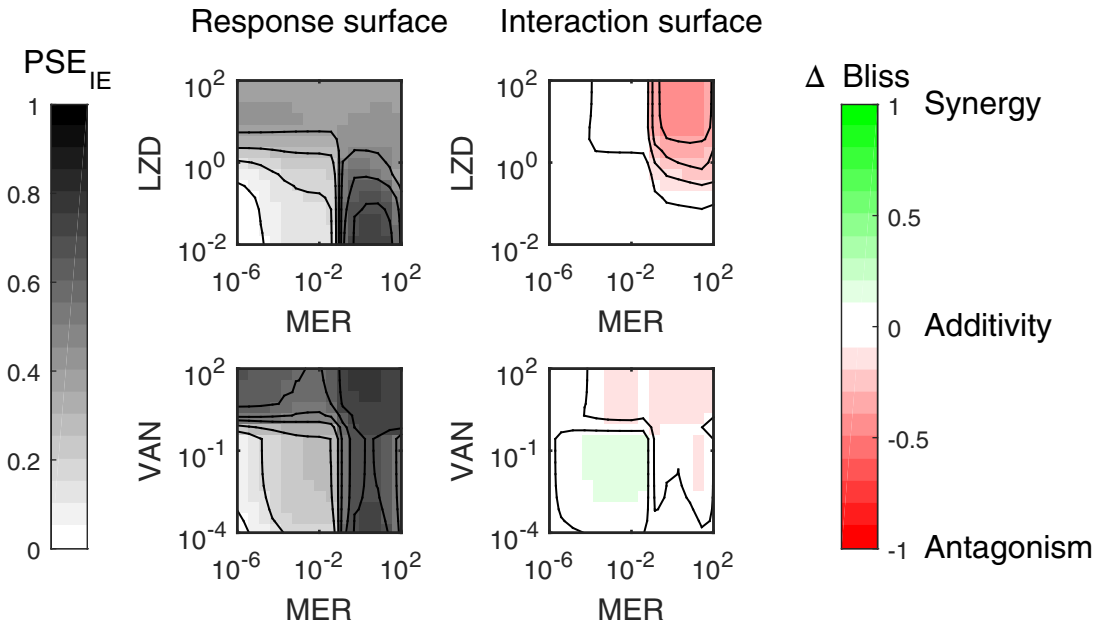

Figure 6.4: Response and interaction surfaces. Response surfaces for integral summary endpoint PSE_{IE} predicted for lag phase *S. aureus* cultures observed over 24 h using maximum a posteriori estimate (darker shade represents stronger response). Based on Bliss independence, we derived corresponding deviation from additivity (Δ_{Bliss}), i.e., the interaction surface. While the meropenem–linezolid combination exhibited a large fraction of antagonistic interactions, the vancomycin–meropenem combination interacted mostly additive. Initial antibiotic concentrations for vancomycin (VAN), meropenem (MER) and linezolid (LZD) in mg/l. Contour lines indicate trajectories of equal response and interaction levels, respectively.

6.2.2 Systematic exploration of different experimental protocols

A key ability of our approach is that the model allows to predict TKC for different experimental protocols. In particular the ability to switch the growth phase for the prediction of the antibiotic combinations is unique and was leveraged to systematically explore the impact of the experimental protocol on antibiotic interactions. To this end, we determined response and interaction surfaces for lag and exponential growth phase and both endpoint definitions (PSE_{IE} or PSE_N). Instead of a graphical representation, we quantified the fractions of the interaction surface categorized as antagonistic, additive or synergistic. The classification was based on a significance test against the null hypothesis that the drug combination interacts additively, as described in "Stochastic interaction surface analysis" (p. 61). Additionally we reported the strength of the interaction with respect to antagonism and synergy as the 5th and 95th percentiles across the whole interaction surface, i.e., the central 90% range. The results are compiled in Table 6.3.

While we observed considerable impact of the growth phase on TKC dynamics for some drugs, in particular linezolid, this was not the case for the pharmacodynamic summary endpoints of the combinations. For both tested antibiotic combinations, the growth phase (lag/exponential) did not strongly impact the fractions of classifications and range. Assuming that any potential impact of the initial growth phase subsides with time, this observation is to be expected. In contrast, the endpoint definition clearly showed an impact on the fractions of classifications. The integral endpoint PSE_{IE} resulted in a lower fraction of additive classifications compared to snapshot endpoint PSE_N, in particular for the meropenem–linezolid combination. The ratio of antagonism to synergy, however, remained comparable, as well as the overall strength of the interaction, i.e., the Δ_{Bliss} range. This agreed with our expectations, since integrating over multiple time points to obtain PSE_{IE} resulted in a narrower distribution of Δ_{Bliss} compared to the exclusive reference to a single time point for PSE_N due to the independent and identical distribution of the

residual error, see "Bayesian inference" (p. 60).

6.2.3 Time and concentration dependency of interactions

As expected, most tested interactions surfaces did not describe a flat landscape. The deviations from additivity were confined to specific concentration regions on the interaction surface, as shown in Figure 6.4 and indicated by a large Δ_{Bliss} range in Table 6.3. In addition, antibiotic interactions depended on time, i.e., they were sensitive to the experimental duration (see Table 6.3). The impact of the experimental duration on the classification depended on the endpoint definition. For the snapshot endpoint PSE_{N}, we observed a tendency to shift from antagonistic to additive classifications with increasing experimental durations. This tendency was much weaker for the integral endpoint PSE_{IE} (see Table 6.3). A possible explanation is that for very long experimental durations the system reaches a steady state close to $N = N_{\max}$ due to adaptive resistance development and drug degradation. To analyze the time dependency in more detail, we focused on the meropenem–linezolid interaction in lag phase *S. aureus* cultures. As shown in Figure 6.5, the interaction pattern changed from clear antagonism ($0 \leq \tau_{\text{E}} \leq 12\,\text{h}$) to a mixed additive and antagonistic interaction surface for longer experimental durations. A potential reason might be the comparatively fast degradation of meropenem. However, the emergent additivity prevailed also in simulations with $k_{\text{deg,MER}} = 0$. Rather, the phenomenon resulted from the adaptive resistance development against meropenem, while susceptibility against linezolid remained high.

Table 6.3: Impact of the experimental protocol on antibiotic interactions. The interaction surfaces were partitioned in antagonistic (ant.), additive (add.) and synergistic (syn.) fractions. The strength of the interactions with respect to antagonism and synergy is reported as the central 90% range of the interaction surface (5th and 95th percentiles denoted by $\Delta_{\text{Bliss}}^{0.05}$ and $\Delta_{\text{Bliss}}^{0.95}$).

		Experimental protocol			Fractions			Range	
Drug A	Drug B	Endpoint	Growth phase	Duration	ant.	add.	syn.	$\Delta_{\text{Bliss}}^{0.05}$	$\Delta_{\text{Bliss}}^{0.95}$
LZD	MER	PSE_{IE}	exponential	6 h	0.89	0.11	0.00	[-0.33	0.00]
LZD	MER	PSE_{IE}	exponential	12 h	0.61	0.19	0.20	[-0.40	0.01]
LZD	MER	PSE_{IE}	exponential	24 h	0.55	0.19	0.26	[-0.44	0.01]
LZD	MER	PSE_{IE}	exponential	48 h	0.48	0.20	0.32	[-0.37	0.03]
LZD	MER	PSE_{IE}	lag	24 h	0.52	0.22	0.26	[-0.42	0.01]
LZD	MER	PSE_{N}	exponential	6 h	0.93	0.07	0.00	[-0.39	-0.01]
LZD	MER	PSE_{N}	exponential	12 h	0.46	0.40	0.13	[-0.44	0.03]
LZD	MER	PSE_{N}	exponential	24 h	0.40	0.43	0.17	[-0.43	0.05]
LZD	MER	PSE_{N}	exponential	48 h	0.26	0.44	0.29	[-0.32	0.10]
LZD	MER	PSE_{N}	lag	24 h	0.37	0.44	0.19	[-0.44	0.05]
VAN	MER	PSE_{IE}	exponential	6 h	0.60	0.00	0.40	[-0.27	0.09]
VAN	MER	PSE_{IE}	exponential	12 h	0.60	0.04	0.36	[-0.28	0.10]
VAN	MER	PSE_{IE}	exponential	24 h	0.60	0.00	0.40	[-0.20	0.11]
VAN	MER	PSE_{IE}	exponential	48 h	0.47	0.01	0.52	[-0.14	0.13]
VAN	MER	PSE_{IE}	lag	24 h	0.59	0.00	0.40	[-0.15	0.11]
VAN	MER	PSE_{N}	exponential	6 h	0.63	0.05	0.32	[-0.28	0.09]
VAN	MER	PSE_{N}	exponential	12 h	0.56	0.04	0.40	[-0.21	0.12]
VAN	MER	PSE_{N}	exponential	24 h	0.45	0.05	0.50	[-0.19	0.14]
VAN	MER	PSE_{N}	exponential	48 h	0.00	0.01	0.99	[0.04	0.17]
VAN	MER	PSE_{N}	lag	24 h	0.40	0.11	0.49	[-0.11	0.14]
simulations without drug degradation ($k_{\text{deg,VAN}} = k_{\text{deg,MER}} = k_{\text{deg,LZD}} = 0$)									
LZD	MER	PSE_{N}	exponential	24 h	0.77	0.20	0.04	[-0.43	0.01]
VAN	MER	PSE_{N}	exponential	24 h	0.49	0.10	0.40	[-0.19	0.11]
LZD	MER	PSE_{IE}	exponential	24 h	0.70	0.09	0.20	[-0.44	0.01]
VAN	MER	PSE_{IE}	exponential	24 h	0.60	0.00	0.40	[-0.20	0.11]

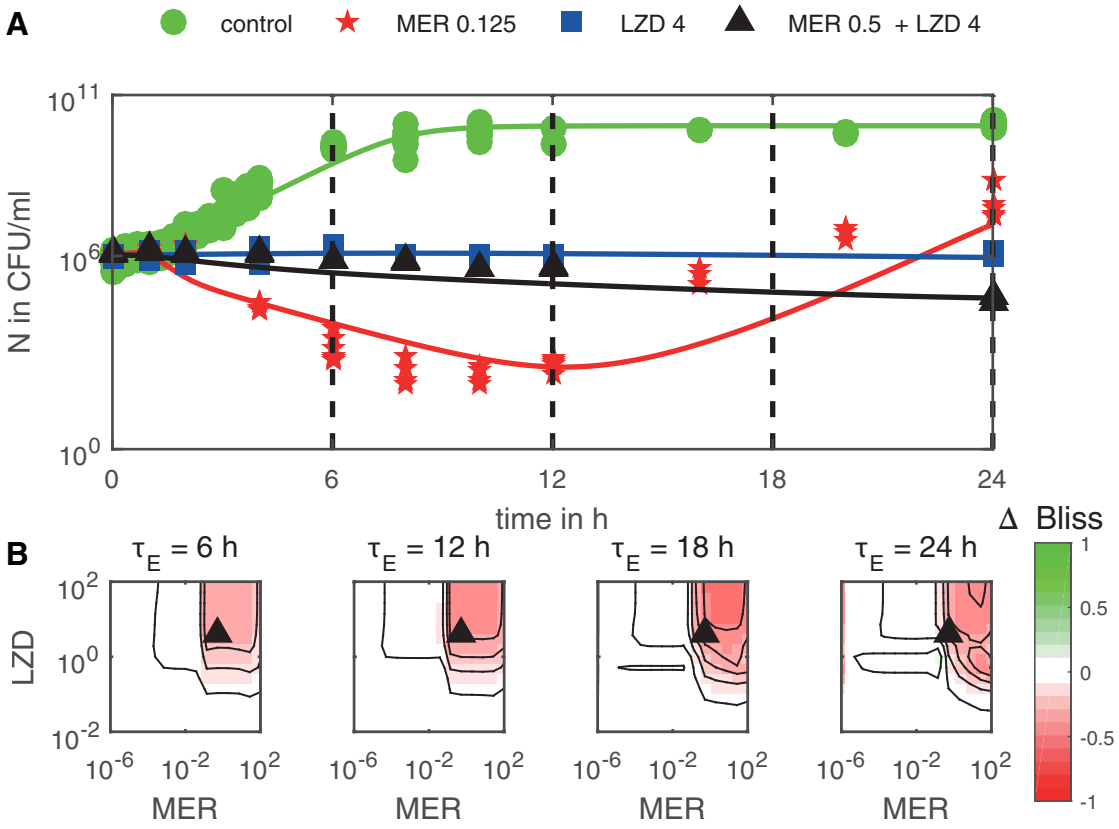

Figure 6.5: Time dependency of interactions. Lag phase *S. aureus* cells exposed to different initial concentrations of meropenem (MER) and linezolid (LZD), both in mg/l. **(A)** Bacterial concentration N over time (symbols denote experimental data and solid lines the corresponding model prediction based on the maximum a posteriori estimate). Compared to meropenem exposure alone, the combination with linezolid exerted inferior initial killing. On the long term, however, the combination was at least on par. **(B)** The interaction surface, i.e., the deviation from expected additivity (Δ_{Bliss}) over time, predicted for pharmacodynamic summary endpoint PSE_{N}. The initially pronounced antagonism (red) shifts towards higher concentrations and a new, slightly synergistic plateau emerges. The black triangle marks the concentrations of the meropenem–linezolid combination which is also depicted in the time-kill curves.

Chapter 7

Discussion

In the following, we critically discuss limitations, assumptions and possible generalizations of the developed cell-level approach. The discussion complements the evaluation of the prototype model in "Interim evaluation of the prototype model" (p. 44).

Time dependency of interactions and experimental implications. We demonstrated that the experimental duration strongly impacted the classification of antibiotic interactions. For example, when too short experimental durations censored regrowth dynamics, see Figure 6.5. Our analysis showed that in this case, the interaction surface changed remarkably over time—especially when evaluating snapshot endpoints, because of the exclusive reference to the end of the experiment. The classification of antibiotic interactions are expected to strongly differ between experimental protocols without standardization of the experimental duration with respect to regrowth. Our findings are in line with Firsov [148] in urging experimenters to prevent unjustified shortening of TKC experiments. In light of the demonstrated variability in the interaction classifications, the observed variability in literature reports is now more understandable, see Figure 6.3.

Link between pharmacokinetic and pharmacodynamic interactions. In this thesis, we studied the antibacterial effects in terms of TKC data for several antibiotics. Some of these drugs were not stable under the experimental conditions. We exploited the developed *in silico* approach to study the impact of the stability on the corresponding interaction for two example drugs: meropenem (fast degraded, $k_{\mathrm{deg,MER}} = 0.019/\mathrm{h}$) and linezolid (stable, $k_{\mathrm{deg,LZD}} \approx 0$) and simulated the interaction surface without degradation ($k_{\mathrm{deg,VAN}} = k_{\mathrm{deg,MER}} = k_{\mathrm{deg,LZD}} = 0$, exponential phase, 24 h using $\mathrm{PSE_N}$). We found that the fast degradation of meropenem weakened the observed antagonism. Thus, linezolid perpetrated meropenem effects even more than observed in the TKC data where drug degradation took place in the growth medium. In simulations without degradation, the antagonism was more pronounced (the antagonistic fraction of the interaction surface increased from 0.40 to 0.77) and the slight synergy even less pronounced (synergistic fraction of the interaction surface reduced from 0.17 to 0.04) compared to simulations including degradation processes. For a full overview, see Table 6.3. The strength of the interactions remained comparable. This is an example of how PK properties influence PD interactions. It highlights the necessity of a combined PKPD approach to determine any "true interaction" with respect to clinical importance.

Alternate additivity criteria. In order to classify synergy and antagonism, we exclusively used Bliss independence to define additivity. An alternate additivity criterion is given by Loewe [107], as introduced in "Drug-drug interactions" (p. 25). In his concept, instead of response additivity, dose additivity is assumed, i.e., one drug is exchanged for an equipotent dose of the combination partner. The resulting response defines the expected additivity. This approach was not applicable in our case: to determine a (unique) equipotent dose, the dose response relationship needed to be invertible. This condition was at least not satisfied for meropenem due to the Eagle effect.

Inter-species translation of the cell-level data. The developed approach integrated cell-level data into the bacterial population growth dynamics as introduced in "Balanced growth and the cell-state" (p. 11). Our analysis of the cell-level data revealed a surprising correlation: the strong dependence of the intracellular ribosomal concentration and efficiency on growth was remarkably conserved across the two bacterial species *S. aureus* and *E. coli*, as shown in Figure 2.3. This may suggest a generalizable pattern of inter-species conservation. When no or very sparse cell-level data are available, the presented Bayes approach would offer rigorous implementation of such patterns as prior knowledge. Yet,

the validity of such assumptions has to be critically considered: external model validations and a check of the physiological plausibility of the parameters including proportions of cell size and mass are mandatory.

Limitations of the growth rate to cell-state interrelationship. A prerequisite for our modeling approach is an invertible relationship between growth rate and cellular characteristics of some reference cell under balanced growth condition, as exploited in "Linking the cell-state to bacterial population growth and *vice versa*" (p. 48). This assumption holds true in nutritional rich media, as typically used to assess antibiotic action. In nutritionally highly unfavorable media, however, cells may employ alternative metabolic pathways to prevent starvation. Then, the descriptions of the reference cell may not be representative for the culture of interest. Thus, extrapolation beyond the tested control growth rate constants should be ideally supported with additional cell-level data in the corresponding media.

Another aspect concerns the applicability of the growth rate to cell-state interrelationship. During drug exposure, as shown for chloramphenicol in Figure 3.7, the relation of growth rate and cell-state was not one-to-one anymore. Instead of a one-to-one relation, a combination of growth rate and drug concentration determined the cell-state. Thus, the assumption related to eqs. (3.10), (3.11) and (3.12) is violated for long term drug exposure. In the following we explain, why this does not impair our approach. We exploited the link of the growth rate to cell-state exclusively for the initialization of the cell-state. More precisely, the link was used for experiments starting in the exponential growth phase, as we estimated the initial cell-state for lag-phase bacteria. Using nutrient rich and drug free media, this is the same growth condition under which Bremer and Dennis performed the corresponding experiments to determine cellular characteristics at different growth rates [24]. Thus, the use of the growth rate to cell-state relation is valid for all used experimental setups where the addition of antibiotics was at the beginning of the experimental duration, see Figure 2.5. Assuming validity of the inverse direction of the link (cell-state to growth rate), it follows that drug effects do not impair the general use of the growth rate to cell-state interrelationship.

Count data and analytical challenges. As it is the common approach [15, 18], we treated the bacterial concentration, stated in unit CFU/ml, as a continuous variable—ignoring the discrete count nature of the data. Such simplification is appropriate for high counts, but may result in unrealistic predictions for very small population sizes with respect to regrowth. Especially, the interpretation of zero colony counts after plating and incubation clearly depends on the (adaptively chosen) dilution scheme. Furthermore, when we inferred the bacterial concentration via viable plating, we assumed that all individual cells had the same probability to form colonies after incubation. Clearly, the number and size of the colonies depends on the incubation time. The validity of the assumption has been demonstrated for the performed viable plating assay by Scheerans [162, p. 56]. He has found no significant change in CFU counts when increasing the incubation time from 24 to 48 h.

Death of a bacterial cell or its division may be modeled as events effecting a discrete bacterial population size. Accordingly, bacterial population dynamics could be described by time to event models. Time to event models would naturally account for both—the count nature of the plating process and also for the related analytical challenges—and represent a more mechanistic alternative compared to treating counts as continuous data.

Explanations for increased RNA levels. A key ability of our approach is the description of cell-level characteristics during antibiotic exposure as exemplified in "Applications

of the prototype model" (p. 37). The predicted increased RNA levels during exposure to protein biosynthesis inhibitors was in agreement with other literature reports: in [163] increased transcription of ribosomal mRNA has been linked to rising intracellular energy levels. In our prototype model these energy levels were represented as the peptide chain elongation rate of the *active* ribosomes during antibiotic perturbation. This is also in line with the hypothesis that the main drivers for this rate are the levels of intracellular amino acid pools. The amino acid supply has been described to generally impact cellular metabolism of clinically relevant bacteria, including *S. pneumoniae*, *S. aureus*, *E. faecalis* and *P. aeruginosa* [164]. In particular, rising amino acid pools release the ppGpp-mediated repression of rRNA synthesis [165]—a mechanism which we integrated in the prototype model. Passive regulation could be an additional mechanism resulting in increased RNA levels: while translation is inhibited, transcription continues, leading to an excess of RNA [166], which in return causes defects in ribosome assembly [56]. Our decision to omit increasing RNA levels in the interaction model is based on the gap of mechanistic knowledge of how RNA levels impact drug action. We estimated that linezolid does not significantly increase the rate of persister formation (see Table 6.1), which is now understandable in light of the link between rising amino acid pools and a relaxation of the stringent response.

Death effect corrected prediction of the RNA mass fraction. We predicted the RNA mass fraction during exposure to chloramphenicol in Figure 3.7. Overall, the predictions were in good agreement with the experimental data. Yet, we observed a trend of increasing deviations at higher chloramphenicol concentrations. Based on the bacteriostatic nature of chloramphenicol we assumed negligible death effects for the applied concentrations. In light of an assumed Emax model for the death effects and the larger deviations at higher concentrations, the validity of the assumption has to be critically discussed. A consideration of death effects could possibly improve this minor misfit.

Parallels between tumor and bacterial growth. Modeling a cell population as the combination of growing and non-growing cells is one of many examples (among drug resistance, carrying capacity and stress response) where elements of bacterial and tumor growth models overlap. In both cases persisting or quiescent cells prevent an eradication of the population—possibly leading to a relapse of tumor growth or to the re-occurrence of an infection. Accordingly, theoretical considerations for tumor growth models could be applicable in bacterial growth models and *vice versa*. In eq. (3.5), we stated an approximation for the fraction of non-growing cells in an exponentially growing population. Analyzing tumor growth, Hartung derived in [167] an analytical solution for the same problem, see eq. (A.13). Simulations showed that for all datasets the approximation in eq. (3.5) leads to similar results (absolute deviation for $f_{\mathrm{p,exp}} \leq 5\%$).

Chapter 8

Conclusion

We successfully developed a cell-level model of bacterial population growth for antibiotic combinations. The novel combination of cell-level and time-kill curve data did not only allow to describe complex population growth dynamics, but also to systematically disentangle the impact of drug effects, assay readouts and experimental protocols on antibiotic interactions. In scenarios involving bacterial regrowth, the experimental duration critically impacted antibiotic interactions, as exemplified by the exposure of *S. aureus* to meropenem, vancomycin and linezolid. Although the impact of the initial growth phase on time-kill curve dynamics was considerable for linezolid, observable for meropenem and negligible for vancomycin, the corresponding impact on interaction surfaces turned out to be always minor. The performed stochastic simulation studies to evaluate time-kill curve data showed that the application of integral summary endpoints resulted in lower proportions of additive interactions compared to the use of snapshot endpoints. The reason was the increased variability of the interaction surfaces due the exclusive reference to a single point implied by the snapshot character. Yet, across tested scenarios, we confirmed the recently found antagonistic interaction between linezolid and meropenem [16].

Overall, the consideration of cell-level processes in the developed pharmacokinetic-pharmacodynamic model to describe time-kill curve data was advantageous regarding some aspects compared to conventional models which are confined to bacterial population growth: an increased versatility allowed to integrate prior knowledge from literature, as demonstrated with the prototype model for *E. coli*. Prior knowledge integration included the correction for different experimental protocols via identification of experiment specific parameters. Moreover, consideration of ribosomal dynamics allowed to explain the reduced potency of linezolid against lag phase *S. aureus* cultures. The increased level of detail implied high model complexity and necessitated the availability of cell-level data. We showed that the cell-level approach can be tailored to specific mechanisms of drug action and thereby we reduced the amount of necessary cell-level data.

In view of the currently emerging antibiotic resistance crisis there is a dire need to improve the understanding of the effects of multiple antibiotics on bacteria. Therefore the developed approach contributes a well-timed piece of research bridging mathematics and biology. The ultimate aim remains to predict antibiotic effects *in vivo*. To this end, this thesis may serve as a starting point for further research. To further advance to this aim, next steps should additionally account for a potential impact of the immune system, the target site pharmacokinetics and the particularities of the *in vivo* habitats, like biofilm formation.

Nomenclature

PSE Pharmacodynamic summary endpoint

(p)ppGpp Guanosin tetraphosphate (phosphorylated)

i.i.d. Independent and identically distributed

aa Amino acid

aa-tRNA Aminoacyl tRNA, charged tRNA

ATP Adenosine triphosphate

DNA Deoxyribonucleic acid

DRAM-MCMC Delayed Rejection Adaptive Metropolis MCMC

ESBL Extended spectrum beta-lactamases

FACS Fluorescence-activated cell scanning/sorting

fMet-tRNA N-formylmethionyl tRNA

LLOQ Lower limit of quantification

MAP Maximum a posteriori

MBC Minimal bactericidal concentration

MCMC Markov chain Monte Carlo (sampler)

MIC Minimal inhibitory concentration

ML Maximum likelihood

mRNA Messenger RNA

MRSA Methicillin resistant *Staphylococcus aureus*

ODE Ordinary differential equation

PBP Penicillin binding protein

PD Pharmacodynamics, "What the drug does to the body"

PK Pharmacokinetics, "What the body does to the drug"

QSS Quasi steady state

RNA Ribonucleic acid

RNAP RNA polymerase

rRNA Ribosomal RNA

THF Tetrahydrofolate

TKC Time-kill curve

tRNA Transfer RNA

UV-VIS Spectrum covering ultraviolet to visible light wavelengths (200 to 800 nm)

VRE Vancomycin resistant enterococci

Bibliography

[1] J. M. A. Blair et al. “Molecular mechanisms of antibiotic resistance”. In: *Nat. Rev. Microbiol.* 13.13 (2015), pp. 42–51.

[2] E. D. Brown and G. D. Wright. “Antibacterial drug discovery in the resistance era”. In: *Nature* 529.7586 (2016), pp. 336–343.

[3] D. S. Jones, S. H. Podolsky, and J. a. Greene. “The Burden of Disease and the Changing Task of Medicine”. In: *N. Engl. J. Med.* 366.25 (2012), pp. 2333–2338.

[4] C. of Disease Control and t. Prevention. *Leading Causes of Death 1900-1998*. `https://www.cdc.gov/nchs/data/dvs/lead1900_98.pdf`. [Online; accessed 06-June-2017].

[5] M. A. Cooper and D. Shlaes. “Fix the antibiotics pipeline”. In: *Nature* 472.7341 (2011), p. 32.

[6] R. Laxminarayan et al. “Antibiotic resistance - the need for global solutions”. In: *Lancet Infect. Dis.* 13 (2013), pp. 1057–1098.

[7] L. L. Silver. “Challenges of antibacterial discovery”. In: *Clin. Microbiol. Rev.* 24.1 (2011), pp. 71–109.

[8] K. Lewis. “Platforms for antibiotic discovery”. In: *Nat. Rev. Drug Discov.* 12.5 (2013), pp. 371–87.

[9] A. T. Society. “Guidelines for the Management of Adults with Hospital-acquired, Ventilator-associated, and Healthcare-associated Pneumonia”. In: *Am. J. Respir. Crit. Care Med.* 171.4 (2005), pp. 388–416.

[10] A. C. Kalil et al. “Management of Adults With Hospital-acquired and Ventilator-associated Pneumonia: 2016 Clinical Practice Guidelines by the Infectious Diseases Society of America and the American Thoracic Society”. In: *Clin. Infect. Dis.* 63.5 (2016), e61–e111.

[11] J. P. Torella, R. Chait, and R. Kishony. “Optimal drug synergy in antimicrobial treatments”. In: *PLoS Comput. Biol.* 6.6 (2010), e1000796.

[12] S.-J. J. Yang et al. “Daptomycin-oxacillin combinations in treatment of experimental endocarditis caused by daptomycin-nonsusceptible strains of methicillin-resistant Staphylococcus aureus with evolving oxacillin susceptibility (the ”seesaw effect”)”. In: *Antimicrob. Agents Chemother.* 54.8 (2010), pp. 3161–3169.

[13] J.-B. Michel et al. “Drug interactions modulate the potential for evolution of resistance”. In: *Proc. Natl. Acad. Sci. U. S. A.* 105.39 (2008), pp. 14918–23.

[14] C. R. Bonapace et al. “Comparison of methods of interpretation of checkerboard synergy testing”. In: *Diagn. Microbiol. Infect. Dis.* 44.4 (2002), pp. 363–366.

[15] E. I. Nielsen and L. E. Friberg. “Pharmacokinetic-pharmacodynamic modeling of antibacterial drugs”. In: *Pharmacol. Rev.* 65.3 (2013), pp. 1053–90.

[16] S. G. Wicha et al. “Pharmacodynamic and response surface analysis of linezolid or vancomycin combined with meropenem against Staphylococcus aureus”. In: *Pharm. Res.* (2015).

[17] P. Yeh, A. I. Tschumi, and R. Kishony. “Functional classification of drugs by properties of their pairwise interactions”. In: *Nat. Genet.* 38.4 (2006), pp. 489–94.

[18] J. B. Bulitta et al. “Development and qualification of a pharmacodynamic model for the pronounced inoculum effect of ceftazidime against Pseudomonas aeruginosa”. In: *Antimicrob. Agents Chemother.* 53.1 (2009), pp. 46–56.

[19] K. N. Agwuh and A. MacGowan. “Pharmacokinetics and pharmacodynamics of the tetracyclines including glycylcyclines”. In: *J. Antimicrob. Chemother.* 58.2 (2006), pp. 256–265.

[20] C. Nightingale et al. *Antimicrobial pharmacodynamics in theory and clinical practice, 2nd Edition*. 2nd. Informa Healthcare, 2007.

[21] D. Czock et al. “Pharmacokinetics and pharmacodynamics of antimicrobial drugs”. In: *Expert Opin. Drug Metab. Toxicol.* 5.5 (2009), pp. 475–87.

[22] S. G. Wicha et al. “TDMx: A novel web-based open-access support tool for optimising antimicrobial dosing regimens in clinical routine”. In: *Int. J. Antimicrob. Agents* 45.4 (2015), pp. 442–444.

[23] C. Scheerans et al. “Concentration-response studies and modelling of the pharmacodynamics of linezolid: Staphylococcus aureus versus Enterococcus faecium”. In: *Int. J. Antimicrob. Agents* 45.1 (2015), pp. 54–60.

[24] H. Bremer and P. P. P. Dennis. “Modulation of Chemical Composition and Other Parameters of the Cell by Growth Rate”. In: *Escherichia Coli Salmonella Typhimurium Vol 2 Cell. Mol. Biol.* Ed. by F. C. Neidhardt. 2. 122. American Society for Microbiology, 1987. Chap. 96, pp. 1527–1540.

[25] S. Cooper. *Bacterial growth and division: biochemistry and regulation of prokaryotic and eukaryotic division cycles*. San Diego: Academic Press, 1991, pp. 1–501.

[26] S. G. Wicha. “Integrated in vitro and in silico studies for optimisation of broad-spectrum antibiotic combination therapy”. PhD thesis. FU Berlin, 2015.

[27] R. E. Buchanan. “Life Phases in a Bacterial Culture”. In: *J. Infect. Dis.* 23.2 (1918), pp. 109–125.

[28] E. Bosdriesz et al. “How fast-growing bacteria robustly tune their ribosome concentration to approximate growth-rate maximization”. In: *FEBS J.* 282.10 (2015), pp. 2029–2044.

[29] M. Scott et al. “Emergence of robust growth laws from optimal regulation of ribosome synthesis”. In: *Mol. Syst. Biol.* 10.8 (2014), p. 747.

[30] D. Schultz and R. Kishony. “Optimization and control in bacterial lag phase”. In: *BMC Biol.* 11 (2013), pp. 120–123.

[31] M. D. Rolfe et al. “Lag phase is a distinct growth phase that prepares bacteria for exponential growth and involves transient metal accumulation”. In: *J. Bacteriol.* 194.3 (2012), pp. 686–701.

[32] K. Kath and A. L. Koch. “Protein degradation in Escherichia coli”. In: *J. Biol. Chem.* 246.22 (1971), pp. 6956–6967.

[33] M. Nomura, R. Gourse, and G. Baughman. “Regulation of the synthesis of ribosomes and ribosomal components”. In: *Annu. Rev. Biochem.* 53 (1984), pp. 75–117.

[34] K. Piir et al. “Ribosome degradation in growing bacteria”. In: *EMBO Rep.* 12.5 (2011), pp. 458–62.

[35] A. Ishihama. “Modulation of the nucleoid, the transcription apparatus, and the translation machinery in bacteria for stationary phase survival”. In: *Genes to Cells* 4.3 (1999), pp. 135–143.

[36] D. Ren et al. “Stationary-Phase Quorum-Sensing Signals Affect Autoinducer-2 and Gene Expression in Escherichia coli”. In: *Appl. Environ. Microbiol.* 70.4 (2004), pp. 2038–2043.

[37] M. H. Zwietering et al. “Modeling of the bacterial growth curve”. In: *Appl. Environ. Microbiol.* 56.6 (1990), pp. 1875–81.

[38] N Nanninga, L. J. H. Koppes, and F. C. de Vries-Tijssen. “The Cell Cycle of Bacillus subtilis as Studies by Electron Microscopy”. In: *Arch. Microbiol.* 123 (1979), pp. 173–181.

[39] M. E. Sharpe, P. M. Hauser, and R. G. Sharpe. “Bacillus subtilis Cell Cycle as Studied by Fluorescence Microscopy : Constancy of Cell Length at Initiation of DNA Replication and Evidence for Active Nucleoid Partitioning”. In: *J. Bacteriol.* 180.3 (1998), pp. 547–555.

[40] S. Cooper and C. E. Helmstetter. “Chromosome replication and the division cycle of Escherichia coli B/r”. In: *J. Mol. Biol.* 31.3 (1968), pp. 519–40.

[41] M. Watve et al. “Aging may be a conditional strategic choice and not an inevitable outcome for bacteria”. In: *Proc. Natl. Acad. Sci. U. S. A.* 103.40 (2006), pp. 14831–5.

[42] P. H. Leslie. *On the use of matrices in certain population mathematics.* 1945.

[43] H Bremer, G Churchward, and R Young. “Relation between growth and replication in bacteria”. In: *J. Theor. Biol.* 81.3 (1979), pp. 533–45.

[44] M. Scott et al. “Interdependence of Cell Growth Origins and Consequences”. In: *Science.* 330.November (2010), pp. 1099–1102.

[45] D.-J. Scheffers. “Bacterial Reproduction and Growth”. In: *eLS* (2013).

[46] M Schaechter, O Maaloe, and N Kjeldgaard. “Dependency on Medium and Temperature of Cell Size and Chemical Composition during Balanced Growth of Salmonella typhimurium”. In: *J. gen. Microbiol.* 19 (1958), pp. 592–606.

[47] S. E. Martin and J. J. Iandolo. “Translational Control of Protein Synthesis in Staphylococcus aureus”. In: *J. Bacteriol.* 122.3 (1975), pp. 1136–1143.

[48] R. Milo. “What is the total number of protein molecules per cell volume? A call to rethink some published values”. In: *BioEssays* 35.12 (2013), pp. 1050–1055.

[49] M. S. VanNieuwenhze et al. “The total synthesis of lipid I”. In: *J. Am. Chem. Soc.* 123.29 (2001), pp. 6983–6988.

[50] A. L. Lovering, S. S. Safadi, and N. C. J. Strynadka. “Structural Perspective of Peptidoglycan Biosynthesis and Assembly”. In: *Annu. Rev. Biochem.* 81 (2012), pp. 451–478.

[51] B. Alberts et al. *Molecular Biology of THE CELL.* 5. Garland Science, 2008.

[52] I. Chopra. “Tetracycline Analogs Whose Primary Target Is Not the Bacterial Ribosome”. In: *Antimicrob. Agents Chemother.* 38.4 (1994), pp. 637–640.

[53] G. A. Pankey and L. D. Sabath. “Clinical Relevance of Bacteriostatic versus Bactericidal Mechanisms of Action in the Treatment of Gram- Positive Bacterial Infections”. In: *Clin. Infect. Dis.* 38.15 (2004).

[54] T. R. Tritton. “Ribosome-tetracycline interactions”. In: *Biochemistry* 16.18 (1977), pp. 4133–4138.

[55] M. A. Kohanski, D. J. Dwyer, and J. J. Collins. “How antibiotics kill bacteria: from targets to networks”. In: *Nat. Rev. Microbiol.* 8.6 (2010), pp. 423–35.

[56] D. N. Wilson. “The A-Z of bacterial translation inhibitors”. In: *Crit. Rev. Biochem. Mol. Biol.* 44.6 (2009), pp. 393–433.

[57] U Geigenmüller and K. H. Nierhaus. “Tetracycline can inhibit tRNA binding to the ribosomal P site as well as to the A site”. In: *Eur. J. Biochem.* 161.3 (1986), pp. 723–726.

[58] I. Chopra and M. Roberts. “Tetracycline Antibiotics: Mode of Action, Applications, Molecular Biology, and Epidemiology of Bacterial Resistance”. In: *Microbiol. Mol. Biol. Rev.* 65.2 (2001), pp. 232–260.

[59] J. Wu, Q. Long, and J. Xie. “(p)ppGpp and Drug Resistance”. In: *J. Cell. Physiol.* 300.March (2010), pp. 300–304.

[60] E. Maisonneuve, M. Castro-Camargo, and K. Gerdes. “(p)ppGpp controls bacterial persistence by stochastic induction of toxin-antitoxin activity”. In: *Cell* 154.5 (2013), pp. 1140–1150.

[61] R. M. Corrigan et al. “ppGpp negatively impacts ribosome assembly affecting growth and antimicrobial tolerance in Gram-positive bacteria”. In: *Proc. Natl. Acad. Sci.* 113.12 (2016), E1710–E1719.

[62] D. Nguyen et al. “Active starvation responses mediate antibiotic tolerance in biofilms and nutrient-limited bacteria”. In: *Science* 334.6058 (2011), pp. 982–6.

[63] R. A. VanBogelen and F. C. Neidhardt. “Ribosomes as sensors of heat and cold shock in Escherichia coli”. In: *Proc. Natl. Acad. Sci. U. S. A.* 87.15 (1990), pp. 5589–93.

[64] P. Greulich et al. “Growth-dependent bacterial susceptibility to ribosome-targeting antibiotics”. In: *Mol. Syst. Biol.* 11.796 (2014), pp. 1–11.

[65] S. Rudorf et al. “Deducing the kinetics of protein synthesis in vivo from the transition rates measured in vitro”. In: *PLoS Comput. Biol.* 10.10 (2014), e1003909.

[66] R. Cox. “Quantitative relationships for specific growth rates and macromolecular compositions of Mycobacterium tuberculosis, Streptomyces coelicolor A3(2) and Escherichia coli B/r: an integrative theoretical approach.” In: *Microbiology* 150 (2004), pp. 1413–1426.

[67] L. L. Barton. *Structural and Functional Relationships in Prokaryotes*. 2005.

[68] J. Abranches et al. “The Molecular Alarmone (p)ppGpp Mediates Stress Responses, Vancomycin Tolerance, and Virulence in Enterococcus faecalis”. In: *J. Bacteriol.* 191.7 (2009), pp. 2248–2256.

[69] W. Gao et al. “Two novel point mutations in clinical Staphylococcus aureus reduce linezolid susceptibility and switch on the stringent response to promote persistent infection”. In: *PLoS Pathog.* 6.6 (2010).

[70] C. Kim et al. “The mechanism of heterogeneous beta-lactam resistance in MRSA: Key role of the stringent stress response”. In: *PLoS One* 8.12 (2013), pp. 1–10.

[71] N. Eliakim-Raz et al. “Efficacy and safety of chloramphenicol: Joining the revival of old antibiotics? Systematic review and meta-analysis of randomized controlled trials”. In: *J. Antimicrob. Chemother.* 70.4 (2015), pp. 979–996.

[72] F Schlünzen et al. “Structural basis for the interaction of antibiotics with the peptidyl transferase centre in eubacteria”. In: *Nature* 413.6858 (2001), pp. 814–821.

[73] N. Koyama, J. Inokoshi, and H. Tomoda. “Anti-infectious agents against MRSA”. In: *Molecules* 18.1 (2012), pp. 204–24.

[74] W. A. Craig. “The pharmacology of meropenem, a new carbapenem antibiotic”. In: *Infect. Dis. Soc. Am.* 24 Suppl 2 (1997), S266–S275.

[75] K. M. Papp-Wallace et al. “Carbapenems: Past, Present, and Future”. In: *Antimicrob. Agents Chemother.* 55.11 (2011), pp. 4943–4960.

[76] M. S. Wilke, A. L. Lovering, and N. C. Strynadka. “β-Lactam antibiotic resistance: a current structural perspective”. In: *Curr. Opin. Microbiol.* 8.5 (2005), pp. 525–533.

[77] M. S. Dryden. “Linezolid pharmacokinetics and pharmacodynamics in clinical treatment”. In: *J. Antimicrob. Chemother.* 66 Suppl 4 (2011), pp. iv7–iv15.

[78] D. J. Diekema and R. N. Jones. “New drug classes Oxazolidinone antibiotics”. In: *Lancet* 358 (2001), pp. 1975–1982.

[79] C. R. Woese, O Kandler, and M. L. Wheelis. “Towards a natural system of organisms: proposal for the domains Archaea, Bacteria, and Eucarya”. In: *Proc. Natl. Acad. Sci. U. S. A.* 87.12 (1990), pp. 4576–4579.

[80] P. a. Vaishampayan et al. “Survival of Bacillus pumilus spores for a Prolonged Period of Time in Real Space Conditions”. In: *Astrobiology* 12.5 (2012), pp. 487–497.

[81] J. Bartholomew and T Mittwer. “The gram stain”. In: *Bacteriol. Rev.* 16 (1952), pp. 1–29.

[82] S. Trifiro et al. “Ghost mycobacteria on Gram stain”. In: *J. Clin. Microbiol.* 28.1 (1990), pp. 146–147.

[83] H. W. Boucher et al. “Bad bugs, no drugs: no ESKAPE! An update from the Infectious Diseases Society of America”. In: *Clin. Infect. Dis.* 48.1 (2009), pp. 1–12.

[84] C. Garzoni and W. L. Kelley. “Staphylococcus aureus: new evidence for intracellular persistence”. In: *Trends Microbiol.* 17.2 (2009), pp. 59–65.

[85] F Kunst and et Al. “The complete genome sequence of the gram-positive bacterium Bacillus subtilis”. In: *Nature* 390.6657 (1997), pp. 249–256.

[86] CLSI. “Performance Standards for Antimicrobial Susceptibility Testing ; Twenty-First Informational Supplement”. In: *CLSI Doc. M100-S21* 31.1 (2011), pp. 42–58.

[87] A. Brauner et al. “Distinguishing between resistance, tolerance and persistence to antibiotic treatment”. In: *Nat. Rev. Microbiol.* 14.5 (2016), pp. 320–30.

[88] J. W. Mouton et al. “The role of pharmacokinetics/pharmacodynamics in setting clinical MIC breakpoints: the EUCAST approach.” In: *Clin. Microbiol. Infect.* 18.3 (2012), E37–45.

[89] E. I. Nielsen and L. E. Friberg. “Pharmacokinetic-pharmacodynamic modeling of antibacterial drugs”. In: *Pharmacol. Rev.* 65.3 (2013), pp. 1053–90.

[90] V. H. Tam, A. N. Schilling, and M. Nikolaou. “Modelling time-kill studies to discern the pharmacodynamics of meropenem”. In: *J. Antimicrob. Chemother.* 55.5 (2005), pp. 699–706.

[91] R. Wax et al. *Bacterial resistance to antimicrobials*. 2. CRC Press, 2008.

[92] B. R. Levin and D. E. Rozen. "Non-inherited antibiotic resistance". In: *Nat Rev Microbiol.* 4.7 (2006), pp. 556–562.

[93] S. Motta-Sandoval, P. Cluzel, and M. Aldana. "Adaptive resistance in bacteria requires epigenetic inheritance, genetic noise, and cost of efflux pumps". In: *PLoS One* 10.3 (2015), pp. 3–8.

[94] S. Sandoval-Motta and M. Aldana. "Adaptive resistance to antibiotics in bacteria: A systems biology perspective". In: *Wiley Interdiscip. Rev. Syst. Biol. Med.* 8.3 (2016), pp. 253–267.

[95] N. Q. Balaban et al. "Bacterial Persistenceas a Phenotypic Switch". In: *Science.* 305.September (2004), pp. 1622–1625.

[96] T. K. Wood, S. J. Knabel, and B. W. Kwan. "Bacterial persister cell formation and dormancy". In: *Appl. Environ. Microbiol.* 79.23 (2013), pp. 7116–21.

[97] K. Gerdes and E. Maisonneuve. "Bacterial persistence and toxin-antitoxin loci". In: *Annu. Rev. Microbiol.* 66 (2012), pp. 103–23.

[98] M. A. Orman and M. P. Brynildsen. "Inhibition of stationary phase respiration impairs persister formation in E. coli". In: *Nat. Commun.* 6 (2015), p. 7983.

[99] B. P. Conlon et al. "Persister formation in Staphylococcus aureus is associated with ATP depletion". In: *Nat. Microbiol.* 1.May (2016), p. 16051.

[100] E. Maisonneuve and K. Gerdes. "Molecular mechanisms underlying bacterial persisters". In: *Cell* 157.3 (2014), pp. 539–548.

[101] S. Helaine and E. Kugelberg. "Bacterial persisters: Formation, eradication, and experimental systems". In: *Trends Microbiol.* 22.7 (2014), pp. 417–424.

[102] E. Kussell et al. "Bacterial persistence: a model of survival in changing environments". In: *Genetics* 169.4 (2005), pp. 1807–14.

[103] P. F. Gallagher et al. "Inappropriate prescribing in an acutely ill population of elderly patients as determined by Beers' Criteria". In: *Age Ageing* 37.1 (2008), pp. 96–101.

[104] J. Jia et al. "Mechanisms of drug combinations: interaction and network perspectives". In: *Nat. Rev. Drug Discov.* 8.2 (2009), pp. 111–28.

[105] A. S. Narang, D. Desai, and S. Badawy. "Impact of Excipient Interactions on Drug Bioavailability from Solid Dosage Forms". In: *Pharm. Res.* 29.10 (2012), pp. 2639–2659.

[106] P. J. Yeh et al. "Drug interactions and the evolution of antibiotic resistance". In: *Nat. Rev. Microbiol.* 7.6 (2009), pp. 460–466.

[107] S. Loewe. "The Problem of Synergism and Antagonism of Combined Drugs". In: *Arzneimittelforschung* 3 (1953), pp. 1–5.

[108] G. Koch, J. Schropp, and W. J. Jusko. "Assessment of non-linear combination effect terms for drug–drug interactions". In: *J. Pharmacokinet. Pharmacodyn.* 43.5 (2016), pp. 461–479.

[109] Y. Wang et al. "Past, present and future applications of flow cytometry in aquatic microbiology". In: *Trends Biotechnol.* 28.8 (2010), pp. 416–24.

[110] M. Ehrenberg, H. Bremer, and P. P. Dennis. "Medium-dependent control of the bacterial growth rate". In: *Biochimie* 95.4 (2013), pp. 643–58.

[111] J. H. Christian and J Waltho. “The Composition of Staphylococcus Aureus in Relation To the Water Activity of the Growth Medium”. In: *J. Gen. Microbiol.* 35 (1964), pp. 205–213.

[112] H. D. Hooker. “Liebig’s Law of the Minimum in Relation to general Biological Problems”. In: *Science.* 46.1183 (1917), pp. 197–204.

[113] B. A. Rasmussen, Y Gluzman, and F. P. Tally. “Inhibition of protein synthesis occurring on tetracycline-resistant, TetM-protected ribosomes by a novel class of tetracyclines, the glycylcyclines”. In: *Antimicrob. Agents Chemother.* 38.7 (1994), pp. 1658–1660.

[114] C. Balsalobre. “Concentration matters!! ppGpp, from a whispering to a strident alarmone”. In: *Mol. Microbiol.* 79.4 (2011), pp. 827–9.

[115] H Bremer and P Dennis. “Feedback control of ribosome function in Escherichia coli”. In: *Biochimie* 90.3 (2008), pp. 493–9.

[116] L. D. Plank and J. D. Harvey. “Generation Time Statistics of Escherichia coli B Measured by Synchronous Culture Techniques”. In: *J. Gen. Microbiol.* 115.1 (1979), pp. 69–77.

[117] J. a. Gregory, E. C. Becker, and K. Pogliano. “Bacillus subtilis MinC destabilizes FtsZ-rings at new cell poles and contributes to the timing of cell division”. In: *Genes Dev.* 22.24 (2008), pp. 3475–88.

[118] J Forchhammer and L Lindahl. “Growth rate of polypeptide chains as a function of the cell growth rate in a mutant of Escherichia coli”. In: *J. Mol. Biol.* 55.3 (1971), pp. 563–8.

[119] G Churchward, H Bremer, and R Young. “Macromolecular composition of bacteria”. In: *J. Theor. Biol.* 94.3 (1982), pp. 651–70.

[120] S. Klumpp et al. “Molecular crowding limits translation and cell growth”. In: *Proc. Natl. Acad. Sci. U. S. A.* 110.42 (2013), pp. 16754–9.

[121] M. R. W. Brown and E. R. Garret. “Kinetics and Mechanisms of Action of Antibiotics on Microorganisms I - Reproducibility of Escherichia coli Growth Curves and Dependence Upon Tetracycline Concentration”. In: *J. Pharm. Sci.* 53.2 (1964), pp. 179–183.

[122] E. R. Garrett and C. M. Won. “Kinetics and Mechanisms of Drug Action on Microorganisms XVII: Bactericidal Effects of Penicillin, Kanamycin, and Rifampin with and without Organism Pretreatment with Bacteriostatic Chloramphenicol, Tetracycline, and Novobiocin”. In: *J. Pharm. Sci.* 62.10 (1973), pp. 1666–1673.

[123] W. A. Hussin and W. M. El-Sayed. “Synergic Interaction Between Selected Botanical Extracts and Tetracycline Against Gram Positive and Gram Negative Bacteria”. In: *J. Biol. Sci.* 11.7 (2011), pp. 433–441.

[124] L. J. L. Norcia and A. M. Silvia. “Studies on Time-Kill Kinetics of Different Classes of Antibiotics Against Veterinary Pathogenic Bacteria Including Pasteurella, Actinobaciluus and Escherichia coli”. In: *J. Antibiot. (Tokyo).* 52.1 (1999), pp. 52–60.

[125] I. S. Radzishevsky et al. “Improved antimicrobial peptides based on acyl-lysine oligomers”. In: *Nat. Biotechnol.* 25.6 (2007), pp. 657–9.

[126] L. Migliore, A. Rotini, and M. C. Thaller. “Low Doses of Tetracycline Trigger the E. coli Growth: A Case of Hormetic Response.” In: *Dose-response* 11.4 (2013), pp. 565–572.

[127] E. R. Garrett and G. H. Miller. “Kinetics and Mechanisms of Action of Antibiotics on Microorganisms III - Inhibitory Action of Tetracycline and Chloramphenicol on Escherichia coli Established By Total and Viable Counts”. In: *J. Pharm. Sci.* 54.3 (1965), pp. 427–431.

[128] H. Funakoshi and A. Yamada. “Transition Phenomena in Bacterial Growth Between Logarithmic and Stationary Phases”. In: *J. Math. Biol.* 9 (1980), pp. 369–387.

[129] I. a. M. Swinnen et al. “Predictive modelling of the microbial lag phase: a review”. In: *Int. J. Food Microbiol.* 94.2 (2004), pp. 137–59.

[130] S. Klumpp, Z. Zhang, and T. Hwa. “Growth rate-dependent global effects on gene expression in bacteria”. In: *Cell* 139.7 (2009), pp. 1366–75.

[131] M. Ueta, C. Wada, and A. Wada. “Formation of 100S ribosomes in Staphylococcus aureus by the hibernation promoting factor homolog SaHPF”. In: *Genes to Cells* 15.1 (2010), pp. 43–58.

[132] T. L. Smith et al. “Emergence of vancomycin resistance in Staphylococcus aureus”. In: *N. Engl. J. Med.* 345.19 (2011), pp. 1359–1367.

[133] I. C. V. Palazzo, M. L. C. Araujo, and A. L. C. Darini. “First Report of Vancomycin-Resistant Staphylococci Isolated from Healthy Carriers in Brazil”. In: *J. Clin. Microbiol.* 43.1 (2005), pp. 179–185.

[134] L Cui et al. “Cell wall thickening is a common feature of vancomycin resistance in Staphylococcus aureus”. In: *J Clin Microbiol* 41.1 (2003), pp. 5–14.

[135] K. Sieradzki, M. G. Pinho, and A. Tomasz. “Inactivated pbp4 in Highly Glycopeptide-resistant Laboratory Mutants of Staphylococcus aureus”. In: *J Biol Chem* 274.27 (1999), pp. 18942–18946.

[136] C. Kreutz et al. “Profile likelihood in systems biology”. In: *FEBS J.* 280.11 (2013), pp. 2564–2571.

[137] T. R. Paul et al. “Localization of penicillin-binding proteins to the splitting system of Staphylococcus aureus septa by using a mercury-penicillin V derivative”. In: *J. Bacteriol.* 177.13 (1995), pp. 3631–3640.

[138] P. Giesbrecht et al. “Staphylococcal Cell Wall: Morphogenesis and Fatal Variations in the Presence of Penicillin”. In: *Microbiol. Mol. Biol. Rev.* 62.4 (1998), pp. 1371–1414.

[139] C. C. S. Fuda, J. F. Fisher, and S. Mobashery. “Beta-Lactam resistance in Staphylococcus aureus: The adaptive resistance of a plastic genome”. In: *Cell. Mol. Life Sci.* 62.22 (2005), pp. 2617–2633.

[140] F. Lowy. “Antimicrobial resistance: the example of Staphylococcus aureus”. In: *J. Clin. Invest.* 111.9 (2003), pp. 1265–1273.

[141] Z. Yao, D. Kahne, and R. Kishony. “Distinct Single-Cell Morphological Dynamics under Beta-Lactam Antibiotics”. In: *Mol. Cell* 48 (2012), pp. 705–712.

[142] R. L. White et al. “Comparative in vitro pharmacodynamics of imipenem and meropenem against ATCC strains of Escherichia coli, Staphylococcus aureus and Bacteroides fragilis”. In: *Diagn. Microbiol. Infect. Dis.* 39.1 (2001), pp. 39–47.

[143] S. G. Wicha and C. Kloft. “Simultaneous determination and stability studies of linezolid, meropenem and vancomycin in bacterial growth medium by high-performance liquid chromatography”. In: *J. Chromatogr. B* 1028 (2016), pp. 242–248.

[144] L. Fernández and R. E. W. Hancock. “Adaptive and mutational resistance: role of porins and efflux pumps in drug resistance”. In: *Clin. Microbiol. Rev.* 25.4 (2012), pp. 661–81.

[145] R. A. Villet et al. “Regulation of Expression of abcA and Its Response to Environmental Conditions”. In: *J. Bacteriol.* 196.8 (2014), pp. 1532–1539.

[146] S. Kumar, M. M. Mukherjee, and M. F. Varela. “Modulation of Bacterial Multidrug Resistance Efflux Pumps of the Major Facilitator Superfamily”. In: *Int. J. Bacteriol.* 2013 (2013), pp. 1–15.

[147] H Eagle and A. D. Musselman. “The rate of bactericidal action of penicillin in vitro as a function of its concentration, and its paradoxically reduced activity at high concentrations against certain organisms.” In: *J. Exp. Med.* 88.1 (1948), pp. 99–131.

[148] A. A. Firsov et al. “Parameters of bacterial killing and regrowth kinetics and antimicrobial effect examined in terms of area under the concentration-time curve relationships: Action of ciprofloxacin against Escherichia coli in an in vitro dynamic model”. In: *Antimicrob. Agents Chemother.* 41.6 (1997), pp. 1281–1287.

[149] A. Solms. “Integrating Nonlinear Mixed Effects and Physiologically-Based Modeling Approaches for the Analysis of Repeated Measurement Studies”. PhD thesis. University of Potsdam, 2017.

[150] H. Haario et al. “DRAM: Efficient adaptive MCMC”. In: *Stat. Comput.* 16 (2006), pp. 339–354.

[151] H. Haario, E. Saksman, and J. Tamminen. “Componentwise adaptation for high dimensional MCMC”. In: *Comput. Stat.* 20 (2005), pp. 265–273.

[152] A. Gelman and D. B. Rubin. “Inference from Iterative Simulation Using Multiple Sequences”. In: *Stat. Sci.* 7.4 (1992), pp. 457–511.

[153] W. L. Martinez and A. R. Martinez. *Computational Statistics Handbook with Matlab.* 2nd. 2008.

[154] S. R. Singh et al. “In vitro 24-hour time-kill studies of vancomycin and linezolid in combination versus methicillin-resistant Staphylococcus aureus”. In: *Antimicrob. Agents Chemother.* 53.10 (2009), pp. 4495–4497.

[155] T. Geiger et al. “Two Small (p)ppGpp Synthases in Staphylococcus aureus Mediate Tolerance against Cell Envelope Stress Conditions”. In: *J. Bacteriol.* 196.4 (2014), pp. 894–902.

[156] V. Dengler et al. “Induction kinetics of the Staphylococcus aureus cell wall stress stimulon in response to different cell wall active antibiotics”. In: *BMC Microbiol.* 11.1 (2011), p. 16.

[157] R. Fontana et al. “Paradoxical Response of Enterococcus faecalis to the Bactericidal Activity of Penicillin Is Associated with Reduced Activity of One Autolysin”. In: *Antimicrob. Agents Chemother.* 34.2 (1990), pp. 314–320.

[158] T. Nishino and S. Nakazawa. “Bacteriological Study on Effects of Beta-Lactam Group Antibiotics in High Concentrations”. In: *Antimicrob. Agents Chemother.* 9.6 (1976), pp. 1033–1042.

[159] E. Yourassowsky et al. “Paradoxical Action of Penicillin G on Staphylococcus aureus: a Time Study of the Effect of a Zonal Antibiotic Concentration Gradient on Bacterial Growth”. In: *Antimicrob. Agents Chemother.* 8.3 (1975), pp. 262–265.

[160] R. J. Doyle, J Chaloupka, and V Vinter. “Turnover of cell walls in microorganisms”. In: *Microbiol. Rev.* 52.4 (1988), pp. 554–567.

[161] R. L. White et al. “Comparison of three different in vitro methods of detecting synergy: time-kill , checkerboard , and E test”. In: *Antimicrob. Agents Chemother.* 40.8 (1996), pp. 1914–1918.

[162] C. Scheerans. "In vitro pharmacodynamics, pharmacokinetic/pharmacodynamic modelling, in silico simulation and evaluation of dosing regimens for linezolid". PhD thesis. Martin-Luther-Universität Halle-Wittenberg, 2010, pp. 1–183.

[163] A. Y. Weiße et al. "Mechanistic links between cellular trade-offs, gene expression, and growth". In: *Proc. Natl. Acad. Sci.* 112.9 (2015), E1038–E1047.

[164] J. Shepherd and M. Ibba. "Direction of aminoacylated transfer RNAs into antibiotic synthesis and peptidoglycan-mediated antibiotic resistance". In: *FEBS Lett.* 587.18 (2013), pp. 2895–2904.

[165] B. J. Paul et al. "rRNA transcription in Escherichia coli". In: *Annu. Rev. Genet.* 38 (2004), pp. 749–770.

[166] T. Siibak et al. "Erythromycin- and chloramphenicol-induced ribosomal assembly defects are secondary effects of protein synthesis inhibition". In: *Antimicrob. Agents Chemother.* 53.2 (2009), pp. 563–571.

[167] N. Hartung. "Parameter non-identifiability of the Gyllenberg-Webb ODE model". In: *J. Math. Biol.* 68.1-2 (2014), pp. 41–55.

Appendix A

Appendix

A.1 Persister fraction during exponential growth

In the following, we derive the approximation stated in eq. (3.5). Consider the following ODE system describing the rate of change of a population consisting of normal $n = n(t)$ and persisting $p = p(t)$ cells during exponential growth

$$\frac{\mathrm{d}}{\mathrm{d}t}n = k_{\text{net}} \cdot n - k_{\text{np,eff}} \cdot n + k_{\text{pn,eff}} \cdot p \tag{A.1}$$

$$\frac{\mathrm{d}}{\mathrm{d}t}p = k_{\text{np,eff}} \cdot n - k_{\text{pn,eff}} \cdot p. \tag{A.2}$$

As it is typically the case, we assumed $k_{\text{np,eff}} \ll k_{\text{net}}$ and $k_{\text{pn,eff}} \ll k_{\text{net}}$. For convenience we set $n(0) = 1$ and $p(0) = 0$. Thus, n was to good approximation given by $n = \exp(k_{\text{net}} \cdot t)$. This resulted to

$$\frac{\mathrm{d}}{\mathrm{d}t}p = k_{\text{np,eff}} \cdot \exp(k_{\text{net}} \cdot t) - k_{\text{pn,eff}} \cdot p. \tag{A.3}$$

Solving for p gave

$$\begin{aligned}
p &= p(0) \cdot \exp(-k_{\text{pn,eff}} \cdot t) \\
&\quad + \int_0^t k_{\text{np,eff}} \cdot \exp(k_{\text{net}} \cdot s) \cdot \exp(-k_{\text{pn,eff}} \cdot (t-s))\,\mathrm{d}s && \text{(A.4)} \\
&= k_{\text{np,eff}} \cdot \int_0^t \exp((k_{\text{net}} + k_{\text{pn,eff}})s)\,\mathrm{d}s \cdot \exp(-k_{\text{pn,eff}} \cdot t) && \text{(A.5)} \\
&= k_{\text{np,eff}} \cdot \exp(-k_{\text{np,eff}} \cdot t) \cdot \frac{1}{k_{\text{net}} + k_{\text{pn,eff}}} \cdot \exp((k_{\text{net}} + k_{\text{pn,eff}}) \cdot s)\Big|_0^t && \text{(A.6)} \\
&= k_{\text{np,eff}} \cdot \exp(-k_{\text{np,eff}} \cdot t) \frac{1}{k_{\text{net}} + k_{\text{pn,eff}}} \cdot \big(\exp((k_{\text{net}} + k_{\text{pn,eff}}) \cdot t) - 1\big) && \text{(A.7)} \\
&= \frac{k_{\text{np,eff}}}{k_{\text{net}} + k_{\text{pn}}}\big(\exp(k_{\text{net}} \cdot t) - \exp(-k_{\text{np,eff}} \cdot t)\big). && \text{(A.8)}
\end{aligned}$$

From this one can show that the persister fraction defined in eq. (3.4) is approximated by

$$f_{\text{p,exp}} \approx \frac{k_{\text{np,eff}}}{k_{\text{np,eff}} + k_{\text{net}} + k_{\text{pn,eff}}}. \tag{A.9}$$

An alternative to this approximation has been pointed out in [167]: considering the system of ODEs in eqs. (A.1) and (A.2) with the same assumptions ($k_{\text{np,eff}} \ll k_{\text{net}}$ and $k_{\text{pn,eff}} \ll k_{\text{net}}$) and defining the total bacteria count $N = N(t) = n + p$, this implies

$$\frac{\mathrm{d}}{\mathrm{d}t}N = k_{\text{net}} \cdot n \qquad \text{and} \qquad \frac{\mathrm{d}^2}{\mathrm{d}t^2}N = k_{\text{net}} \cdot \frac{\mathrm{d}}{\mathrm{d}t}n, \tag{A.10}$$

leading to the second order equation

$$\frac{\mathrm{d}^2}{\mathrm{d}t^2}N = (k_{\text{net}} - k_{\text{np,eff}} - k_{\text{pn,eff}}) \cdot \frac{\mathrm{d}}{\mathrm{d}t}N + k_{\text{net}} \cdot k_{\text{pn,eff}} \cdot N, \tag{A.11}$$

which is a Sturm-Liouville equation and has the known solution

$$N(t) = N(0) \cdot [\alpha \cdot \exp(0.5t \cdot (A + \sqrt{A^2 + 4B})) + (1-\alpha) \cdot \exp(0.5t \cdot (A - \sqrt{A^2 + 4B}))], \tag{A.12}$$

with $A = k_{\text{net}} - k_{\text{np,eff}} - k_{\text{pn,eff}}$, $B = k_{\text{net}} \cdot k_{\text{pn,eff}}$ and some proportionality factor α. Since we have $n = 1/k_{\text{net}} \cdot \frac{\mathrm{d}}{\mathrm{d}t}N$, it follows that $n/N = 1/k_{\text{net}} \cdot \frac{\mathrm{d}}{\mathrm{d}t}N \cdot 1/N$. Finally we write the quotient using the derivative of the solution, where the $1 - \alpha$ weighted term approaches zero for large t, and α cancels out yielding

$$f_{\text{p,exp}} = 1 - \frac{k_{\text{net}} - k_{\text{np,eff}} - k_{\text{pn,eff}} + \sqrt{(k_{\text{net}} - k_{\text{np,eff}} - k_{\text{pn,eff}})^2 + 4k_{\text{net}} \cdot k_{\text{pn,eff}}}}{2k_{\text{net}}}. \tag{A.13}$$

A.2 Comprehensive effect equations

Find below the effect equations used in "Cell-level model of bacterial population growth for antibiotic combinations" (p. 56). The corresponding parameter estimates are compiled in Table 6.1 and Table 6.2.

TET growth reduction
$$E_{\mathrm{TET,g}} = \frac{\mathrm{Emax}_{\mathrm{TET,g}} \cdot \mathrm{TET}^{\gamma_{\mathrm{TET,g}}}}{(\frac{\mathrm{rib_c}}{\mathrm{rib}} \cdot \mathrm{EC50}_{\mathrm{TET,g}})^{\gamma_{\mathrm{TET,g}}} + \mathrm{TET}^{\gamma_{\mathrm{TET,g}}}} \quad \text{(A.14)}$$

TET death effect
$$E_{\mathrm{TET,d}} = \frac{\mathrm{Emax}_{\mathrm{TET,d}} \cdot \mathrm{TET}^{\gamma_{\mathrm{TET,d}}}}{(\frac{\mathrm{rib_c}}{\mathrm{rib}} \cdot \mathrm{EC50}_{\mathrm{LZD,d}})^{\gamma_{\mathrm{TET,d}}} + \mathrm{TET}^{\gamma_{\mathrm{TET,d}}}} \quad \text{(A.15)}$$

TET persister formation
$$E_{\mathrm{TET,p}} = \frac{\mathrm{Emax}_{\mathrm{TET,p}} \cdot \mathrm{TET}^{\gamma_{\mathrm{TET,p}}}}{\mathrm{EC50}_{\mathrm{LZD,p}}^{\gamma_{\mathrm{TET,p}}} + \mathrm{TET}^{\gamma_{\mathrm{TET,p}}}} \quad \text{(A.16)}$$

VAN death effect
$$E_{\mathrm{VAN_t,d}} = \frac{\mathrm{Emax}_{\mathrm{VAN_t,d}} \cdot \mathrm{VAN_t}^{\gamma_{\mathrm{VAN_t,d}}}}{\mathrm{EC50}_{\mathrm{VAN_t,d}}^{\gamma_{\mathrm{VAN_t,d}}} + \mathrm{VAN_t}^{\gamma_{\mathrm{VAN_t,d}}}} \quad \text{(A.17)}$$

VAN adaptive resistance
$$E_{\mathrm{VAN_t,ARV}} = \frac{k_{\mathrm{g}} \cdot \frac{\mathrm{rib}}{\mathrm{rib_c}} \cdot \mathrm{Emax}_{\mathrm{VAN_t,ARV}} \cdot \mathrm{VAN_t}^{\gamma_{\mathrm{VAN_t,ARV}}}}{\mathrm{EC50}_{\mathrm{VAN_t,ARV}}^{\gamma_{\mathrm{VAN_t,ARV}}} + \mathrm{VAN_t}^{\gamma_{\mathrm{VAN_t,ARV}}}} \quad \text{(A.18)}$$

VAN persister formation
$$E_{\mathrm{VAN,p}} = \frac{\mathrm{Emax}_{\mathrm{VAN,p}} \cdot \mathrm{VAN}^{\gamma_{\mathrm{VAN,p}}}}{\mathrm{EC50}_{\mathrm{VAN,p}}^{\gamma_{\mathrm{VAN,p}}} + \mathrm{VAN}^{\gamma_{\mathrm{VAN,p}}}} \quad \text{(A.19)}$$

MER death effect
$$E_{\mathrm{eMER,d}} = \frac{k_{\mathrm{g}} \cdot \mathrm{Emax}_{\mathrm{eMER,d}} \cdot \mathrm{eMER}^{\gamma_{\mathrm{eMER,d}}}}{\mathrm{EC50}_{\mathrm{eMER,d}}^{\gamma_{\mathrm{eMER,d}}} + \mathrm{eMER}^{\gamma_{\mathrm{eMER,d}}}} \quad \text{(A.20)}$$

MER Eagle effect
$$E_{\mathrm{eMER,E}} = \frac{\mathrm{Emax}_{\mathrm{eMER,g}} \cdot \mathrm{eMER}^{\gamma_{\mathrm{eMER,g}}}}{\mathrm{EC50}_{\mathrm{eMER,g}}^{\gamma_{\mathrm{eMER,g}}} + \mathrm{eMER}^{\gamma_{\mathrm{eMER,g}}}} \quad \text{(A.21)}$$

MER adaptive resistance
$$E_{\mathrm{eMER,ARM}} = \frac{\mathrm{Emax}_{\mathrm{eMER,ARM}} \cdot \mathrm{eMER}^{\gamma_{\mathrm{eMER,ARM}}}}{\mathrm{EC50}_{\mathrm{eMER,ARM}}^{\gamma_{\mathrm{eMER,ARM}}} + \mathrm{eMER}^{\gamma_{\mathrm{eMER,ARM}}}} \quad \text{(A.22)}$$

MER persister formation
$$E_{\mathrm{MER,p}} = \frac{\mathrm{Emax}_{\mathrm{MER,p}} \cdot \mathrm{MER}^{\gamma_{\mathrm{MER,p}}}}{\mathrm{EC50}_{\mathrm{MER,p}}^{\gamma_{\mathrm{MER,p}}} + \mathrm{MER}^{\gamma_{\mathrm{MER,p}}}} \quad \text{(A.23)}$$

LZD growth reduction
$$E_{\mathrm{LZD,g}} = \frac{\mathrm{Emax}_{\mathrm{LZD,g}} \cdot \mathrm{LZD}^{\gamma_{\mathrm{LZD,g}}}}{(\frac{\mathrm{rib_c}}{\mathrm{rib}} \cdot \mathrm{EC50}_{\mathrm{LZD,g}})^{\gamma_{\mathrm{LZD,g}}} + \mathrm{LZD}^{\gamma_{\mathrm{LZD,g}}}} \quad \text{(A.24)}$$

LZD death effect	$E_{\mathrm{LZD,d}}$	$=\frac{\mathrm{Emax}_{\mathrm{LZD,d}} \cdot \mathrm{LZD}^{\gamma_{\mathrm{LZD,d}}}}{(\frac{\mathrm{rib_c}}{\mathrm{rib}} \cdot \mathrm{EC50}_{\mathrm{LZD,d}})^{\gamma_{\mathrm{LZD,d}}} + \mathrm{LZD}^{\gamma_{\mathrm{LZD,d}}}}$	(A.25)
LZD persister formation	$E_{\mathrm{LZD,p}}$	$=\frac{\mathrm{Emax}_{\mathrm{LZD,p}} \cdot \mathrm{LZD}^{\gamma_{\mathrm{LZD,p}}}}{\mathrm{EC50}_{\mathrm{LZD,p}}^{\gamma_{\mathrm{LZD,p}}} + \mathrm{LZD}^{\gamma_{\mathrm{LZD,p}}}}$	(A.26)

A.3 *E. coli* exposed to tetracycline

Table A.1: Parameter estimates (*E. coli*, growth and tetracycline related).

Parameter	Unit	Comment	Maximum a posteriori estimate with 0.05 and 0.95 quantiles of the marginals in brackets exponential phase	lag phase	Bounds / Reference
$\log(N_0)$	log(CFU/ml)	initial inoculum	14.34 (14.15–14.52)		$[0, \log(10^7)]$
rib0	10^{-5}/aa	initial ribosomal concentration	rib_c		fixed
f_p	-	initial persister fraction	0		fixed
$k_{\text{g,c}}$	1/h	control growth rate constant	2.01 (1.71–2.35)		$[0, +\infty]$
$\log(N_{\max})$	log(CFU/ml)	carrying capacity	22.31 (21.71–23.08)		$[\log(10^7), +\infty]$
k_{np}	1/h	switching rate constant (stationary phase, $n \to p$)	1		fixed
k_{pn}	1/h	switching rate constant ($p \to n$)	0.1		fixed
$k_{\text{deg,TET}}$	1/h	degradation rate constant	0		fixed
$\text{EC50}_{\text{TET,g}}$	mg/l	tetracycline growth inhibition, scales with rib_c/rib	0.000142 (0.000122–0.000163)		$[0, +\infty]$
$\gamma_{\text{TET,g}}$	-	tetracycline growth inhibition	4.02 (2.51–8.61)		$[0, +\infty]$
$\text{EC50}_{\text{TET,d}}$	mg/l	tetracycline death induction, scales with rib_c/rib	0.0194 (0.0132–0.0292)		$[0, +\infty]$
$\text{Emax}_{\text{TET,d}}$	1/h	tetracycline death induction	5		fixed
$\text{EC50}_{\text{TET,p}}$	mg/l	tetracycline persister formation	0.0000003		fixed
$\text{Emax}_{\text{TET,p}}$	-	tetracycline persister formation	100		fixed

The maximum effect $\text{Emax}_{\text{TET,g}}$ and slope factors $\gamma_{\text{TET,d}}$, $\gamma_{\text{TET,p}}$ were fixed to 1 to increase parameter identifiability

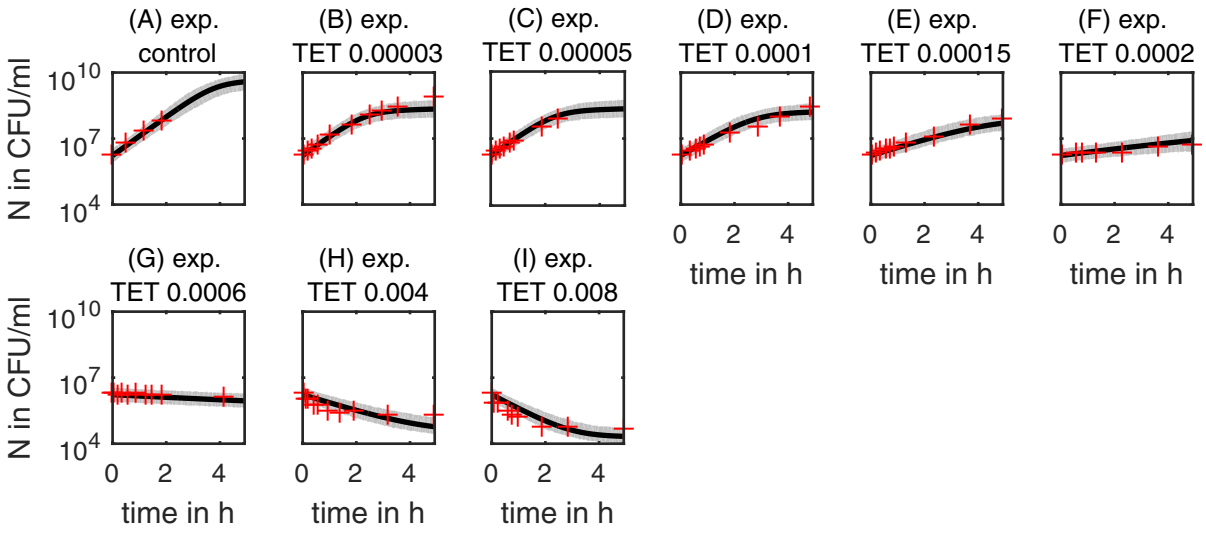

Figure A.1: Time-kill curves (*E. coli*, TET, exp. phase). Exponential phase cultures exposed to different initial concentrations of tetracycline (TET) in mg/l. Data from [121, Fig. 3] shown as red crosses. Solid black line is simulation based on the maximum a posteriori estimate. Gray area represents 0.05 to 0.95 quantile of prediction interval. Note the sparse data situation in the control curve.

A.4 Comprehensive time-kill curves *S. aureus*

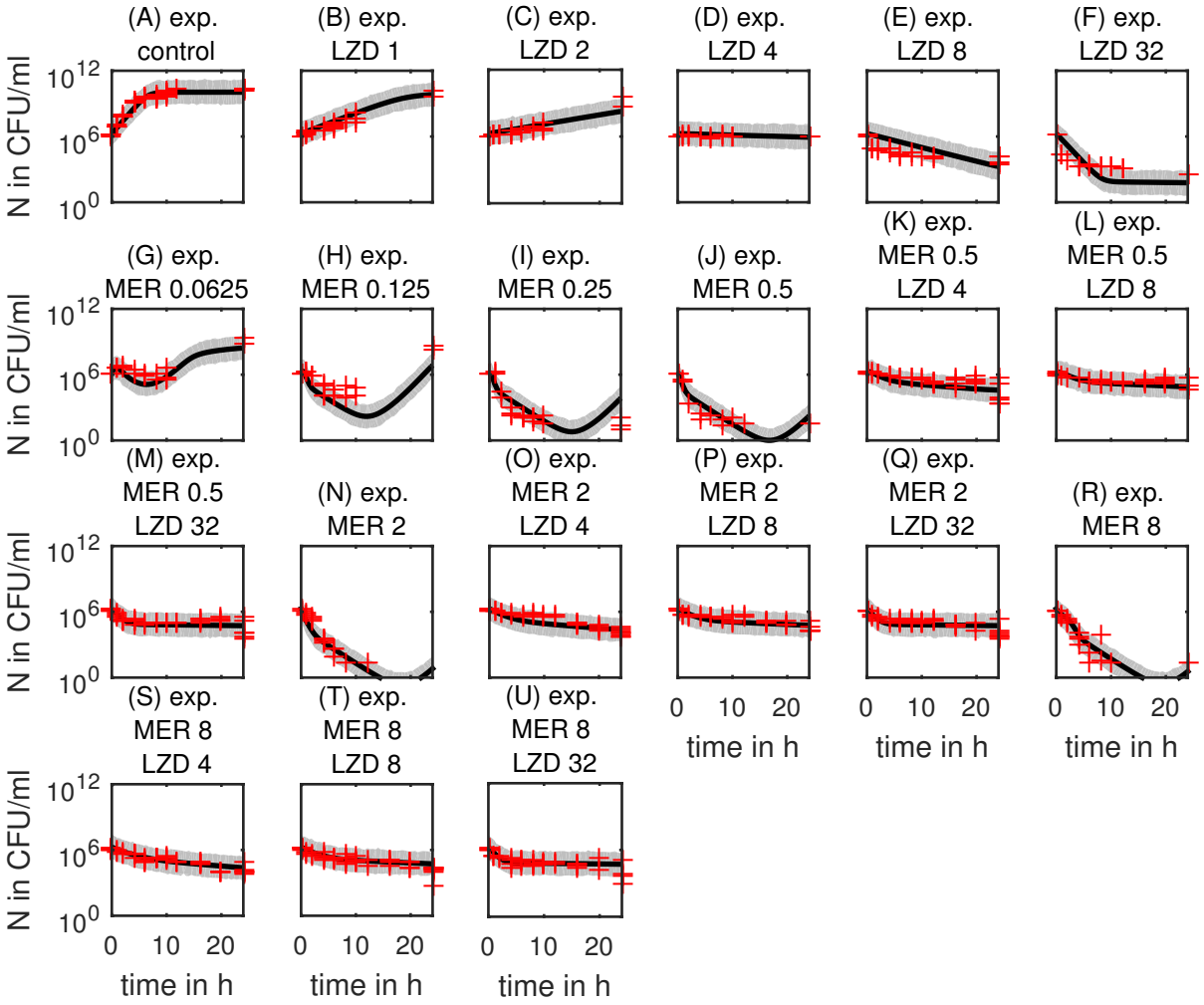

Figure A.2: Time-kill curves (*S. aureus*, MER, LZD, exp. phase). Exponential phase cultures exposed to different initial concentrations of meropenem (MER) and linezolid (LZD) in mg/l. Data as red crosses. Solid black line is simulation based on the maximum a posteriori estimate. Gray area represents 0.05 to 0.95 quantile of prediction interval.

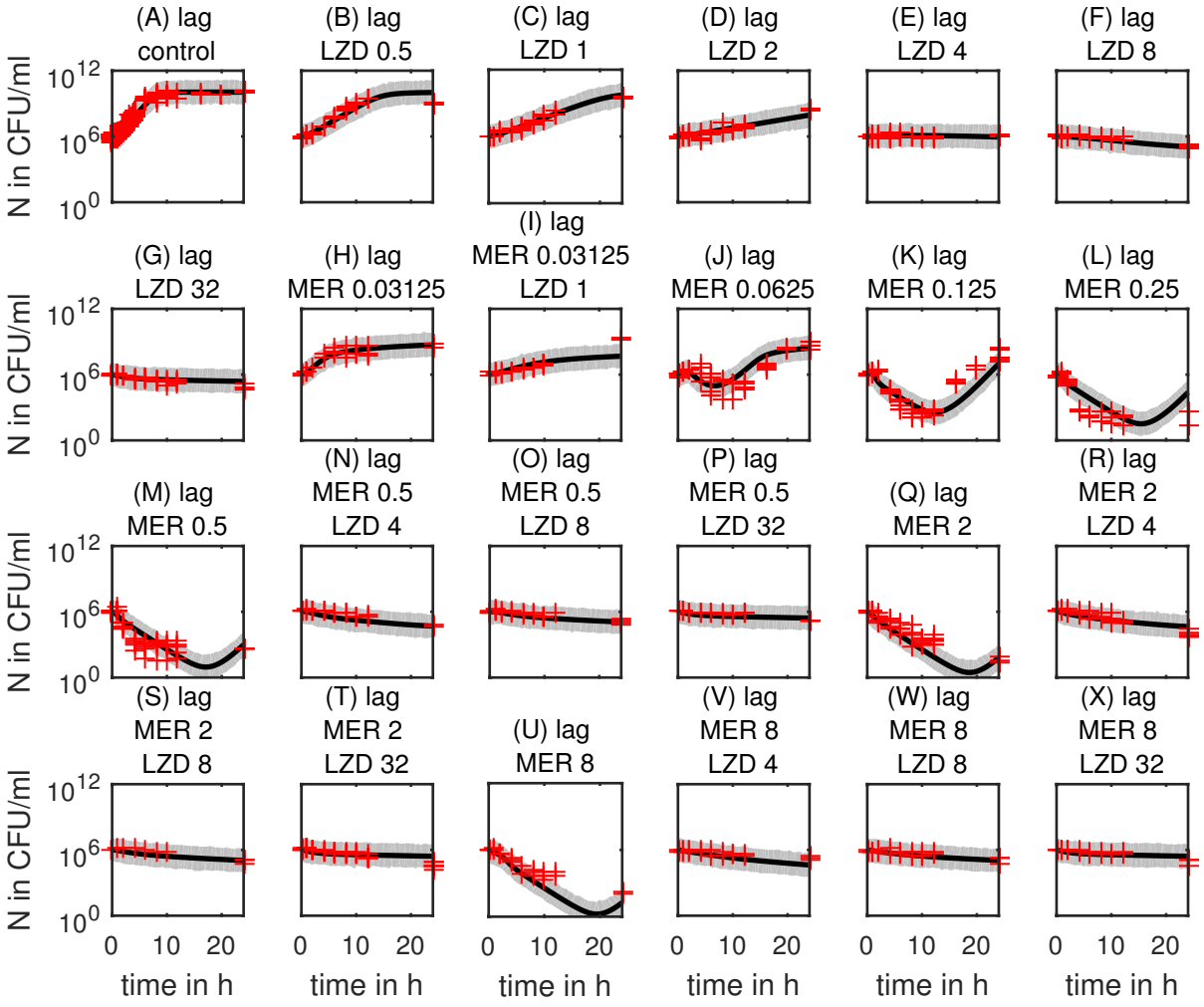

Figure A.3: Time-kill curves (*S. aureus*, MER, LZD, lag phase). Lag phase cultures exposed to different initial concentrations of meropenem (MER) and linezolid (LZD) in mg/l. Data as red crosses. Solid black line is simulation based on the maximum a posteriori estimate. Gray area represents 0.05 to 0.95 quantile of prediction interval.

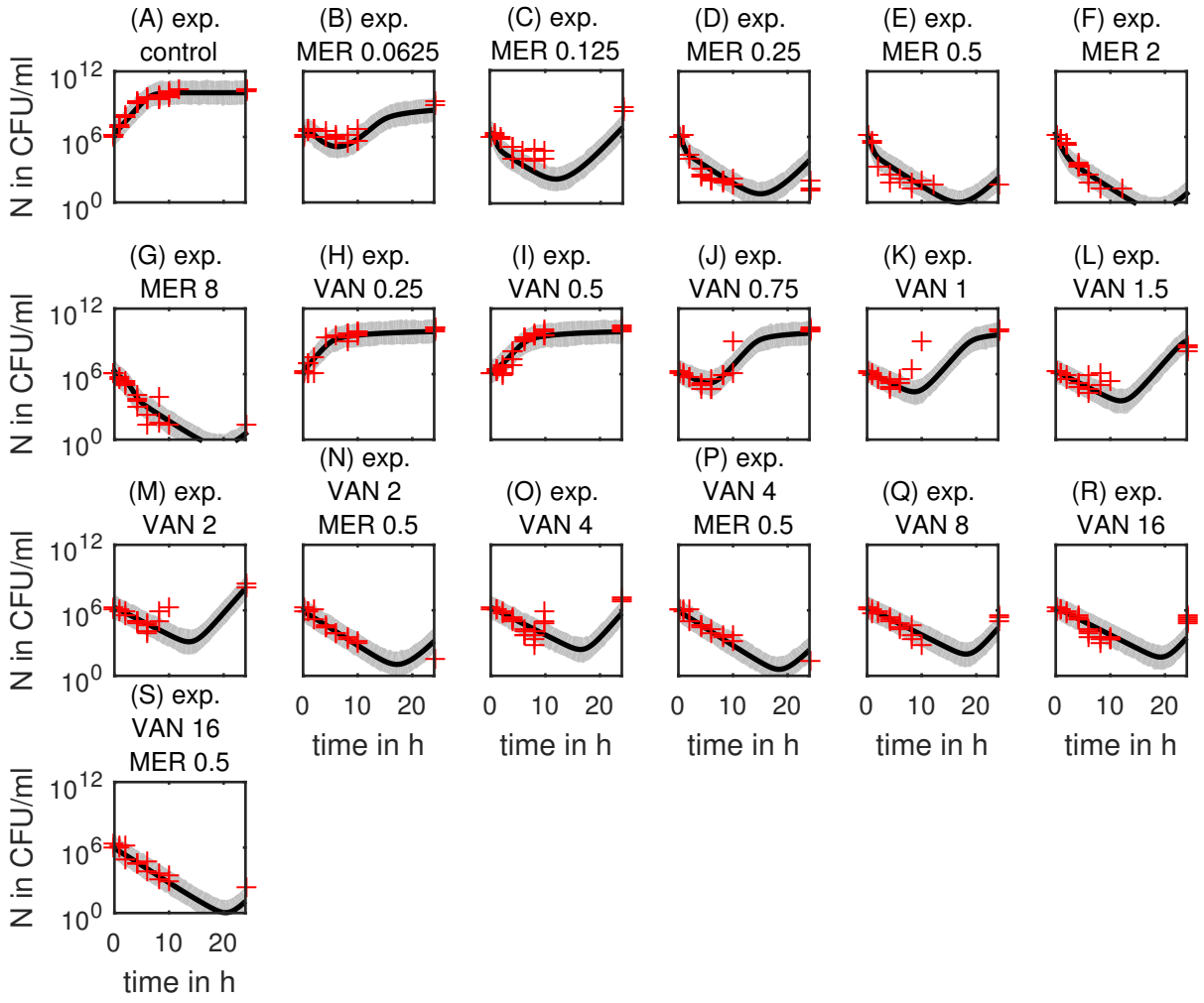

Figure A.4: Time-kill curves (*S. aureus*, VAN, MER, exp. phase). Exponential phase cultures exposed to different initial concentrations of vancomycin (VAN) and meropenem (MER) in mg/l. Data as red crosses. Solid black line is simulation based on the maximum a posteriori estimate. Gray area represents 0.05 to 0.95 quantile of prediction interval.

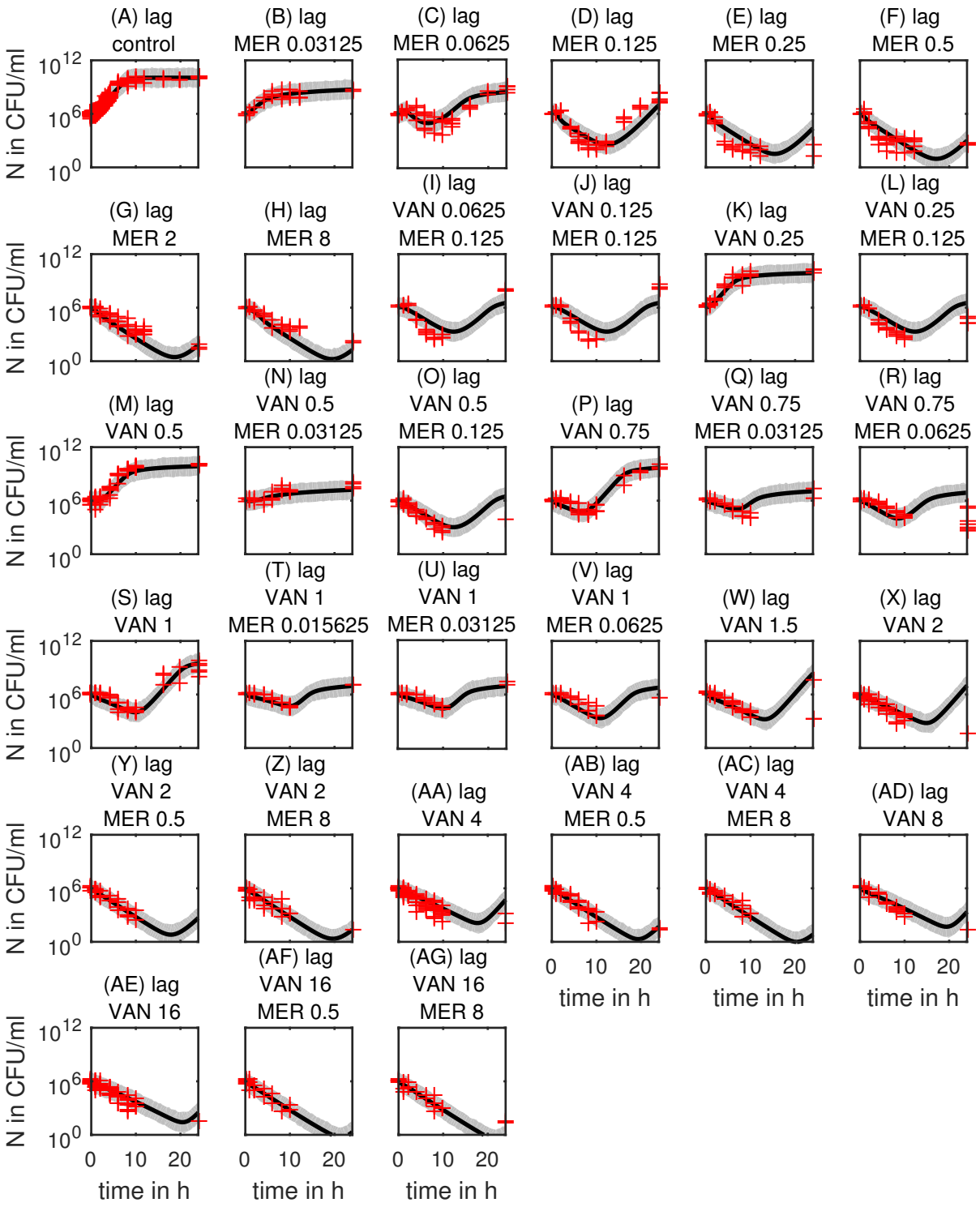

Figure A.5: Time-kill curves (*S. aureus*, VAN, MER, lag phase). Lag phase cultures exposed to different initial concentrations of vancomycin (VAN) and meropenem (MER) in mg/l. Data as red crosses. Solid black line is simulation based on the maximum a posteriori estimate. Gray area represents 0.05 to 0.95 quantile of prediction interval.